TRANSPORTATION RESEARCH

RECORD

No. 1370

Pavement Design, Management, and Performance

Pavement Design and Rehabilitation

A peer-reviewed publication of the Transportation Research Board

TRANSPORTATION RESEARCH BOARD
NATIONAL RESEARCH COUNCIL

NATIONAL ACADEMY PRESS
WASHINGTON, D.C. 1992

Transportation Research Record 1370
Price: $17.00

Subscriber Category
IIB pavement design, management, and performance

TRB Publications Staff
Director of Reports and Editorial Services: Nancy A. Ackerman
Senior Editor: Naomi C. Kassabian
Associate Editor: Alison G. Tobias
Assistant Editors: Luanne Crayton, Norman Solomon, Susan E. G. Brown
Graphics Specialist: Terri Wayne
Office Manager: Phyllis D. Barber
Senior Production Assistant: Betty L. Hawkins

Printed in the United States of America

Library of Congress Cataloging-in-Publication Data
National Research Council. Transportation Research Board.

Pavement design and rehabilitation.
p. cm.—(Transportation research record ISSN 0361-1981; no. 1370)
"A peer-reviewed publication of the Transportation Research Board."
ISBN 0-309-05411-7
1. Pavements, Concrete—Testing. 2. Pavements, Concrete—Joints. I. Series: Transportation research record; 1370.
TE7.H5 no. 1370
[TE278]
388 s—dc20 92-42007
[625.8] CIP

Sponsorship of Transportation Research Record 1370

GROUP 2—DESIGN AND CONSTRUCTION OF TRANSPORTATION FACILITIES
Chairman: Charles T. Edson, New Jersey Department of Transportation

Pavement Management Section
Chairman: Joe P. Mahoney, University of Washington

Committee on Rigid Pavement Design
Chairman: Gary Wayne Sharpe, Kentucky Transportation Cabinet
Don R. Alexander, Ernest J. Barenberg, Brian T. Bock, Kathleen Theresa Hall, Amir N. Hanna, John E. Hunt, Michael P. Jones, Walter P. Kilareski, Starr D. Kohn, Roger M. Larson, Jo A. Lary, Richard A. McComb, B. Frank McCullough, Theodore L. Neff, Mauricio R. Poblete, Robert J. Risser, Jr., Shiraz D. Tayabji, Mang Tia, James H. Woodstrom, John P. Zaniewski, Terrence L. Zoller, Dan G. Zollinger

Frank R. McCullagh, Transportation Research Board staff

The organizational units, officers, and members are as of December 31, 1991.

Transportation Research Record 1370

Contents

Foreword

Smith et al. investigated the effects of early loading of young concrete pavements by construction traffic and determined that slab edge loadings were the most critical and could reduce the life of the pavement. Choubane and Tia present the results of an analytical and experimental study of the temperature distribution within concrete pavement slabs and its effect on the pavement's behavior. Ioannides et al. describe a theoretical and practical approach for determining maximum responses in concrete pavement systems incorporating a base layer.

Seiler developed regression models that permit the use of an equivalent single-wheel radius to determine the free edge stress in a jointed plain concrete pavement. Wu presents the results of a 23-year study of an experimental concrete pavement that included a control and eight test sections and concludes that the base type affects the performance of the concrete surface and also that the current design equation underestimates concrete pavement performance. Krauthammer and Palmieri describe a study on the relationship between aggregate interlock shear transfer across a concrete interface and its dynamic response frequency.

Analysis of Concrete Pavements Subjected to Early Loading

KURT D. SMITH, THOMAS P. WILSON, MICHAEL I. DARTER, AND PAUL A. OKAMOTO

Even before a newly placed concrete pavement has achieved its specified design strength, it is often subjected to loading from construction traffic and equipment. Concrete trucks, haul trucks, and joint-sawing equipment are among several of the different types of construction traffic to which a young pavement may be subjected. Engineers have long speculated whether this early loading of the young pavement by construction traffic causes any significant damage to the pavement. In a research study for the Federal Highway Administration, the effects of early loading of a young pavement by construction traffic at different locations were investigated. Accumulated fatigue damage inflicted by an 18-kip single axle was calculated for the edge, interior, and transverse joint loading conditions for a slab of various concrete strengths. The results indicated that slab edge loadings were the most critical and, depending on their magnitude and the strength of the concrete at the time of loading, could reduce the life of the pavement. The interior and transverse joint stresses were comparable in magnitude, but much less than those produced at the slab edge. Joint-sawing equipment was shown to have a negligible effect on the fatigue life of the slab.

Newly placed concrete pavements are often subjected to traffic loading shortly after they have hardened but long before they have attained their design strength. For example, construction traffic may use the young pavement as a working platform to facilitate subsequent construction activities. Lighter construction equipment, such as joint-sawing equipment, may also load the pavement at a very early age.

The early trafficking of young concrete pavements raises several questions regarding the potential reduction in the service life of the pavement caused by the early loading. Although some argue that the pavement should not be loaded until it has achieved its design strength, others contend that light loads or a small number of heavy load repetitions will not cause any appreciable damage. A methodology for evaluating the effect of early loading is presented here with a demonstration of its use in practical applications.

APPROACH TO EARLY LOADING EVALUATION

In order to determine the damage caused by early loading, a fatigue analysis of concrete pavements subjected to early loading was conducted. The fatigue analysis compares the actual number of early traffic load applications with the allowable number of load applications that the pavement may sustain before cracking. This latter value depends on the critical stresses produced in the slab by the construction traffic and the existing strength of the slab. The greater the strength of the slab, the larger the number of load applications that the slab may sustain before cracking.

K. D. Smith, T. P. Wilson, and M. I. Darter, ERES Consultants, Inc., 8 Dunlap Court, Savoy, Ill. 61874. P. A. Okamoto, Construction Technology Laboratories, 5420 Old Orchard Road, Skokie, Ill. 60077.

Determining Stresses and Compressive Strength

The maximum tensile stresses occurring at the bottom of the slab, which are the critical stresses that can produce fatigue cracking, were determined for typical construction traffic loadings using the ILLI-SLAB finite-element computer program (*1–3*). The program was recently evaluated using field-measured strain data for newly constructed pavements and provided reasonable results (*4*).

In a laboratory evaluation of early-age concrete properties, the following relationship was developed between the concrete elastic modulus and the concrete compressive strength (*4*):

$$E_c = 62{,}000 * (f'_c)^{0.5} \quad (1)$$

where E_c is the elastic modulus of the concrete in pounds per square inch and f'_c is the compressive strength of the concrete in pounds per square inch. This relationship was based on laboratory concrete mixes ranging in age from 1 to 28 days and is believed to be more reflective of early-age concrete strength properties than the more familiar American Concrete Institute (ACI) relationship. However, Equation 1 is used here for demonstration purposes only. The actual relationship for a given project is a function of cement type, cement source, and aggregate type; each agency should therefore develop relationships representative of their materials and conditions. Equation 1 can be used to relate the compressive strength of a concrete slab at any time to the elastic modulus, which is needed by the ILLI-SLAB program to obtain an estimate of the load stresses developing in the slab.

Determining Modulus of Rupture

The modulus of rupture represents the strength of the concrete slab in flexure. As such, it is an important parameter in the estimate of fatigue damage. Since this test typically is not performed by most agencies, it is recommended that each agency develop a relationship between the compressive strength

of the concrete and the modulus of rupture. A general relationship between these factors is given below (*4*):

$$MR = [8.460 \times (f'_c)^{0.5}] + (3.311 \times RH) - 155.91 \quad (2)$$

where

MR = concrete modulus of rupture (psi),
f'_c = concrete compressive strength (psi), and
RH = relative humidity during curing (%).

This model was derived for a number of different materials with different aggregate and cement sources, different relative humidities, and different cement contents. Although Equation 2 will be used here for demonstration purposes, it is recommended that agencies develop their own unique relationships for each individual mix design.

Estimating Concrete Fatigue Damage

The amount of fatigue damage occurring in a slab subjected to early loading was estimated by employing a fatigue-consumption approach similar to the one first proposed by Miner (*5*). This approach theorizes that a concrete pavement has a finite fatigue life and can withstand some maximum number of load repetitions, N, of a given traffic loading before fracture. Every individual traffic loading applied, n, decreases the life of the pavement by an infinitesimal amount. Damage is defined as

$$\text{Damage} = \Sigma\ (n/N) * 100 \quad (3)$$

where

Damage = proportion of life consumed when mean inputs are used (50 percent of slabs cracked when damage is 100),
n = applied number of applied traffic loadings, and
N = allowable number of traffic loadings to slab cracking.

This value provides the percentage of life that is consumed by the applied traffic loads up to a given time. Theoretically, when $\Sigma\ (n/N) = 100$, fracture of the concrete would occur for a given slab; however, because of variability in edge traffic loadings and concrete strength from slab to slab, fracture of some slabs can occur at values both less than and greater than 1. Thus, because mean values are used for all inputs in the fatigue damage analysis, 50 percent of the slabs should be cracked when the calculated fatigue damage is 100.

The allowable number of traffic loadings when 50 percent of the slabs are cracked can be estimated from the following fatigue damage model (*6*):

$$\text{Log}_{10}\ N = 2.13\ (1/SR)^{1.2} \quad (4)$$

where

N = allowable number of traffic loadings at 50 percent slab cracking,
SR = stress ratio = σ/MR,
σ = critical stress in slab due to given loading (psi), and
MR = 28-day cured concrete modulus of rupture (psi) (from beam breaks).

The fatigue model was developed from 60 full-scale test sections built by the Corps of Engineers (*6*). As such, it is believed to be a more realistic model than fatigue models developed from laboratory beam testing since the field-developed model represents supported slab conditions, whereas laboratory beams do not. Furthermore, whereas in theory a crack can occur from one loading if the stress ratio is greater than or equal to 1, the fully supported slab in the field can sustain many more loadings before the crack progresses to the surface.

EARLY CONSTRUCTION TRAFFIC LOADING

An 18,000-lb single axle with dual tires was selected as a typical load for the evaluation of fatigue damage from early construction traffic loading. Tandem-axle loads were not considered, but generally the stresses produced by a tandem axle, which has twice the load of a single axle, are less than those for single axles. Furthermore, only one contact pressure (100 psi) was evaluated.

Five elastic modulus values (1 million to 5 million psi) were investigated, corresponding to a range in compressive strength of the concrete. Although the higher elastic modulus levels (4 million and 5 million psi) are not representative of early loading conditions, they were included to illustrate the effect of load-induced stresses on mature pavements.

Three loading conditions (edge, interior, and transverse joint) were evaluated. The critical stresses for each of these loading conditions were determined using the ILLI-SLAB program for a range of slab thicknesses, elastic modulus values, and effective k-values. The input variables used in the ILLI-SLAB evaluation of pavements subjected to early loading are given in Table 1.

Edge Loading Condition

The edge loading condition consists of the load placed at the slab edge midway between the transverse joints. This represents the most critical loading position because the largest stresses for a free edge develop at this location. On the basis of the relationship presented earlier between the concrete elastic modulus and concrete compressive strength, the critical edge stresses computed from ILLI-SLAB were related directly to the compressive strength. For example, with the previous relationship between elastic modulus and compressive strength (Equation 1), the compressive strength corresponding to a concrete elastic modulus of 2 million psi would be

$$f'_c = (2{,}000{,}000/62{,}000)^2 = 1{,}040 \text{ psi}$$

If the modulus of rupture corresponding to a given compressive strength could be estimated, the stress ratio (stress/modulus of rupture) would be known and an estimate of the fatigue damage done to the pavement by the given construction loading could be obtained. For purposes of illustration, the general relationship between modulus of rupture and com-

TABLE 1 Summary of Input Variables Used in ILLI-SLAB Evaluation of Early Construction Traffic Loading

PAVEMENT TYPE	JPCP
PCC SURFACE PROPERTIES	
Slab Thickness	8 in
	10 in
	12 in
Poisson's Ratio	0.15
Modulus of Elasticity	1,000,000 psi
	2,000,000 psi
	3,000,000 psi
	4,000,000 psi
	5,000,000 psi
SUBGRADE PROPERTIES	
Subgrade Model	Winkler
Subgrade *k*-value	100 psi/in
	300 psi/in
	500 psi/in
JOINT DATA	
Joint Spacing	15 ft
Lane Width	12 ft
Joint Width	0.125 in
Transverse Joint	
Doweled Joint	
Dowel Diameter	1.25 in
Dowel Spacing	12 in
Modulus of Dowel Support	1,500,000 psi/in
Dowel Modulus of Elasticity	29,000,000 psi
Dowel Poisson's Ratio	0.30
Dowel Concrete Interaction (Using Friberg's Analysis)	1,490,000 lb/in
Nondoweled Joint	
Aggregate Interlock Factor	0 (free edge)
WHEEL LOADING	
Type of Axle	Single, dual wheel
Gross Weight of Axle	18,000 lb
Tire Imprint	45 in^2
Contact Pressure	100 psi
TEMPERATURE GRADIENT	
Not considered	

pressive strength given in Equation 2 will be used, assuming 80 percent relative humidity.

The resulting modulus of rupture estimate was then used in the fatigue model to obtain the mean allowable number of load applications before slab fracture. For example, for a slab with a compressive strength of 1,000 psi and a curing relative humidity of 80 percent, the modulus of rupture would be

$$MR = [8.460 \times (1000)^{0.5}] + (3.311 \times 80) - 155.91 = 376 \text{ psi}$$

Using this modulus of rupture estimate and the 195-psi critical stress value previously obtained, the resulting allowable number of edge load applications is

$$N = 10^{2.13*(376/195)^{1.2}} = 48{,}242 \text{ applications}$$

This indicates that when the concrete attains a compressive strength of 1,000 psi, the pavement can sustain 48,242 edge load applications by an 18-kip single-axle load before 50 percent of the slabs are cracked. To calculate the damage done by 100 loads along the unsupported edge, the applied number of load applications (n) is divided by N, so that the percent life consumed is

$$\text{Damage} = (100/48{,}242) \times 100 = 0.21 \text{ percent}$$

This value indicates that the amount of damage from 100 applications of an 18,000-lb single axle with a tire pressure of 100 psi along an unsupported edge would reduce the pavement life by 0.21 percent at that point in time when the concrete possesses a compressive strength of 1,000 psi. The damage done by the same 100 loads for pavements with a compressive strength of 1,500 and 2,000 psi would be 0.05 and 0.014 percent, respectively.

Table 2 provides a summary of the edge load fatigue damage calculations for each combination of slab thickness (t), k-value, and elastic modulus value (E). Table 2 also shows the corresponding compressive strength (f'_c) and modulus of rupture (MR) values, the critical stress in the slab (σ), and the allowable number of load applications (N).

Selected fatigue damage results from Table 2 are plotted in Figures 1 through 3 for 8-, 10-, and 12-in. slabs with a k-value of 300 psi/in. Other cases in which significant fatigue damage occurred could also have been plotted. These charts allow for the immediate determination of the fatigue damage

TABLE 2 Summary of Fatigue Damage Determination for Edge Loading Condition

Pavement Characteristics				Calculated Values			Percent Fatigue Damage Consumed at Different Levels of Early Loading				
t (in)	k (psi/in)	E_c (psi)	f'_c (psi)	MR (psi)	σ (psi)	N_{all} (No. of loads)	1	10	100	1000	10000
8	100	1000000	260	245	290	5.54e+01	2	18	181	1806	18055
8	100	2000000	1041	382	333	3.24e+02	0	3	31	309	3087
8	100	3000000	2341	518	351	2.51e+03	0	0	4	40	398
8	100	4000000	4162	655	364	2.04e+04	0	0	0	5	49
8	100	5000000	6504	791	373	1.78e+05	0	0	0	1	6
8	300	1000000	260	245	243	1.43e+02	1	7	70	699	6990
8	300	2000000	1041	382	285	1.06e+03	0	1	9	94	942
8	300	3000000	2341	518	302	1.18e+04	0	0	1	8	85
8	300	4000000	4162	655	315	1.33e+05	0	0	0	1	7
8	300	5000000	6504	791	325	1.57e+06	0	0	0	0	1
8	500	1000000	260	245	222	2.53e+02	0	4	40	396	3959
8	500	2000000	1041	382	263	2.15e+03	0	0	5	47	465
8	500	3000000	2341	518	280	2.88e+04	0	0	0	3	35
8	500	4000000	4162	655	293	3.89e+05	0	0	0	0	3
8	500	5000000	6504	791	302	5.83e+06	0	0	0	0	0
10	100	1000000	260	245	206	4.25e+02	0	2	24	235	2355
10	100	2000000	1041	382	232	7.47e+03	0	0	1	13	134
10	100	3000000	2341	518	243	1.93e+05	0	0	0	1	5
10	100	4000000	4162	655	249	6.25e+06	0	0	0	0	0
10	100	5000000	6504	791	254	2.13e+08	0	0	0	0	0
10	300	1000000	260	245	174	1.65e+03	0	1	6	61	605
10	300	2000000	1041	382	201	3.99e+04	0	0	0	3	25
10	300	3000000	2341	518	213	1.56e+06	0	0	0	0	1
10	300	4000000	4162	655	221	6.95e+07	0	0	0	0	0
10	300	5000000	6504	791	227	3.39e+09	0	0	0	0	0
10	500	1000000	260	245	160	3.62e+03	0	0	3	28	276
10	500	2000000	1041	382	187	1.04e+05	0	0	0	1	10
10	500	3000000	2341	518	198	5.75e+06	0	0	0	0	0
10	500	4000000	4162	655	206	3.40e+08	0	0	0	0	0
10	500	5000000	6504	791	213	1.94e+10	0	0	0	0	0
12	100	1000000	260	245	156	4.66e+03	0	0	2	21	214
12	100	2000000	1041	382	171	3.85e+05	0	0	0	0	3
12	100	3000000	2341	518	177	5.40e+07	0	0	0	0	0
12	100	4000000	4162	655	181	9.23e+09	0	0	0	0	0
12	100	5000000	6504	791	183	2.20e+12	0	0	0	0	0
12	300	1000000	260	245	131	3.34e+04	0	0	0	3	30
12	300	2000000	1041	382	150	3.44e+06	0	0	0	0	0
12	300	3000000	2341	518	158	7.27e+08	0	0	0	0	0
12	300	4000000	4162	655	164	1.65e+11	0	0	0	0	0
12	300	5000000	6504	791	168	4.75e+13	0	0	0	0	0
12	500	1000000	260	245	122	8.47e+04	0	0	0	1	12
12	500	2000000	1041	382	140	1.26e+07	0	0	0	0	0
12	500	3000000	2341	518	148	3.85e+09	0	0	0	0	0
12	500	4000000	4162	655	154	1.25e+12	0	0	0	0	0
12	500	5000000	6504	791	158	5.27e+14	0	0	0	0	0

done by the standard truck loading (18,000-lb single axle, 100-psi contact pressure) on a pavement of known compressive strength. For simplification in graphing, the compressive strength values have been rounded off to the nearest 50 psi.

It is observed from Figure 1, which is for an 8-in. slab with a *k*-value of 300 psi/in., that 100 load applications of the standard truck loading will consume 70 percent of the concrete fatigue life if the slab is loaded when it has a compressive strength of only 250 psi. However, if the pavement is not loaded until the concrete has attained a compressive strength of 2,350 psi, then 100 load applications of the standard loading will reduce the fatigue life by only about 1 percent.

Interior Loading Condition

The interior loading condition calls for the wheels to be situated at some distance from the edge. The interior load was placed 2 ft from the edge to represent the case in which an 8-ft-wide truck would center itself in a 12-ft-wide lane. The

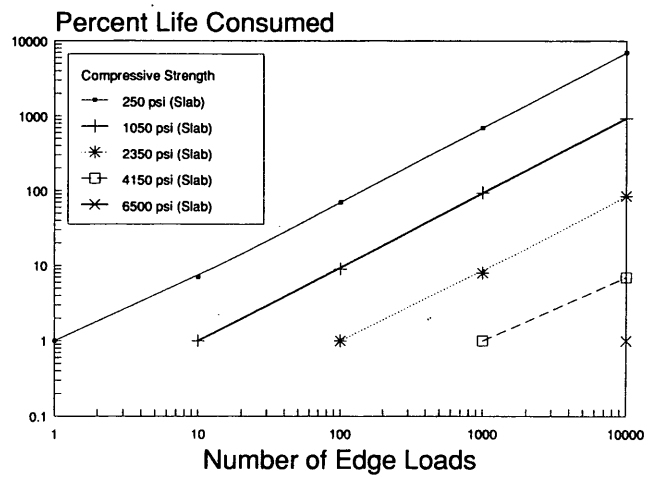

FIGURE 1 Percent life consumed versus number of 18-kip single-axle edge load applications for an 8-in. slab (k = 300 psi/in.)

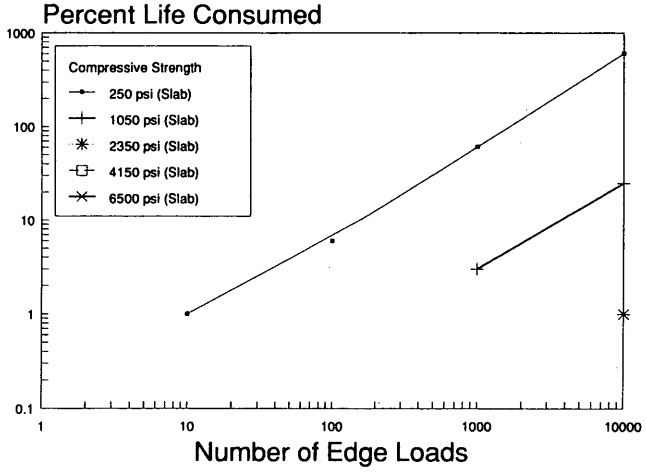

FIGURE 2 Percent life consumed versus number of 18-kip single-axle edge load applications for a 10-in. slab (k = 300 psi/in.).

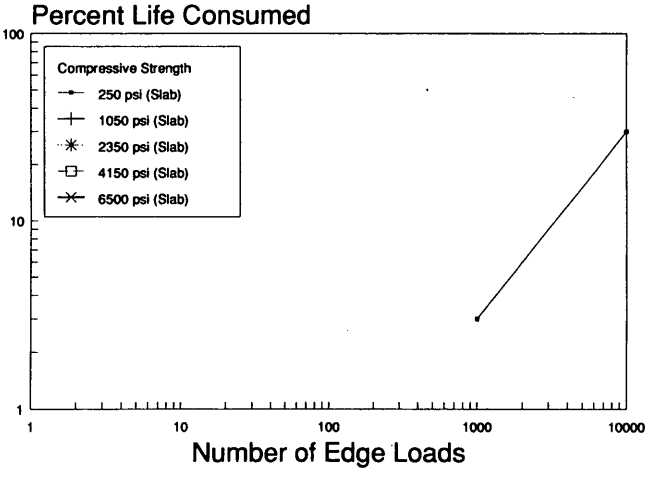

FIGURE 3 Percent life consumed versus number of 18-kip single-axle edge load applications for a 12-in. slab (k = 300 psi/in.).

ILLI-SLAB program again was used to determine the stresses occurring in the slab for the 18,000-lb single-axle load with a contact pressure of 100 psi.

The maximum stress in the slab was calculated as a function of the compressive strength of the concrete following the same procedure as that used in the edge loading analysis. Then, again for purposes of illustration, the modulus of rupture was estimated from the general relationship with compressive strength. These results were then evaluated using the fatigue damage model to obtain an estimate of the slab fatigue damage for a range of slab thicknesses and load applications. Table 3 summarizes the results of the fatigue damage evaluation for the interior loading condition.

An examination of Table 3 shows that the interior loading condition produces much less damage than the edge loading condition and indicates that if the trucks that load a pavement at an early age stay away from the edge (in this case, 2 ft from the edge), little damage may result. Charts could have been developed to illustrate the percent life consumed as a function of the number of load applications, but this was not done since the amount of fatigue damage was so small.

In the example cited for the edge loading condition, it was noted that 100 applications of the 18,000-lb single axle consumed 70 percent of the life of an 8-in. slab that had a k-value of 300 psi/in. and a compressive strength of 250 psi. However, if on that same pavement those 100 applications stay 2 ft away from the slab edge, Table 3 indicates that virtually no fatigue damage occurs.

Transverse Joint Loading Condition

The transverse joint loading condition was evaluated with the ILLI-SLAB program for a few selected cases. A 10-in. slab (with and without dowel bars) was evaluated for a k-value of 300 psi/in. and portland cement concrete (PCC) elastic modulus values of 2 million and 4 million psi. The tranverse joint was loaded with an 18,000-lb single-axle load 6 ft from the edge.

Doweled Transverse Joint

ILLI-SLAB was used to calculate the stresses occurring for the doweled transverse joint loading condition. The doweled transverse joint was analyzed assuming no aggregate interlock at the joint; that is, load transfer was provided only by the dowel bars. This provides a conservative estimate of the actual stresses because a portion of the load will be transferred through aggregate interlock. Typical stress load transfer efficiencies (LTE) for the doweled joints ranged between 46 and 58 percent.

Nondoweled Transverse Joint

ILLI-SLAB was also used to calculate stresses for the nondoweled transverse joint loading condition. The analysis was conducted assuming a "free edge" and then the various stresses

TABLE 3 Summary of Fatigue Damage Determination for Interior Loading Condition

Pavement Characteristics				Calculated Values			Percent Fatigue Damage Consumed at Different Levels of Early Loading				
t (in)	k (psi/in)	E_c (psi)	f'_c (psi)	MR (psi)	σ (psi)	N_{all} (No. of loads)	1	10	100	1000	10000
8	100	1000000	260	245	165	2.69e+03	0	0	4	37	372
8	100	2000000	1041	382	185	1.21e+05	0	0	0	1	8
8	100	3000000	2341	518	197	6.32e+06	0	0	0	0	0
8	100	4000000	4162	655	205	3.82e+08	0	0	0	0	0
8	100	5000000	6504	791	212	2.21e+10	0	0	0	0	0
8	300	1000000	260	245	139	1.64e+04	0	0	1	6	61
8	300	2000000	1041	382	155	1.93e+06	0	0	0	0	1
8	300	3000000	2341	518	165	2.58e+08	0	0	0	0	0
8	300	4000000	4162	655	173	3.32e+10	0	0	0	0	0
8	300	5000000	6504	791	179	4.72e+12	0	0	0	0	0
8	500	1000000	260	245	129	4.06e+04	0	0	0	2	25
8	500	2000000	1041	382	143	8.37e+06	0	0	0	0	0
8	500	3000000	2341	518	153	1.62e+09	0	0	0	0	0
8	500	4000000	4162	655	160	3.58e+11	0	0	0	0	0
8	500	5000000	6504	791	165	9.45e+13	0	0	0	0	0
10	100	1000000	260	245	118	1.35e+05	0	0	0	1	7
10	100	2000000	1041	382	131	4.90e+07	0	0	0	0	0
10	100	3000000	2341	518	139	2.16e+10	0	0	0	0	0
10	100	4000000	4162	655	144	1.29e+13	0	0	0	0	0
10	100	5000000	6504	791	147	1.13e+16	0	0	0	0	0
10	300	1000000	260	245	99	2.15e+06	0	0	0	0	0
10	300	2000000	1041	382	110	3.05e+09	0	0	0	0	0
10	300	3000000	2341	518	118	3.79e+12	0	0	0	0	0
10	300	4000000	4162	655	123	6.95e+15	0	0	0	0	0
10	300	5000000	6504	791	128	8.98e+18	0	0	0	0	0
10	500	1000000	260	245	91	1.01e+07	0	0	0	0	0
10	500	2000000	1041	382	102	2.42e+10	0	0	0	0	0
10	500	3000000	2341	518	108	9.75e+13	0	0	0	0	0
10	500	4000000	4162	655	114	2.26e+17	0	0	0	0	0
10	500	5000000	6504	791	118	7.89e+20	0	0	0	0	0
12	100	1000000	260	245	89	1.57e+07	0	0	0	0	0
12	100	2000000	1041	382	98	7.85e+10	0	0	0	0	0
12	100	3000000	2341	518	103	6.43e+14	0	0	0	0	0
12	100	4000000	4162	655	106	8.66e+18	0	0	0	0	0
12	100	5000000	6504	791	107	3.17e+23	0	0	0	0	0
12	300	1000000	260	245	75	6.84e+08	0	0	0	0	0
12	300	2000000	1041	382	84	1.28e+13	0	0	0	0	0
12	300	3000000	2341	518	89	4.42e+17	0	0	0	0	0
12	300	4000000	4162	655	93	1.44e+22	0	0	0	0	0
12	300	5000000	6504	791	96	5.86e+26	0	0	0	0	0
12	500	1000000	260	245	69	5.82e+09	0	0	0	0	0
12	500	2000000	1041	382	77	3.56e+14	0	0	0	0	0
12	500	3000000	2341	518	82	2.94e+19	0	0	0	0	0
12	500	4000000	4162	655	86	2.18e+24	0	0	0	0	0
12	500	5000000	6504	791	89	2.06e+29	0	0	0	0	0

corresponding to selected load transfer efficiencies were determined using the following relationship:

$$\sigma = \sigma_{fe} / (1 + LTE) \quad (5)$$

where

σ = calculated edge stress for a given LTE (psi),
σ_{fe} = maximum free edge stress (zero LTE) (psi), and
LTE = stress load transfer efficiency across transverse joint.

Comparison of Interior and Transverse Joint Stresses

The stresses for the doweled and nondoweled joints (assuming 50 percent LTE) are plotted in Figure 4 along with the corresponding interior stresses. Generally speaking, there is little difference in the magnitude of the stresses, indicating that the stresses occurring at the transverse joints are comparable with the stresses occurring in the interior portions of the slab. It is interesting to note that as the elastic modulus increases,

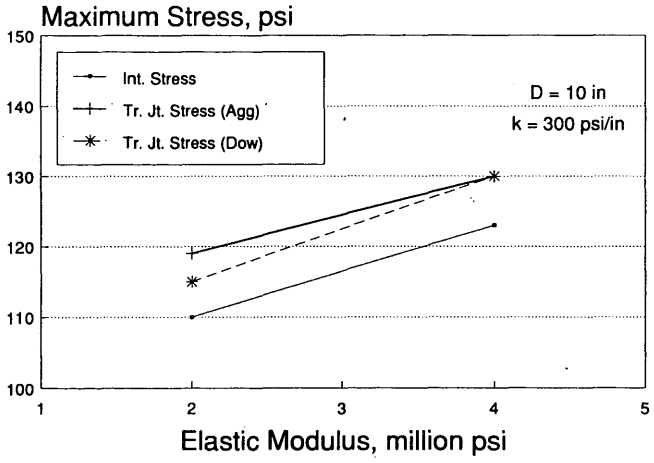

FIGURE 4 Comparison of interior and transverse joint stresses for a 10-in. slab (k = 300 psi/in.).

the doweled transverse joint stress approaches that of the nondoweled transverse joint stress.

The nondoweled transverse joint stresses were generally higher than those for the doweled joint or the interior loading condition. Again, however, the nondoweled transverse joint stresses were not substantially different from those for the interior loading condition.

For the purposes of this comparison, 50 percent stress load transfer was assumed for the nondoweled transverse joint. In actuality, this value may be much higher because of the high level of aggregate interlock that exists immediately after construction. As calculated from Equation 5, an increase in stress load transfer efficiency to even 75 percent greatly reduces the magnitude of the stress. The same type of argument can be made for the stresses developing in the doweled joint, because these neglected aggregate interlock load transfer and the actual stresses would probably be less.

DOWEL BEARING STRESSES

The maximum bearing stresses exerted by the dowels on the concrete are a critical aspect in the design of doweled concrete pavements. It has been shown that the magnitude of the bearing stresses has a great effect on the development of transverse joint faulting (*7*). If the bearing stresses due to early loading exceed the compressive strength of the concrete, fracture or crushing of the concrete around the dowel bar could occur.

The modified Friberg analysis was used to calculate the maximum bearing stresses (*7–9*). The maximum bearing stress is given by the following formula:

$$\sigma_{max} = K * \delta_0 \quad (6)$$

where

K = modulus of dowel support (psi/in.),
δ_0 = deflection of the dowel at the face of the joint (in.),
= $P_t (2 + \beta z) / 4\beta^3 E_s I$, in which
P_t = shear force acting on dowel (lb),
z = width of joint opening (in.),
E_s = modulus of elasticity of dowel bar (psi),
I = moment of inertia of dowel bar cross section (in.^{4}),
= $0.25 * \pi * (d/2)^4$ for dowel diameter d in inches, and
β = relative stiffness of the dowel concrete system (l/in.)
= $[(Kd)/(4E_sI)]^{0.25}$.

The analysis assumes a 9,000-lb wheel load placed at the corner, which will produce the maximum stress in the outermost dowel bar. Only dowel bars within a distance of 1.0 $* l$ from the center of the load are considered to be active, where l is the radius of relative stiffness, defined as

$$l = [Eh^3/12k(1 - \mu^2)]^{0.25} \quad (7)$$

where

E = concrete modulus of elasticity (psi),
h = slab thickness (in.),
k = effective modulus of subgrade reaction (psi/in.), and
μ = Poisson's ratio.

Finally, the modified Friberg analysis is based on the assumption that 45 percent of the *load* (not the stress) was transferred across the joint, which has been shown to provide conservative results (*7*).

The modulus of dowel support, K, has been suggested to range from 300,000 to 1,500,000 psi/in., with a value of 1,500,000 psi/in. typically assumed in design. However, this value is probably less than that when the concrete is newly placed and its compressive strength is low. One recent study showed that the modulus of dowel support increased with increasing compressive strength (*10*). Since K is a measure of the support provided to the dowel bar by the slab, it is intuitive that this support value will increase with increasing compressive strength. It would follow, then, that the parameter also increases with increasing concrete elastic modulus and that different K-values corresponding to increases in the concrete elastic modulus should be used in the evaluation of early-age bearing stresses.

Unfortunately, very little research has been done on the relation between the modulus of dowel support and PCC compressive strength or elastic modulus. Limited data from Tayabji and Colley (*10*) indicated that K increased with increasing compressive strength, and these data were used to develop some very crude approximations of the modulus of dowel support at various compressive strengths. Since only 28-day compressive strengths were measured in that study, strengths at earlier times were obtained using the concrete strength development model provided by Davis and Darter (*11*). The average modulus of dowel support values shown below were estimated for the corresponding elastic modulus values evaluated in this study.

PCC Elastic Modulus (psi)	*PCC Compressive Strength (psi)*	*Modulus of Dowel Support (psi/in.)*
1,000,000	260	375,000
2,000,000	1,041	650,000
3,000,000	2,341	1,000,000
4,000,000	4,162	1,750,000
5,000,000	6,504	2,500,000

It must be reiterated that the values shown above are based on very limited data, particularly in the area of early concrete

strengths. Additional research is definitely needed to quantify this relationship more accurately.

Assuming the modulus of dowel support values given above, dowel bearing stresses were computed using ILLI-SLAB. Dowel bar diameters were assumed to be one-eighth of the slab thickness. The resulting bearing stresses are plotted in Figures 5 through 7 for a range of design factors. The diagonal line shown in Figures 5 through 7 represents the line of equality between the bearing stress and the compressive strength; those bearing stresses that fall to the left of the line are unacceptable (i.e., bearing stress exceeds compressive strength) and those that fall to the right of the line are acceptable (i.e., compressive strength exceeds bearing stress).

It is observed from Figures 5 through 7 that the bearing stresses decrease with increasing slab thickness (and dowel bar diameter, since larger dowels were assumed for thicker slabs). Because of this, thinner slabs are much more susceptible to bearing stress fracture from early loading than the thicker slabs.

Another observation from Figures 5 through 7 is that the bearing stress increases with an increase in the foundation support. However, the impact of the foundation support on the dowel bearing stresses is not as substantial for thicker slabs with larger dowel bars.

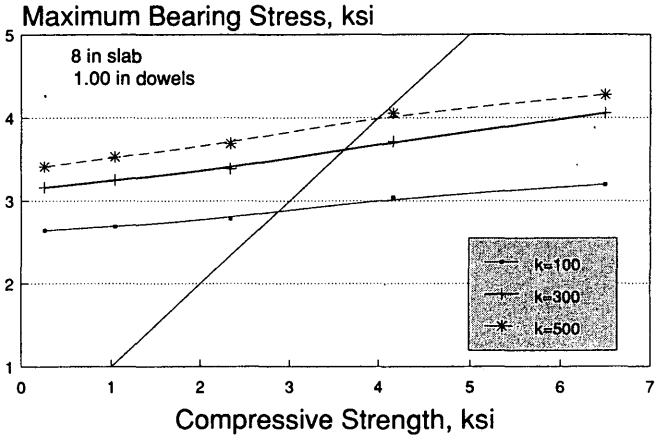

FIGURE 5 Maximum bearing stress versus compressive strength for 8-in. slab.

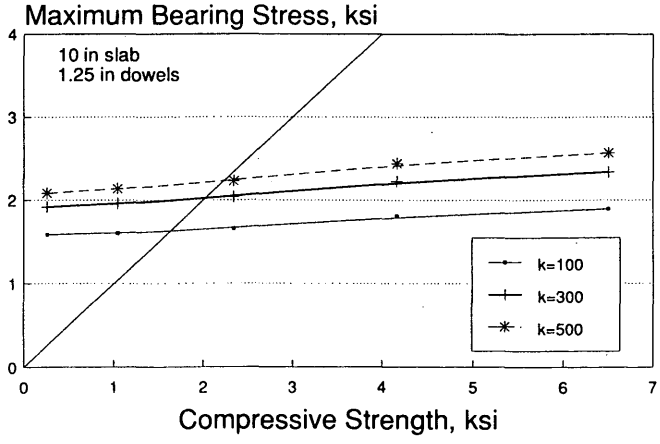

FIGURE 6 Maximum bearing stress versus compressive strength for 10-in. slab.

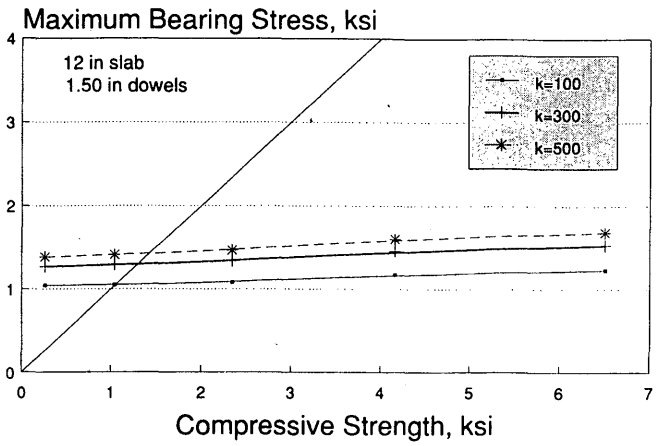

FIGURE 7 Maximum bearing stress versus compressive strength for 12-in. slab.

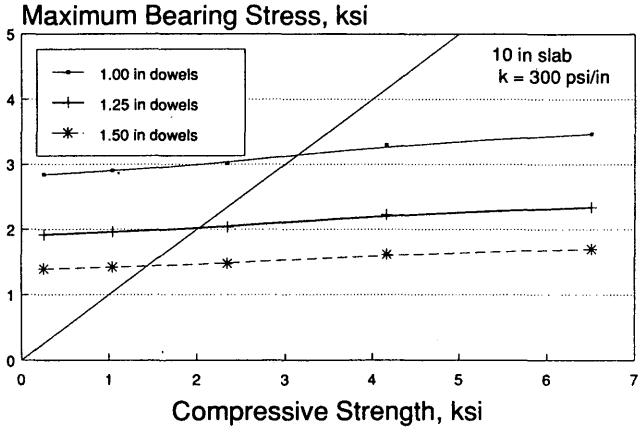

FIGURE 8 Maximum bearing stress versus compressive strength for 10-in. slab with varying dowel diameters.

It has been mentioned that dowel diameters are an important factor influencing the magnitude of the bearing stresses. To illustrate this, maximum bearing stresses were determined using ILLI-SLAB for a 10-in. slab with 1-, 1.25-, and 1.5-in. dowel diameters and assuming a foundation support of 300 psi/in. These bearing stresses are plotted in Figure 8. As would be expected, the larger-diameter dowel resulted in lower bearing stresses, with a particularly big reduction in bearing stresses obtained by moving from a 1-in. to a 1.25-in. dowel.

LOADING BY SAWING EQUIPMENT

Other than construction truck traffic, the spansaw, a piece of heavy equipment used to cut the transverse joint in the slab, could load a pavement at an early age. Hence, the fatigue damage done by the spansaw was also evaluated by placing it in the interior portions of the slab. The inputs for the ILLI-SLAB evaluation are given in Table 4.

TABLE 4 Summary of Input Variables Used in ILLI-SLAB Evaluation of Spansaw Interior Loading

PAVEMENT TYPE	JPCP
PCC SURFACE PROPERTIES	
Slab Thickness	8 in
	10 in
	12 in
Poisson's Ratio	0.15
Modulus of Elasticity	1,000,000 psi
	2,000,000 psi
	3,000,000 psi
	4,000,000 psi
	5,000,000 psi
SUBGRADE PROPERTIES	
Subgrade Model	Winkler
Subgrade *k*-value	100 psi/in
	300 psi/in
	500 psi/in
JOINT DATA	
Joint Spacing	20 ft
Lane Width	24 ft
WHEEL LOADING	
Gross Weight of Spansaw	14,500 lb
Number of Tires	4
Tire Imprint	48 in^2
Contact Pressure	75.5 psi
TEMPERATURE GRADIENT	
Not considered	

The spansaw configuration and input variables were analyzing using ILLI-SLAB. A fatigue damage analysis was conducted using the same relationships and procedures previously described. The results of that analysis indicated that no fatigue damage occurs for any combination, even up to a maximum of 10,000 load applications of the spansaw. Thus, it is believed that none of the lighter construction equipment causes any damage on the pavement after a minimum compressive strength of 250 psi (corresponding to an elastic modulus of 1,000,000 psi) has been obtained.

SUMMARY

A methodology has been presented that allows for the estimation of concrete fatigue damage due to early loading. The fatigue damage sustained by a slab of known compressive strength from a certain number of early load applications can be estimated or, conversely, the minimum compressive strength required to minimize the fatigue damage caused by those early load applications can be determined. The early loading analysis was conducted using relationships between compressive strength, flexural strength, and modulus of elasticity.

The longitudinal edge loading condition, in which the load is placed in the midpoint of the slab at the edge, was determined to be the most critical. The stresses that develop in the slab at this location are much larger than those that develop at the slab interior or at the transverse joint for the same loading. This indicates that a slab can be subjected to early loading with very little fatigue damage if the loads are located away from the longitudinal slab edge.

An evaluation of the transverse joint loading condition showed that the maximum slab stresses for both the nondoweled and doweled joints were compatible with the stresses developing for the interior loading condition, and both conditions yielded virtually no fatigue damage. If higher levels of aggregate interlock were assumed (which is not unrealistic for a newly placed concrete pavement), the critical transverse joint stresses would be even less than the interior stresses.

An evaluation of dowel bearing stresses at early ages indicated that thinner slabs, which typically use smaller-diameter dowel bars, may be more susceptible to early loading damage than thicker slabs. Indeed, larger-diameter dowels were observed to be very effective in reducing bearing stresses. All of the work evaluating bearing stresses was based on modulus of dowel support values that were assumed to change with compressive strength. Rough approximations of the modulus of dowel support value were made, but much more research on this topic is needed.

A fatigue damage analysis was also conducted for the use of spansaws. The evaluation indicated that this equipment causes no fatigue damage to a slab (for a minimum compressive strength of 250 psi).

If early loading of a concrete slab becomes desirable or necessary, it is important to identify the maximum amount of fatigue damage that the slab should sustain from early loading without sacrificing its design life. That maximum amount of early loading damage is ultimately up to the highway agency, but it is critical that the agency consider the design traffic and the performance period of the pavement.

As an illustration, consider a pavement that was designed for 10 million 18-kip equivalent single-axle load (ESAL) ap-

plications over a 20-year period. Of those 10 million ESAL applications, assume that about 6 percent (0.6 million) of these would be edge loads. If early edge loading consumed 10 percent of the fatigue damage, this would mean that about 60,000 edge load applications were consumed. This translates to a reduction in life of roughly 2 years, assuming a linear distribution of traffic loading over the 20-year period. For this particular example, with the unknowns in actual traffic loadings and the historic inaccuracies of past traffic projections, the loss of 2 years of service life is probably unacceptable. Thus, the design traffic and the performance period must be evaluated for each design in order to evaluate what may be an acceptable level of fatigue damage from early loading.

ACKNOWLEDGMENTS

This paper is based on the results of a research project conducted by Construction Technology Laboratories, Inc. (CTL) for the Federal Highway Administration. ERES Consultants, Inc., served as a subcontractor to CTL and was responsible for the early loading analyses using the laboratory results obtained by CTL. The authors are grateful for the assistance provided by Pete Nussbaum of CTL and for the support provided by Steve Forster of FHWA.

REFERENCES

1. A. M. Tabatabaie and E. J. Barenberg. Structural Analysis of Concrete Pavement Systems. *Transportation Engineering Journal*, ASCE, Vol. 106, No. TE5, Sept. 1980.
2. A. M. Ioannides. Analysis of Slabs-on-Grade for a Variety of Loading and Support Conditions. Ph.D. dissertation. University of Illinois, Urbana-Champaign, 1984.
3. G. T. Korovesis. Analysis of Slab-on-Grade Pavement Systems Subjected to Wheel and Temperature Loading. Ph.D. dissertation. University of Illinois, Urbana-Champaign, 1990.
4. P. A. Okamoto, P. J. Nussbaum, K. D. Smith, M. I. Darter, T. P. Wilson, C. L. Wu, and S. D. Tayabji. *Guidelines for Timing Contraction Joint Sawing and Earliest Loading for Concrete Pavements,* Volume I—*Final Report*. Report FHWA-RD-91-079. FHWA, U.S. Department of Transportation, Oct. 1991.
5. M. A. Miner. Cumulative Damage in Fatigue. *Transactions, American Society of Mechanical Engineers,* Vol. 67, 1945.
6. M. I. Darter. *A Comparison Between Corps of Engineers and ERES Consultants, Inc. Rigid Pavement Design Procedures*. Technical Report. U.S. Air Force SAC Command, Aug. 1988.
7. K. W. Heinrichs, M. J. Liu, M. I. Darter, S. H. Carpenter, and A. M. Ioannides. *Rigid Pavement Analysis and Design*. Report FHWA-RD-88-068. FHWA, U.S. Department of Transportation, June 1989.
8. B. F. Friberg. Design of Dowels in Transverse Joints of Concrete Pavements. *Transactions of the American Society of Civil Engineers,* Vol. 105, 1940.
9. A. M. Ioannides, Y.-H. Lee, and M. I. Darter. Control of Faulting Through Joint Load Transfer Design. In *Transportation Research Record 1286*, TRB, National Research Council, Washington, D.C., 1990.
10. S. D. Tayabji and B. E. Colley. *Improved Rigid Pavement Joints*. Report FHWA/RD-86/040. FHWA, U.S. Department of Transportation, Feb. 1986.
11. D. D. Davis and M. I. Darter. Early Opening of PCC Full-Depth Repairs. Presented at the 63rd Annual Meeting of the Transportation Research Board, 1984.

Nonlinear Temperature Gradient Effect on Maximum Warping Stresses in Rigid Pavements

BOUZID CHOUBANE AND MANG TIA

The results are presented of an experimental and analytical study to determine the actual temperature distribution within typical concrete pavement slabs and to evaluate the effects of nonlinear thermal gradients on the behavior of concrete pavements. The temperature data obtained in this study indicated that the temperature variations within the pavement slabs were mostly nonlinear. The temperature distribution throughout the depth of a concrete pavement slab can be represented fairly well by a quadratic equation. When the distribution is nonlinear, the maximum computed tensile stresses in the slab tend to be lower for the daytime condition and higher for the nighttime condition as compared with the stresses computed with the consideration of a linear temperature distribution.

Daily temperature fluctuation within the concrete slab is an important factor affecting concrete pavement behavior. Thermally induced slab movements could significantly influence (a) the load transfer between adjacent slabs and (b) the degree of support offered by the subgrade, which affect the maximum load-induced stresses in the concrete slab. Several methods for rigid pavement design and analysis that take into account the effect of these temperature fluctuations have been developed over the years. These methods are all based, for simplicity, on the assumption that the temperature variation in the concrete slab from top to bottom is linear, even though the nonlinearity of the temperature distribution throughout the slab has long been recognized.

The nonlinearity of temperature distribution within the concrete pavement slab was first measured in the Arlington Road tests in the early 1930s. Teller and Sutherland, the investigators, concluded then that a uniform temperature gradient would result in the most critical stress condition, even though the curved gradient was the more usual temperature distribution (*1*). In 1940 Thomlinson reached the same conclusion by assuming a simple harmonic temperature variation at the slab top surface in combination with the heat flow laws (*2*). The magnitudes of the stresses derived in both cases were compared with those given by Westergaard's equations. Bradbury used a temperature differential in the concrete slab in his warping stress equations in plain and reinforced concrete pavements (*3*). According to Lang (*4*), the variations of the temperature distribution from the straight-line relationship are relatively small. The maximum measured temperature difference between a straight line and the actual distribution was less than 2°F at 2.5 and 4.5 in. below the slab surface for a 7-in. slab thickness. Lang concluded that considering the importance of the warping stress and the many variables affecting the design, these small variations from a straight line are not important, and consequently the temperature gradient can be approximated as linear for convenience.

With the advent of the computer age, various finite-element computer models that allow considerable freedom in loading configuration, flexural stiffness, and boundary conditions have been developed. Most of the currently used computer programs, such as WESLIQID (*5*), WESLAYER (*5*), JSLAB (*6*), ILLI-SLAB (*7*), and FEACONS (*8,9*), consider only the linear temperature gradient effects on the concrete slab.

In this paper the results are presented of an experimental and analytical study to determine the actual temperature distribution within typical concrete pavement slabs and to evaluate the effect of a nonlinear thermal gradient on the behavior of concrete pavements.

SLAB INSTRUMENTATION AND DATA COLLECTION

A six-slab concrete pavement constructed at the Materials Office of the Florida Department of Transportation (FDOT) was used to monitor pavement temperatures for this investigation. Each slab is 20 ft long, 12 ft wide, and 9 in. thick. The adjoining Slabs 1 and 2 and Slabs 4 and 5 are connected by dowels, as shown in Figure 1.

The test pavement was constructed to be representative of in-service Florida concrete pavements in August 1982. The slabs were laid on a native roadbed soil consisting mainly of granular materials classified as A-3 according to the AASHTO Soil Classification. The average limerock bearing ratio (LBR) of the compacted subgrade was 50 (*9*).

Five thermocouples to monitor pavement temperatures were embedded in the slab concrete at different levels at the time of construction. These thermocouples are positioned at 1, 2.5, 4.5, 6.5 and 8 in. below the top surface at the center of the fourth slab. The ambient temperature was measured by another thermocouple that was housed inside a wooden box mounted on a 5-ft pole. The thermocouples were connected to a Fluke programmable data logger. For the purpose of this study, the data logger was programmed to take the temperature measurements from all five sensors at 15-min intervals.

Department of Civil Engineering, University of Florida, Gainesville, Fla. 32611.

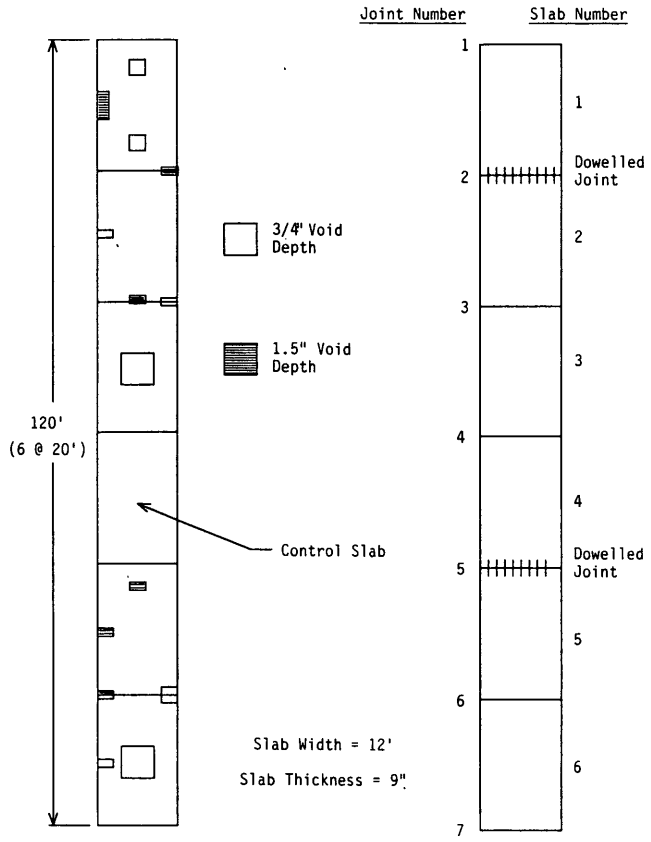

FIGURE 1 Plan of test slabs.

THERMAL GRADIENT ANALYSIS

Recorded Temperature Distribution

Figures 2 through 5 show the typical recorded variations in temperature distribution throughout the test slab for various times of the day at different periods of the year. It can be seen that the temperature differential in the slab tends to be positive in the daytime and negative at night. The nonlinearity of the temperature distribution is apparent. In addition, the curvature of the temperature distribution tends to be inward when ΔT is positive and outward when ΔT is negative. The temperature distributions for the nighttime and daytime conditions, which are used in the thermal stress analyses in this study, are based on the characteristics of these typical recorded temperature data.

Typical Thermal Gradient Components

The temperature distribution in the pavement slab can be typically divided into three components: (a) a component that causes axial displacement, that is, overall expansion or contraction; (b) a component that causes the bending; and (c) the nonlinear component, as shown in Figure 6.

The division of the temperature distribution into these three components is based on the assumption used in classical plate-bending theory that the cross section of a plate remains plane after bending. Thus, the plate can deform in only two ways:

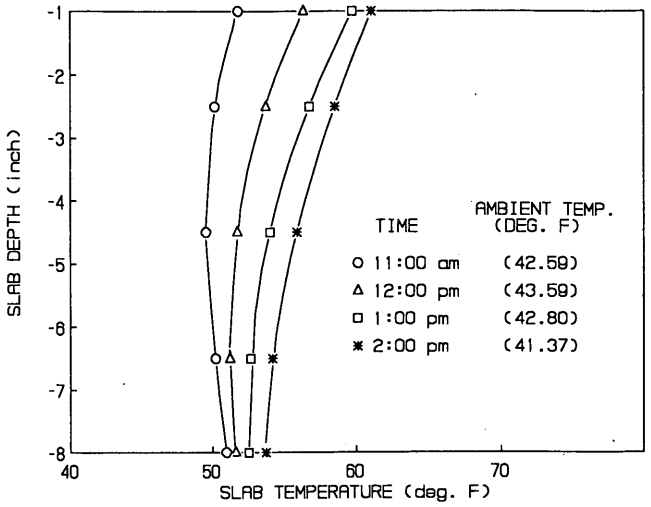

FIGURE 2 Typical daily temperature variations throughout the test slab corresponding to a positive temperature differential as recorded in January.

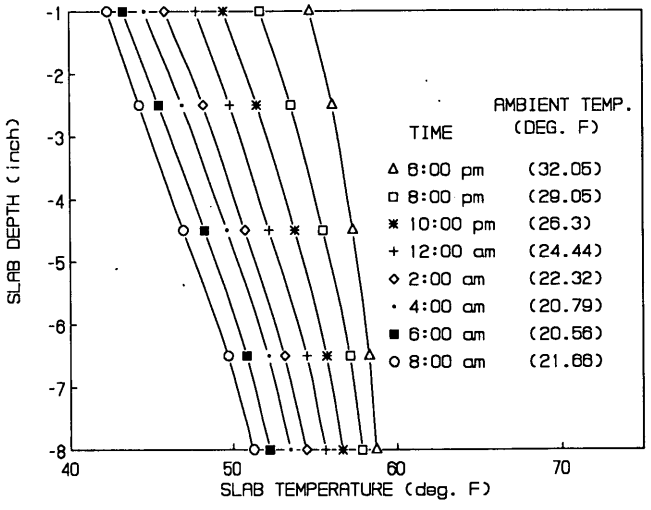

FIGURE 3 Typical daily temperature variations throughout the test slab corresponding to a negative temperature differential as recorded in January.

it can expand or contract axially, or it can bend with its cross section remaining plane. The first type of deformation is caused by a uniform temperature component. The second type is caused by a linear temperature distribution. The nonlinear temperature component is the remaining temperature component after the uniform and the linear temperature components have been subtracted from the total temperature distribution. These three temperature components are shown in Figure 6(a–c).

Mathematical Modeling of the Thermal Gradient

In order to isolate and study the effect of the nonlinearity of temperature variation, a mathematical model was used. From

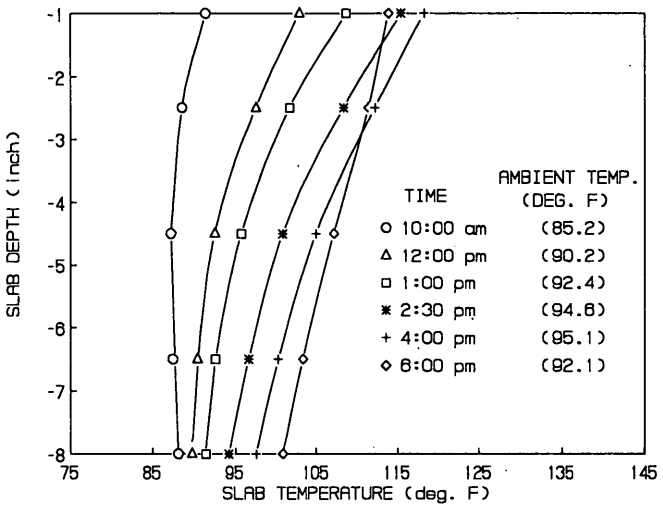

FIGURE 4 Typical daily temperature variations throughout the test slab corresponding to a positive temperature differential as recorded in July.

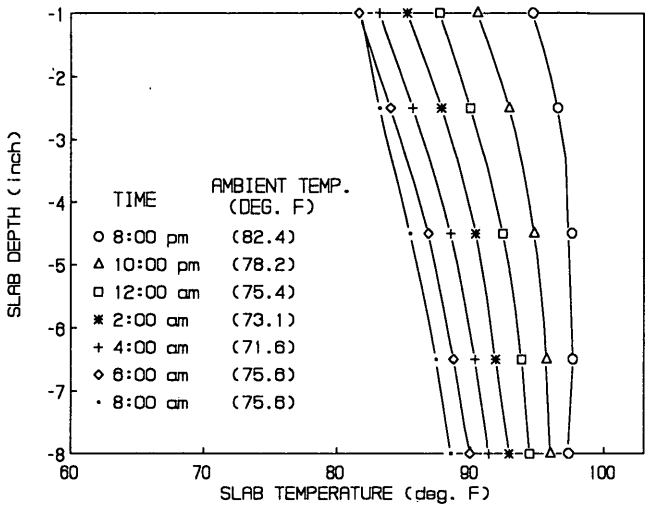

FIGURE 5 Typical daily temperature variations throughout the test slab corresponding to a negative temperature differential as recorded in July.

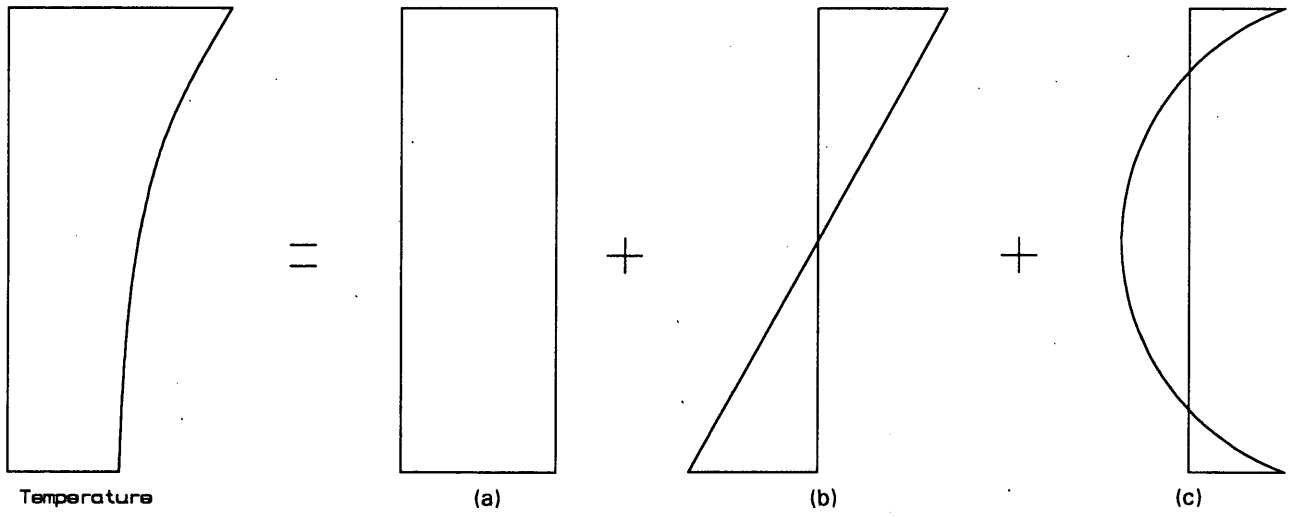

FIGURE 6 Typical temperature variation profile throughout a slab and its three components: (a) component causing axial displacement, (b) component causing bending, and (c) nonlinear temperature component.

an analysis of the temperature data and comparative study of the existing models for predicting actual temperature distributions, it appeared that a quadratic equation could be used to express the temperature as a function of depth. This is shown in Figures 7 and 8. The general form of the equation is

$$t = A + By + Cy^2 \tag{1}$$

where t is the temperature in degrees Fahrenheit and y is the slab depth, with $y = 0$ at the top and $y = d$ at the bottom.

Since a quadratic equation can be defined by three points, the quadratic equation is determined by matching the equation with the measured temperatures at three points. If these three temperature readings were taken at the top (t_t), at the middle (t_m), and at the bottom of the slab (t_b), the coefficients A, B, and C would be defined as follows:

$$A = t_t \tag{2}$$

$$B = (4t_m - 3t_t - t_b)/d \tag{3}$$

$$C = 2(t_t + t_b - 2t_m)/d^2 \tag{4}$$

Table 1 summarizes the representative values of these coefficients A, B, and C as well as the corresponding temperature differentials for a daily cycle at various time periods.

The temperature component causing axial displacement is determined by integrating the temperature across the section and dividing the integral (area under the curve) by the slab thickness as follows:

$$t_{\text{axial}} = \frac{1}{d}\int_0^d (A + By + Cy^2)dy$$

$$= A + B(d/2) + C(d^2/3) \tag{5}$$

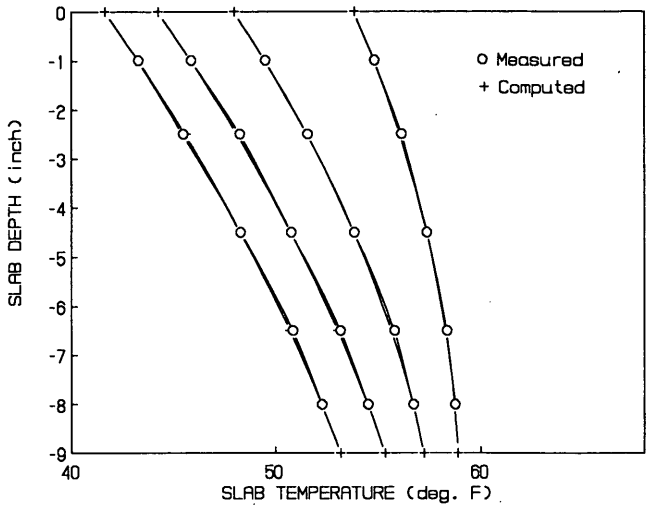

FIGURE 7 Computed versus measured temperature variations throughout the test slab corresponding to a negative temperature differential as recorded in a typical daily cycle in January.

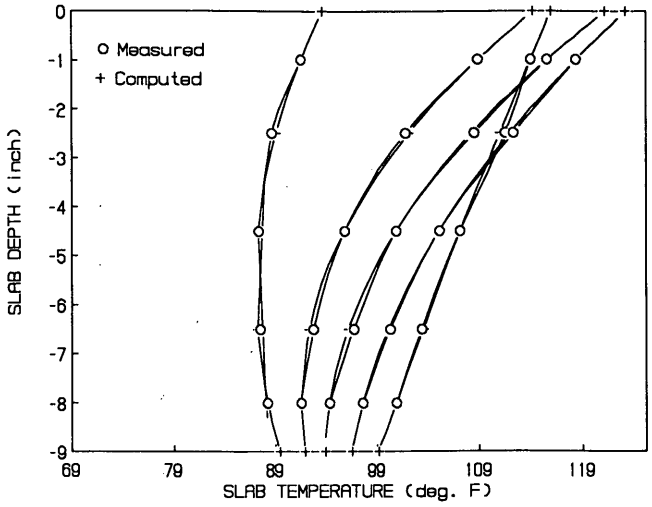

FIGURE 8 Computed versus measured temperature variations throughout the test slab corresponding to a positive temperature differential as recorded in a typical daily cycle in January.

TABLE 1 Representative Values of the Coefficients *A*, *B*, and *C* of Quadratic Equation 1 as Computed for a Daily Cycle at Various Time Periods

Period of the Year	Typical Daily Cycle Time	A	B	C	Temp. Diff. DT
Jan.	11:00 am	53.03836	-1.45816	0.149795	0.99
	01:00 pm	62.11836	-2.58102	0.172653	9.24
	02:00 pm	63.05142	-2.13142	0.12	9.46
	06:00 pm	53.80979	1.010408	-0.05020	- 5.03
	08:00 pm	50.41081	1.408367	-0.05918	- 7.88
	10:00 pm	47.97265	1.578979	-0.06163	- 9.22
	00:00 am	46.37285	1.477142	-0.04	-10.05
	02:00 am	44.24959	1.669387	-0.04897	-11.06
	04:00 am	42.90612	1.734897	-0.05102	-11.48
	06:00 am	41.67204	1.671632	-0.04367	-11.51
June	09:00 am	98.73816	-3.31775	0.239591	10.45
	11:00 am	112.3161	-4.91938	0.263265	22.95
	01:00 pm	122.8802	-5.95183	0.281632	30.75
	03:00 pm	109.18	-0.35714	-0.14285	14.78
	05:00 pm	115.2114	-2.54857	0.057142	18.31
	08:00 pm	96.50530	1.727959	-0.18326	- 0.71
	10:00 pm	91.15979	1.796122	-0.13591	- 5.16
	00:00 am	87.80530	1.662244	-0.09755	- 7.06
	02:00 am	85.18428	1.605714	-0.08	- 7.97
	06:00 am	82.31448	1.246734	-0.04122	- 7.88
Nov.	10:00 pm	59.27816	2.189387	-0.11755	-10.18
	02:00 am	54.90693	2.133265	-0.09020	-11.89
	04:00 am	53.41183	2.090612	-0.08244	-12.14
	07:00 am	51.39204	2.085918	-0.07795	-12.46
	10:00 am	68.82632	-2.87265	0.256326	5.09
	12:00 pm	82.05326	-4.76653	0.323265	16.71
	01:18 pm	87.53387	-4.97346	0.299591	20.49
	04:00 pm	74.87102	0.336530	-0.09755	4.87

The temperature component causing bending of the slab is determined by taking the moment of the area that remains after the axial component is subtracted from the total area under the curve and then finding a linear temperature distribution that would produce the same moment.

The moment is taken with respect to the mid-depth of the slab. Let $y' = (d/2) - y$
Then

$$t_{total} - t_{axial} = By + Cy^2 - B(d/2) - C(d^2/3)$$
$$= -C(d^2/12) - (B + Cd)y' + Cy'^2 \quad (6)$$

The moment, taken with respect to slab mid-depth, will then be as follows:

$$M = \int_{-d/2}^{d/2} (t_{total} - t_{axial})y'dy' = -(B + Cd)d^3/12 \quad (7)$$

For a linear temperature distribution varying from $+T_{curling}$ to $-T_{curling}$, the moment caused by this temperature distribution is

$$M = 2T_{curling}\,(d/4)\,(d/3) = T_{curling}\,(d^2/6) \quad (8)$$

By setting this moment equal to the moment as expressed in Equation 7, $t_{curling}$ at any depth y can be solved to be

$$t_{curling} = (B + Cd)\,[y - (d/2)] \quad (9)$$

Last, the nonlinear temperature component is determined as follows:

$$t_{nonlinear} = t_{total} - t_{axial} - t_{curling}$$
$$= C[y^2 - dy + (d^2/6)] \quad (10)$$

From this expression, it is apparent that if the coefficient C is positive, the extreme fibers of the slab would tend to expand. This condition is reversed if the coefficient C is negative. Furthermore, it can also be seen from Table 1 that this coefficient C, the nonlinear temperature component, is not directly correlated with the temperature differential.

In the case of the assumption of a linear temperature gradient, where the coefficient C is zero, only two temperature components would remain: the temperature component related to axial displacement and the curling temperature component related to slab bending.

Comparison with Other Models

Various models for predicting temperatures in concrete pavements have been developed by researchers such as Thomlinson (*2*), Barber (*11*), Bergstrom (*12*), Thompson et al. (*13*), and Hsieh et al. (*14*). Hsieh presented a three-dimensional computer model that uses the finite-difference scheme of Beam and Warming (*15*). The model is based on the coupled theories of heat-moisture conduction through a semifinite, isotropic, and homogeneous porous medium. The inputs required for this computer program are weather data and the material properties of the concrete and soil.

A comparison made between the computed temperature variations using Hsieh's computer model and the quadratic Equation 1 is shown in Figures 9 and 10. The predicted temperature variations from Hsieh's model match well with those from the quadratic equation unless there is a drastic change in temperature in the top 2 in. of the slab, as can be seen in Figure 9. In that case, if the temperature differential is positive, the quadratic equation gives comparatively higher temperatures in the top half of the slab and lower temperatures in the lower half. This observation is reversed in the case of a negative temperature differential.

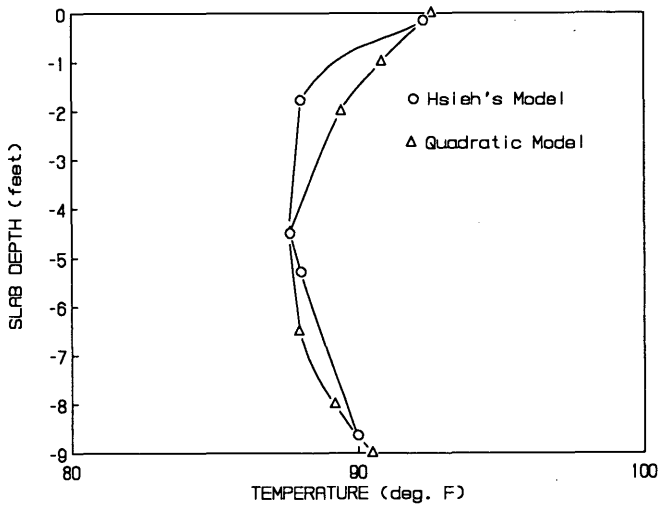

FIGURE 9 Predicted temperature distributions throughout the slab depth using the quadratic equation and Hsieh's model for full-sun simulation at 8:00 a.m.

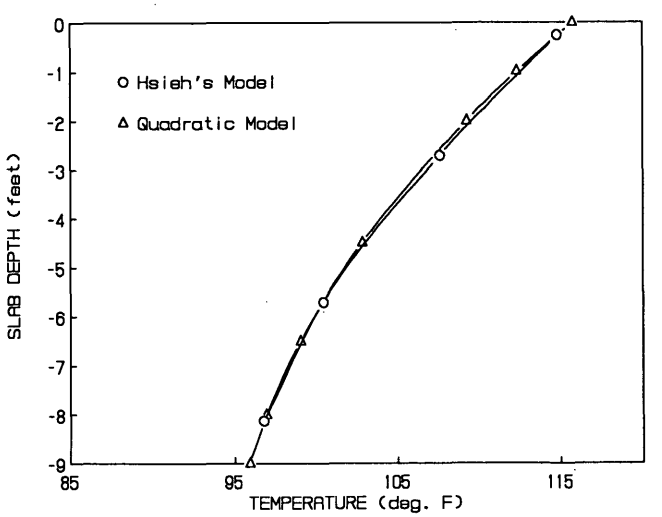

FIGURE 10 Predicted temperature distributions throughout the slab depth using the quadratic equation and Hsieh's model for full-sun simulation at 2:00 p.m.

THERMAL STRESS ANALYSIS

Bradbury's Equations for Computing Thermal Stresses

Several methods of determining thermal warping stresses were proposed as early as 1926 when Westergaard presented his well-known mathematical analysis on the subject. Using Westergaard's concepts, Bradbury (*3*) developed equations for the computation of the temperature-induced warping stresses at different positions of concrete pavement slabs.

The general Bradbury expressions for computing warping stresses due to temperature differential are as follows:

Edge stress:

$$\sigma = C_x E \alpha \Delta T/2 \tag{11}$$

Interior stresses:

$$\sigma_x = (E\alpha\Delta T/2)\,[(C_x + \mu C_y)/(1 - \mu^2)] \tag{12}$$

$$\sigma_y = (E\alpha\Delta T/2)\,[(C_y + \mu C_x)/(1 - \mu^2)] \tag{13}$$

where

E = modulus of elasticity of concrete,
α = thermal coefficient of expansion of concrete,
ΔT = temperature difference between top and bottom of the slab, and
C_x, C_y = warping stress coefficients.

The coefficients C_x and C_y are functions of the free length and width depending on the direction in which the curling stress is required. The values of these warping stress coefficients are given by Bradbury's nomograph (*3*).

FEACONS IV Computer Program

The computer program FEACONS IV (Finite Element Analysis of CONcrete Slabs, version IV) was developed at the University of Florida for analysis of the response of jointed concrete pavements to load and temperature variations (*8,9*). In this program, a jointed concrete pavement is modeled as a three-slab system, whereas a slab is considered as an assemblage of rectangular elements with three degrees of freedom per node as developed by Melosh (*16*) and Zienkiewicz and Cheung (*17*). The subgrade is assumed as a Winkler foundation modeled by a series of vertical springs at the nodes. Load transfers across the joints are modeled by linear and rotational springs connecting the slabs at the nodes of the elements along the joints. The thermal gradient across the depth of the slab is assumed to be uniform, and a temperature differential between the top and bottom surfaces of the slab is used as an input to the program.

Results from FEACONS Versus Bradbury's Equations

The thermal stresses caused by the temperature variation recorded from the test slabs were computed by using FEACONS and also by using Bradbury's equation for comparison purposes. For a slab 20 ft long, 12 ft wide, and 9 in. thick with an assumed coefficient of thermal expansion of 6×10^{-6}/°F, a modulus of elasticity of 4,500 ksi, a Poisson's ratio of 0.2 for the concrete, and a subgrade modulus of 300 pci, the coefficients C_x and C_y are determined to be equal to 1.064 and 0.609, respectively. Then Equations 11 through 13 become the following:

Edge stress:

$$\sigma = 14.364\Delta T \tag{14}$$

Interior stresses:

$$\sigma_x = 16.675\Delta T \tag{15}$$

$$\sigma_y = 11.556\Delta T \tag{16}$$

From the foregoing equations, it can be observed that the maximum computed warping stresses according to Bradbury's formulas occur at the interior of the slab and run in the longitudinal direction. Table 2 gives the typical values of computed thermal stresses according to Bradbury's equations along with the corresponding computed stresses from FEACONS. The computed stresses from Bradbury's equations are slightly higher than those from FEACONS for the daytime conditions, whereas they are very close to one another for the nighttime conditions. It is believed that the differences are due to the fact that FEACONS can take into account the possible loss of contact between the slab and the subgrade, although Bradbury's method does not.

Stress Analysis Considering Nonlinear Temperature Variation

Since the cross section of the slab is assumed to remain plane, the nonlinear temperature component, which does not cause any axial or bending deformation, will induce stresses in the slab as if the slab were totally restrained from deformation. The thermal stresses induced by the nonlinear temperature component as expressed in Equation 10 can be determined by multiplying the negative of the nonlinear temperature component by the coefficient of thermal expansion and the modulus of elasticity of concrete as follows:

$$\sigma = -E_c \alpha t_{\text{nonlinear}} = -E_c \alpha C[y^2 - dy + (d^2/6)] \tag{17}$$

This stress is a function of the coefficient C, the coefficient of thermal expansion, and the concrete modulus of elasticity. It can be seen that the variation of the coefficient of thermal expansion will affect the thermal stresses greatly.

Since the nonlinear temperature component does not affect the bending of the concrete slab, its effects on the total stresses in the concrete slab would be independent of the effects of the other factors. Thus, the total stress can be obtained by adding algebraically the bending stress due to a linear temperature gradient as computed by FEACONS and the corresponding stress due to the nonlinear component of the temperature distribution.

TABLE 2 Representative Values of Maximum Warping Stresses as Computed for a Daily Cycle Using Bradbury's Equations and FEACONS IV

Period of the Year	Typical Daily Cycle Time	Temperature Differential	Stresses (psi)	
			Bradbury	FEACONS IV
January	11:00 am	0.99	17	16
	1:00 pm	9.24	154	147
	2:00 pm	9.46	158	151
	6:00 pm	- 5.03	84	84
	8:00 pm	- 7.88	131	128
	10:00 pm	- 9.22	154	149
	00:00 am	-10.05	168	161
	2:00 am	-11.06	184	176
	4:00 am	-11.48	191	181
	6:00 am	-11.51	192	181
June	9:00 am	10.45	174	164
	11:00 am	22.95	383	310
	1:00 pm	30.75	513	418
	3:00 pm	14.78	246	228
	5:00 pm	18.31	305	263
	8:00 pm	- 0.71	12	12
	10:00 pm	- 5.16	86	86
	00:00 am	- 7.06	118	116
	2:00 am	- 7.97	133	129
	6:00 am	- 7.88	131	128
November	10:00 pm	-10.18	170	163
	2:00 am	-11.89	198	187
	4:00 am	-12.14	202	191
	7:00 am	-12.46	208	194
	10:00 am	5.09	85	84
	12:00 pm	16.71	279	249
	1:18 pm	20.49	342	295
	4:00 pm	4.87	81	80

The temperature data recorded on the test slabs were used to determine the thermal stresses in the concrete slabs by taking the effects of the nonlinear temperature component into account. The concrete was assumed to have a constant coefficient of thermal expansion of 6×10^{-6}/°F and a modulus of elasticity of 4,500 ksi. The stress due to the nonlinear temperature component in a 9-in. thick slab is given by the following expression:

$$\sigma = -27C(y^2 - 9y + 13.5) \quad (18)$$

From this expression, it can be seen that if coefficient C is positive, the extreme fibers of the slab would tend to expand and cause internal compressive stresses at these positions, and tensile stresses would result at slab mid-length. This condition is reversed if coefficient C is negative. This observation is valid for any slab thickness.

Representative values of stresses due to the nonlinear temperature component, bending stresses due to the linear temperature component, and the total stresses as determined in a daily cycle for various time periods are shown in Table 3. As a convention, the tensile stresses are computed as positive values and the compressive stresses are negative. It can be observed from Table 2 that the maximum compressive stresses due to the nonlinear temperature component generally occurred between noon and 1:00 p.m.

Since concrete is much weaker in tension than in compression, the tensile stresses are much more critical than the compressive stresses and thus are of more concern. From Table 3 it can be observed that a nonlinear temperature distribution tends to increase the total maximum tensile stress in the slab at night when the temperature differentials are negative, whereas it tends to reduce the maximum tensile stress during the day when positive temperature differentials occur. A maximum stress of 240 psi due to the consideration of a nonlinear temperature distribution was computed for the condition at 6:00 a.m. during April, whereas the computed stress without the consideration of the nonlinear temperature effects was 216 psi. This amounts to an increase of approximately 11 percent in tensile stress. Conversely, a maximum computed bending stress of 418 psi was obtained for June at 1:00 p.m., whereas the corresponding computed total stress with the

TABLE 3 Representative Computed Total Stresses at the Extreme Slab Fibers Caused by Nonlinear Temperature Distribution in a Daily Cycle

Period of the Year	Typical Daily Cycle Time	STRESSES (psi)				
		Non-Linear	Bending		Total	
		Top & Bottom	Top	Bottom	Top	Bottom
January	11:00 am	-55	-16	16	-71	-39
	12:00 pm	-67	-102	102	-169	35
	01:00 pm	-63	-147	147	-210	84
	02:00 pm	-44	-151	151	-195	107
	06:00 pm	18	84	-84	102	-66
	10:00 pm	22	149	-149	171	-127
	02:00 am	18	176	-176	194	-158
	06:00 am	16	181	-181	197	-165
	08:00 am	6	56	-56	62	-51
April	10:00 am	-106	-154	154	-260	48
	12:00 pm	-116	-309	309	-425	193
	01:00 pm	-97	-352	352	-448	255
	02:00 pm	-79	-359	359	-438	280
	04:00 pm	0	-250	250	-250	250
	08:00 pm	58	112	-112	170	-54
	00:00 am	31	174	-174	205	-143
	04:00 am	27	200	-200	227	-173
	06:00 am	24	216	-216	240	-192
June	11:00 am	-96	-310	310	-406	214
	01:00 pm	-103	-418	418	-521	315
	03:00 pm	52	-228	228	-176	280
	05:00 pm	-21	-263	263	-284	242
	08:00 pm	67	12	-12	79	55
	00:00 am	36	116	-116	152	-80
	06:00 am	15	128	-128	143	-113
July	08:00 pm	48	56	-56	104	-8
	00:00 am	40	139	-139	179	-99
	04:00 am	37	167	-167	204	-130
	06:00 am	31	170	-170	201	-139
	10:00 am	-76	-70	70	-146	-6
	12:00 pm	-116	-250	250	-366	134
	02:30 pm	-119	-371	371	-490	252
	04:00 pm	-85	-362	362	-447	277
	06:00 pm	-6	-249	249	-255	243
August	09:00 am	-19	50	-50	30	-69
	12:00 pm	-107	-258	258	-365	151
	03:16 pm	-116	-378	378	-494	262
	07:00 pm	68	-51	51	17	119
	08:00 pm	60	9	-9	69	51
	00:00 am	54	129	-129	183	-75
	04:00 am	36	145	-145	181	-109
	06:00 am	31	147	-147	178	-116

(*continued on next page*)

TABLE 3 (*continued*)

Period of the Year	Typical Daily Cycle Time	STRESSES (psi)				
		Non-Linear	Bending		Total	
		Top & Bottom	Top	Bottom	Top	Bottom
November	08:00 pm	48	140	-140	188	-92
	12:00 am	40	181	-181	221	-141
	04:00 am	30	191	-191	221	-161
	07:00 am	28	194	-194	222	-166
	10:00 am	-93	-84	84	-177	-9
	12:00 pm	-118	-249	249	-367	131
	01:18 pm	-109	-295	295	-404	186
	02:00 pm	83	-287	287	-370	204
	04:00 pm	36	-80	80	-44	116

consideration of the nonlinear temperature effects was 315 psi. This represents a 25 percent reduction in computed tensile stress. A maximum percent increase in computed tensile stress of 661 percent was obtained in August when the consideration of the effects of nonlinear temperature distribution increased the slab tensile stress from 9 to 69 psi.

SUMMARY OF FINDINGS

The main findings in this study are summarized as follows:

1. The temperature data obtained from the concrete test road in this study indicated that the temperature distribution within the concrete slabs is mostly nonlinear.
2. The temperature distribution throughout the depth of a concrete pavement slab can be represented fairly well by a quadratic equation.
3. When the temperature distribution is assumed to be linear, the maximum computed tensile stresses in the slab tend to be higher for the daytime condition and lower for the nighttime condition as compared with the stresses computed with the consideration of the effects of the nonlinear temperature distribution.

REFERENCES

1. L. W. Teller and E. C. Sutherland. The Structural Design of Concrete Pavements. *Public Roads*, Vol. 23, No. 8, June 1943, pp. 167–211.
2. J. Thomlinson. Temperature Variations and Consequent Stresses Produced by Daily and Seasonal Temperature Cycles in Concrete Slabs. *Concrete and Construction Engineering,* 1940.
3. R. D. Bradbury. *Reinforced Concrete Pavements.* Wire Reinforcement Institute, Washington, D.C., 1938.
4. F. C. Lang. Temperature and Moisture Variations in Concrete Pavements. *HRB Proc.*, Vol. 21, 1941, pp. 260–271.
5. Y. T. Chou. *Structural Analysis Computer Programs for Rigid Multicomponent Pavement Structures with Discontinuities—WESLIQID and WESLAYER.* Technical Reports 1, 2, and 3. U.S. Army Engineering Waterways Experiment Station, Vicksburg, Miss., May 1981.
6. S. P. Tayabji and B. E. Colley. *Analysis of Jointed Concrete Pavements.* FHWA, U.S. Department of Transportation, 1981.
7. A. M. Tabatabaie and E. J. Barenberg. Finite Element Analysis of Jointed or Cracked Concrete Pavements. In *Transportation Research Record 671*, TRB, National Research Council, Washington, D.C., 1978, pp. 11–19.
8. M. Tia, J. M. Armaghani, C. L. Wu, S. Lei, and K. L. Toye. FEACONS III Computer Program for an Analysis of Jointed Concrete Pavements. In *Transportation Research Record 1136*, TRB, National Research Council, Washington, D.C., 1987, pp. 12–22.
9. M. Tia, C. L. Wu, B. E. Ruth, D. Bloomquist, and B. Choubane. *Field Evaluation of Rigid Pavements for the Development of a Rigid Pavement Design System*—Phase III. Final Report, Project 245-D54. Department of Civil Engineering, University of Florida, Gainesville, July 1988.
10. J. M. Armaghani. *Comprehensive Analysis of Concrete Pavement Response to Temperature and Load Effects.* Ph.D dissertation. Department of Civil Engineering, University of Florida, Gainesville, 1987.
11. E. S. Barber. Calculation of Maximum Pavement Temperature from Weather Reports. In *Highway Research Board Bulletin 168,* HRB, National Research Council, Washington, D.C., 1975.
12. K. C. Bergstrom. Temperature Stresses in Concrete Pavements. Proc., Swedish Cement and Concrete Institute, Stockholm, 1950.
13. M. R. Thompson, B. Dempsey, H. Hill, and J. Vogel. Characterizing Temperature Effects for Pavement Analysis and Design. Presented at 66th Annual Meeting of the Transportation Research Board, Washington, D.C., 1987.
14. C. K. Hsieh, Q. Chaobin, and E. E. Ryder. *Development of Computer Modeling for Prediction of Temperature Distribution Inside Concrete Pavements.* Florida Department of Transportation, Department of Mechanical Engineering, University of Florida, Gainesville, Aug. 1989.
15. R. M. Beam and R. F. Warming. An Implicit Factored Scheme for the Compressible Navier-Stokes Equations. *AIAA Journal*, Vol. 16, No. 4, 1978, pp. 393–402.
16. R. M. Melosh. Basis of Derivation of Matrices for the Direct Stiffness Method. *AIAA Journal*, Vol. 1, No. 7, July 1963, pp. 1631–1637.
17. O. C. Zienkiewicz and Y. K. Cheung. The Finite Element Method for Analysis of Elastic Isotropic and Orthotropic Slabs. *Proc. Institute of Civil Engineers,* Vol. 28, 1964, pp. 471–488.

Structural Evaluation of Base Layers in Concrete Pavement Systems

ANASTASIOS M. IOANNIDES, LEV KHAZANOVICH, AND JENNIFER L. BECQUE

A theoretically sound and practical approach is described for determining maximum responses in concrete pavement systems that incorporate a base layer. Equations are presented that may be used with either an elastic solid or a dense liquid foundation under any of the three fundamental loading conditions. These formulas are extensions of available closed-form solutions and account for the compressions in the two placed layers that are ignored by plate theory. The proposed methodology may be easily implemented in a personal computer spreadsheet or on a programmable calculator. Research activities for its full verification and refinement are continuing at this time. It is anticipated that such theoretically based investigations will encourage the elimination of theoretically questionable empirical concepts, such as that of deriving a composite "top-of-the-base" subgrade modulus.

Conventional analysis and mechanistic-based design procedures for portland cement concrete (PCC) pavement systems use closed-form analytical solutions that have been developed over the last 75 years on the basis of quite restrictive assumptions. The idealizations that led to the formulation of the well-known Westergaard equations (*1*) for a slab on a dense liquid foundation and of the less often quoted expressions by Losberg (*2*) and Ioannides (*3*) for the corresponding slab on an elastic solid subgrade treat a pavement system that

1. Considers a slab of infinite dimensions (no slab size effects),
2. Consists of only one slab panel (no load transfer),
3. Includes only one placed layer (no base or subbase),
4. Employs a semiinfinite foundation (no rigid bottom),
5. Is acted upon by a single tire print (no multiple wheel loads), and
6. Experiences no curling or warping (i.e., flat slab, no temperature or moisture differential condition).

Each of these restrictions is violated in actual concrete pavement construction, which dictates that analytical considerations be adjusted or "calibrated" before a reasonable engineering design can be made. In particular, the treatment of the concrete pavement as incorporating only one placed layer, namely, the PCC slab, has been a pervasive obstacle in the effort to arrive at a mechanistic design that would permit comparisons with alternative designs involving asphalt concrete. The inability of conventional plate theory solutions to accommodate multiple placed layers is often cited as one of the primary reasons calling for its abandonment in favor of a unified analysis and design procedure based on layered elastic theory (*4*).

Department of Civil Engineering, University of Illinois at Urbana-Champaign, 205 N. Mathews Avenue #2230C, Urbana, Ill. 61801.

Use of layered elastic theory (*5*) in addressing the single-placed-layer (SPL) limitation of conventional plate theory solutions is not new. In fact, it is the oldest of at least three main approaches to the problem posed by bases underneath concrete pavement slabs. Even before the development of computer codes allowing the analysis of multilayered axisymmetric pavement systems, layered elastic theory was suggested by Odemark (*6*)—in the form of his celebrated method of equivalent thicknesses—as a theoretically sound methodology for extending (not replacing) plate theory applications. The reason for not calling for the outright elimination of plate theory as an analytical tool for concrete pavement systems was a recognition by early investigators of the reciprocal inability of layered elastic theory to consider the all-important phenomena pertaining to the edges and corners of concrete slabs.

With the advent of sophisticated finite-element codes, a second approach to the SPL problem emerged exemplified in the treatment of a concrete pavement system as a two-layered composite plate resting on an elastic foundation. This approach was implemented in computer programs such as ILLI-SLAB (*7*). Although treating both placed layers (slab and base) as plates does address the noted SPL shortcoming—particularly in the case of cement-treated (stiff) bases—predictions on the basis of plate theory are often found to incorporate a significant error. This error arises from the neglected compression experienced by the two layers (especially when softer, granular bases are employed).

The third and most predominant means for accounting for the presence of a base, however, has been by increasing the value of the subgrade modulus, k. Thus, in contrast to the finite-element formulation that considers the base as a structural element reinforcing the upper placed layer, namely, the PCC slab, the more conventional approach has been to regard the base as contributing exclusively to the stiffness of the subgrade. It may be argued that the philosophical basis for this approach is to be found in the work by Odemark (*6*), who suggested increasing the subgrade modulus of elasticity, E_s, to account for the contribution of the base. It appears, however, that the popularity of this approach is due more to the practical expediency and ease of solution it offers than to its theoretical merits. A literature survey conducted at the outset of this investigation identified at least 12 different ways of "bumping the k-value," or defining a composite or "top-of-the-base" subgrade modulus. According to a review of current methods for determining the composite modulus of subgrade reaction conducted by Uzan and Witczak (*8*), "the equivalent k_{comp}-values for granular bases [obtained by dif-

ferent methods] are essentially the same," but for "stabilized materials. . . the k-values can vary within a factor of two."

Of the three approaches to dealing with the SPL assumption outlined above, the process of increasing the value of the subgrade modulus depending on the type and thickness of the base is the least attractive from a theoretical viewpoint. Its origins may be traced to tests conducted in the 1950s by the Portland Cement Association (PCA) and by the Corps of Engineers (*9*). At that time, the "bump the k-value" approach appeared as a minor extrapolation of Methods 2 and 3 described by Teller and Sutherland (*10*) for the determination of the subgrade modulus. It should be remembered, however, that both of these methods (namely, the volumetric approach and the backcalculation approach) aimed at defining a property of the natural subgrade, just as did the plate load test (Teller and Sutherland's Method 1), rather than the property of an "equivalent" supporting medium. It is precisely the development of computerized backcalculation procedures based on matching theoretical and observed deflection basins (by determining the area or volume of the basin) that has revealed the extent of errors that may be committed through the use of top-of-the-base k-values. Such composite values are quite often much higher than those reported in earlier literature (*11*), so much so that the definition of the medium they purport to describe as a dense liquid is brought into question.

This paper offers a theoretically sound yet practical solution to the problem posed by the SPL assumption. Simple equations are presented that may easily be implemented on a personal computer or hand-held calculator and that may be used to calculate with sufficient accuracy maximum responses in concrete pavement systems incorporating a base layer. The formulas presented have been obtained through application of dimensional analysis concepts in interpreting a data base of numerical results from two computer codes, one based on plate theory (ILLI-SLAB) and one using layered elastic analysis [BISAR (*12*)]. It is hoped that such solutions, which are essentially extensions of well-known analytical equations, will eliminate the need to use empirical and theoretically questionable concepts, such as that of the composite top-of-the-base subgrade modulus, thereby preventing any associated errors and miscalculations in the future.

SCOPE OF INVESTIGATION

The proposed analysis procedure for three-layer concrete pavements begins by considering the two placed layers as a composite plate and postulating that there exists an imaginary, homogeneous "effective" plate resting on the same elastic foundation that deforms in the same manner as the real two-layer plate. The purpose of the analysis presented below is

1. To verify the existence of the "effective" plate, that is, ascertain that it is possible to define its properties in terms of the corresponding properties of the two layers in the original composite plate;
2. To obtain elastic solutions for the response of the "effective" plate using available analytical equations;
3. To relate the "effective" plate responses determined in this manner to the corresponding unknown composite plate responses; and
4. To extend the applicability of the formulas developed in Item 3 to the case of a three-layer concrete pavement system of any arbitrary stiffnesses, subject only to the assumption that one of the two placed layers is much stiffer than the foundation.

CLOSED-FORM SOLUTION FOR THREE-LAYER SYSTEM WITH UNBONDED LAYERS

Plate Theory Solution

According to medium-thick plate theory (*13*), when a flat plate of uniform cross section is subjected to elastic bending, the following moment-curvature relationships apply, expressed in polar coordinates (r,ϕ):

$$M_r = -D\left[\frac{\partial^2 w}{\partial r^2} + \mu\left(\frac{1}{r}\frac{\partial w}{\partial r} + \frac{1}{r^2}\frac{\partial^2 w}{\partial \phi^2}\right)\right]$$

$$M_\phi = -D\left(\frac{1}{r}\frac{\partial w}{\partial r} + \frac{1}{r^2}\frac{\partial^2 w}{\partial \phi^2} + \mu\frac{\partial^2 w}{\partial r^2}\right)$$

$$M_{r\phi} = (1-\mu)D\left(\frac{1}{r}\frac{\partial^2 w}{\partial r\partial \phi} - \frac{1}{r^2}\frac{\partial w}{\partial \phi}\right) \quad (1)$$

in which $w(r,\phi)$ denotes the vertical displacement from the originally horizontal neutral axis of the plate. The flexural stiffness of the plate, D, is defined by

$$D = \frac{Eh^3}{12(1-\mu^2)} \quad (2)$$

where E, μ, and h are the Young's modulus, Poisson's ratio, and thickness of the plate, respectively.

Equations 1 may be rewritten in a compact form as

$$\{M\} = -D\{L(\mu)\}\,[w(r,\phi)] \quad (3)$$

in which $\{L(\mu)\}$ is a vector operator depending on the value of μ.

Consider now a composite plate consisting of two dissimilar plate layers resting on an elastic foundation, for example, a dense liquid or an elastic solid. Assuming that during bending the two plate layers do not experience any separation, their respective deflected shapes will be identical; that is,

$$w_1(r,\phi) = w_2(r,\phi) = w_e(r,\phi) \quad (4)$$

Subscripts 1 and 2 denote here plate layers 1 and 2, respectively, in the original composite two-layer plate, and subscript e denotes an imaginary, homogeneous "effective" plate resting on the same elastic foundation. The "effective" plate is required to deform in the same manner as the real composite plate.

At this point, the assumption that the two plate layers in the composite plate act independently, that is, that their interface is unbonded and free of shear stress, is introduced.

Application of Equations 3 and 4 to each of these plate layers yields the following moment expressions:

$$\{M_1\} = -D_1\{L(\mu_1)\}[w_e(r, \phi)] \quad (5)$$

$$\{M_2\} = -D_2\{L(\mu_2)\}[w_e(r, \phi)] \quad (6)$$

The corresponding equation for the moment acting on the "effective" plate is

$$\{M_e\} = -D_e\{L(\mu_e)\}[w_e(r, \phi)] \quad (7)$$

The assumption is also introduced that

$$\mu_1 = \mu_2 = \mu_e \quad (8)$$

and it is noted that the composite as well as the "effective" plates are subjected to the same applied loads, experience the same deflections, and therefore are acted upon by the same foundation reactions. Thus, it is evident that

$$\{M_T\} = \{M_1\} + \{M_2\} = \{M_e\} \quad (9)$$

where $\{M_T\}$ denotes the total moment acting on the composite plate. Equation 9 yields upon substitution from Equations 5 and 6:

$$\{M_e\} = -(D_1 + D_2\{L(\mu_e)\}[w_e(r, \phi)] \quad (10)$$

Comparison of Equation 10 with Equation 7 results in

$$D_e = D_1 + D_2 \quad (11)$$

Equation 11 verifies that the "effective" plate postulated by Equation 4 exists and that its structural parameters can be defined in terms of the corresponding parameters of layers 1 and 2 in the original composite plate. Furthermore, it follows from Equations 7 and 11 that

$$\{M_e\} = \left(1 + \frac{D_2}{D_1}\right)\{M_1\} \quad (12)$$

Thus, the generalized stresses, $\{\sigma_e\}$, in the "effective" plate are written in terms of the corresponding stresses, $\{\sigma_1\}$, in plate layer 1 as

$$\{\sigma_e\} = \frac{6}{h_e^2}\left(1 + \frac{D_2}{D_1}\right)\{M_1\} \quad (13)$$

or

$$\{\sigma_e\} = \frac{h_1^2}{h_e^2}\left(1 + \frac{D_2}{D_1}\right)\{\sigma_1\} \quad (14)$$

$$= \frac{h_1^2}{h_e^2}\left(\frac{E_1h_1^3 + E_2h_2^3}{E_1h_1^3}\right)\{\sigma_1\} \quad (15)$$

It follows from Equations 8 and 11 that

$$E_eh_e^3 = E_1h_1^3 + E_2h_2^3 \quad (16)$$

Substituting Equation 16 into Equation 15 leads to

$$\{\sigma_e\} = \frac{h_1^2}{h_e^2}\frac{E_eh_e^3}{E_1h_1^3}\{\sigma_1\} \quad (17)$$

whence

$$\{\sigma_e\} = \frac{h_e}{h_1}\frac{E_e}{E_1}\{\sigma_1\} \quad (18)$$

Setting $E_e = E_1$, this yields

$$\{\sigma_e\} = \frac{h_e}{h_1}\{\sigma_1\} \quad (19)$$

$$\{\sigma_1\} = \frac{h_1}{h_e}\{\sigma_e\} \quad (20)$$

Furthermore, the thickness of the "effective" plate, h_e, is obtained from Equation 16 as

$$h_e = \left[\left(h_1^3 + \frac{E_2}{E_1}h_2^3\right)\right]^{1/3} \quad (21)$$

Note that Equation 20 implies, in particular, that the maximum bending stress, σ_1, developing at the bottom of plate layer 1 in the composite plate may be obtained by multiplying the corresponding maximum bending stress, σ_e, arising at the bottom of the imaginary, homogeneous "effective" plate (of modulus $E_e = E_1$) by the thickness ratio (h_1/h_e), with h_e defined by Equation 21. For example, considering the case of an elastic solid foundation, Equation 20 implies that

$$\sigma_1 = \frac{h_1}{h_e}\sigma_e = \frac{h_1}{h_e}\sigma(h_e, E_1, E_s) \quad (22)$$

The corresponding expression for a dense liquid foundation is

$$\sigma_1 = \frac{h_1}{h_e}\sigma_e = \frac{h_1}{h_e}\sigma(h_e, E_1, k) \quad (22a)$$

The notation $\sigma(h_i, E_j, F)$ in Equations 22 and 22a denotes the maximum bending stress predicted by plate theory at the bottom of a plate of thickness h_i and modulus E_j resting on a subgrade characterized by generalized stiffness parameter F, that is, Young's modulus, E_s, for an elastic solid foundation or modulus of subgrade reaction, k, for a dense liquid foundation. Furthermore, Equation 20 implies that the thickness ratio (h_1/h_e) is the constant that relates the bending stress at any point (r, ϕ) in layer 1 of the composite plate to the bending stress arising at the corresponding point in the "effective plate." Having thus obtained σ_1, the maximum bending stress at the bottom of plate layer 2 may also be calculated using plate theory as follows, subject to the assumption of Equation 8:

$$\sigma_2 = \sigma_1\frac{E_2}{E_1}\frac{h_2}{h_1} \quad (23)$$

The value of $\sigma_e = \sigma(h_e, E_1, F)$ in Equations 22 and 22a may be obtained using available closed-form analytical solutions pertaining to the particular foundation type and loading condition of interest. An equation for the maximum bending stress arising at the bottom of a homogeneous infinite plate on an elastic solid foundation loaded by an interior load has been presented by Losberg (*2*). More recently, Ioannides (*3*) considered the edge and corner loading conditions for the same plate-foundation system and provided simple formulas for the calculation of the maximum bending stress pertaining to these loading conditions as well. The corresponding equations for a plate on dense liquid foundation were given by Westergaard (*1*) for all three fundamental loading conditions.

With respect to deflections, it is noted that Equation 4 implies that the maximum deflection in the two-layer composite plate is equal to the maximum deflection experienced by the "effective" plate. The latter may be calculated using the pertinent formulas given in the publications cited above. Similarly, the maximum subgrade stress under the composite plate is equal to the corresponding stress under the "effective" plate.

Elimination of Plate Theory Restrictions

To extend the applicability of the proposed approach to layers of any arbitrary stiffness—subject only to the assumption that one of the two layers is much stiffer than the foundation—responses calculated must be adjusted for the compression that occurs within the two layers of the original composite plate and that is ignored by plate theory. To illustrate how such a corrective may be applied, the case of the maximum bending stress, σ_{1L}, occurring at the bottom of layer 1 in a three-layer system of any arbitrary stiffnesses will be considered. This response may be written in the following form:

$$\sigma_{1L} = \sigma_1 + [\vartheta\ \Delta\sigma] \tag{24}$$

where σ_1 is the corresponding stress according to plate theory given by Equation 22 and $[\vartheta\ \Delta\sigma]$ is a "correction increment." The contribution to this increment of the compression of the second layer is usually of overriding importance. In a typical pavement system, the second layer has a lower modulus than the first layer and may therefore be expected to diverge from plate behavior (no compression) more significantly than the first layer. For this reason, an expression for $\Delta\sigma$ accounting only for the compression in the second layer is derived first (i.e., $\vartheta = 1$). Considering the case of an elastic solid foundation, the following assumption is introduced at this point:

$$\frac{\partial(\Delta\sigma)}{\partial(E_s)} = 0 \tag{25}$$

That is, it is assumed that $\Delta\sigma$ (as well as the compression of the second layer) is largely insensitive to changes in the subgrade modulus, E_s. This assumption is a reasonable approximation for material moduli in the range of those typically encountered in concrete pavements, for which E_1 is much higher than E_s. If the assumption of Equation 25 is accepted, the case may be considered in which $E_s = E_2$, which reduces the three-layer system to a two-layer system. Then, for this case,

$$\Delta\sigma(h_1, h_2, E_1, E_2, E_s) = \Delta\sigma(h_1, h_2, E_1, E_2, E_2) \tag{26}$$

in which the parameters listed in parentheses define the properties of the layered system considered in determining $\Delta\sigma$. By referring to Equations 24 and 22, the following expression may be written:

$$\Delta\sigma(h_1, h_2, E_1, E_2, E_2) = \sigma_{1L}(h_1, h_2, E_1, E_2, E_2) - \frac{h_1}{h_e}\sigma(h_e, E_1, E_2) \tag{27}$$

If $E_1 >> E_2$, σ_{1L} may be evaluated according to plate theory, or

$$\sigma_{1L}(h_1, h_2, E_1, E_2, E_2) = \sigma(h_1, E_1, E_2) \tag{28}$$

It is noted that in writing this equation, the effect of an unbonded surface at depth h_2 into the elastic half-space of modulus E_2 is assumed to be negligible. Thus,

$$\Delta\sigma(h_1, h_2, E_1, E_2, E_2) = \sigma(h_1, E_1, E_2) - \frac{h_1}{h_e}\sigma(h_e, E_1, E_2) \tag{29}$$

That is, the correction increment $\Delta\sigma$ may be calculated as the difference between two stresses, each of which is evaluated using available closed-form solutions, such as those by Losberg (*2*) or Ioannides (*3*), for the parameters indicated by Equation 29.

The value of $\Delta\sigma$ obtained as explained above accounts only for the compression of the second layer; that is, it applies when $E_2 << E_1$. This would be the case, for example, of a PCC slab placed on a soft base. As E_2 tends to E_1, Equation 28 becomes increasingly inaccurate. Noting that for such pavements plate theory would apply without the need for corrections (since in this case both E_1 and E_2 are much higher than E_s), the correction increment should tend to zero. In addition, when $E_2 > E_1$, the correction increment must be negative, reflecting the effect of the compression in the first layer. This corresponds to the case, for example, of an asphalt concrete overlay on a PCC slab. For these reasons, therefore, the value of $\Delta\sigma$ obtained above is multiplied by a factor ϑ. Considering the interior loading condition, the following formula was developed for ϑ on the basis of comparisons of the proposed closed-form solution with the results of several three-layer runs of the BISAR computer program:

$$\vartheta = 1 - \exp\left[\frac{1}{3}\left(1 - \frac{E_1}{E_2}\right)\right] \tag{30}$$

Thus, substituting σ_1 from Equation 22 and $\Delta\sigma$ from Equation 29 into Equation 24, the general solution for the maximum bending stress, σ_{1L}, arising at the bottom of the upper layer

in an arbitrary three-layer system may be written as

$$\sigma_{1L} = \frac{h_1}{h_e}\sigma(h_e, E_1, E_s) + \vartheta\left[\sigma(h_1, E_1, E_2) - \frac{h_1}{h_e}\sigma(h_e, E_1, E_2)\right] \quad (31)$$

with h_e as defined by Equation 21 and ϑ as given by Equation 30. Each of the three bending stresses $\sigma(h_i, E_j, E_s)$ in Equation 31 may be calculated using Losberg's formula for the interior load-elastic foundation case, as follows:

$$\sigma = \frac{-6P(1+\mu)}{h_i^2} \times \left[-0.0490 + 0.1833\log_{10}\left(\frac{a}{l_e}\right) - 0.0120\left(\frac{a}{l_e}\right)^2\right] \quad (32)$$

where

$$l_e = \left[\frac{E_j h_i^3(1-\mu_s^2)}{6E_s(1-\mu_j^2)}\right]^{1/3} \quad (33)$$

μ_j, μ_s = Poisson's ratios for the plate and foundation, respectively,
P = total applied load, and
a = radius of applied load.

The proposed procedure for calculating σ_{1L} is well suited for incorporation into a personal computer spreadsheet and may be used to assess the effect on the maximum bending stress of the introduction of a base under a PCC slab.

GRAPHICAL SOLUTION FOR THREE-LAYER SYSTEM WITH UNBONDED LAYERS

Plate Theory Solution

An alternative graphical solution was also developed in this study. Its derivation proceeds from Equation 22, which may be rewritten as

$$\sigma_1 = 6\frac{M_e}{\eta_e^2} \quad (34)$$

where

$$\eta_e^2 = \frac{h_e^3}{h_1} = h_1^2 + h_2^2\left(\frac{E_2 h_2}{E_1 h_1}\right) \quad (35)$$

Noting that as η_e^2 tends to h_1^2, M_e tends to M_1 and σ_1 tends to $\sigma(h_1, E_1, F_1)$—the latter being the plate theory prediction for the maximum bending stress in the PCC slab resting directly on the subgrade—it may be expected that the stress ratio $[\sigma_1/\sigma(h_1, E_1, F)]$ diverges from unity as the ratio (η_e^2/h_1^2) decreases. This assertion has recently been verified by Salsilli (*14*), who considered the results of plate theory for a small factorial of unbonded, three-layer, edge-loading cases using the WINKLER option in ILLI-SLAB (*15*). He demonstrated that the relationship between the two dimensionless parameters defined above shows little sensitivity to the dimensionless load size ratio (a/l) and provided the following best-fit equation for its description:

$$\frac{\sigma_1}{\sigma(h_1, E_1, k)} = 0.0477629 + 0.265264\left(\frac{a}{l}\right) + 0.953195\left(\frac{\eta_e}{h_1}\right)^{-2} - 0.26083\left(\frac{a}{l}\right)\left(\frac{\eta_e}{h_1}\right)^{-2} \quad (36)$$

In this expression l denotes the radius of relative stiffness of the slab-dense liquid system (h_1, E_1, k), which is defined by

$$l = \left(\frac{E_1 h_1^3}{12(1-\mu_1^2)k}\right)^{1/4} \quad (37)$$

The value predicted by the Westergaard edge-loading equation (*1*) may be substituted for $\sigma(h_1, E_1, k)$ in routine applications of Equation 36.

Elimination of Plate Theory Restrictions

A drastically different picture is obtained when the compressions in the two placed layers are accounted for. Interior loading results from computer program BISAR were used to establish the relationship between dimensionless ratios $[\sigma_{1L}/\sigma(h_1, E_1, E_s)]$ and (η_e^2/h_1^2) without plate theory restrictions. Interpretation of these numerical results on the basis of the principles of dimensional analysis showed that for a wide range of practical applied load radius values, the relationship between the two ratios could be defined uniquely for each value of (E_1/E_2). Thus, Figure 1 was prepared. This can

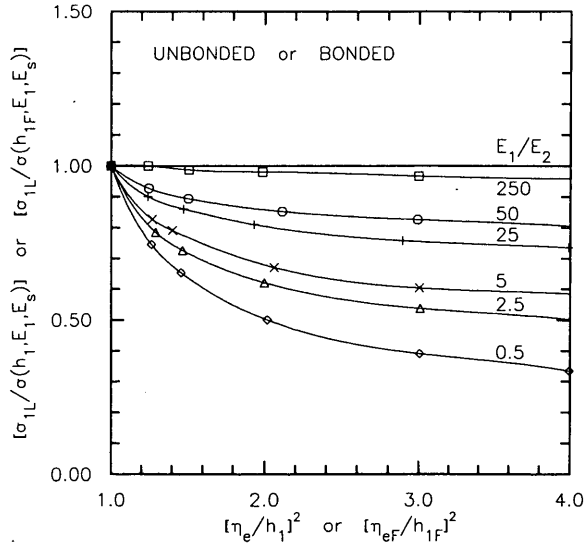

FIGURE 1 Reduction factor for determining maximum bending stress in a three-layer concrete pavement system (elastic solid foundation).

be used to obtain a reduction factor that when multiplied by the available analytical slab-on-grade solution for $\sigma(h_1, E_1, E_s)$ given by Losberg (*2*) provides an estimate for the maximum interior loading bending stress at the bottom of the top layer in a three-layer system.

SOLUTIONS FOR THREE-LAYER SYSTEM WITH BONDED LAYERS

Analytical Solution

The closed-form solution derived above for unbonded layers may be applied, with relatively few modifications, to the case of bonded layers as well. The most significant change is in the definition of the "effective" thickness, h_e (cf. Equation 21). Recall that for unbonded layers, h_e was defined using the condition of equality between flexural stiffnesses of the original composite two-layer plate and of the imaginary, homogeneous "effective" plate. Equation 16, however, applies only to unbonded layers. In the case of bonded layers, the flexural stiffness of the original composite plate may be determined using the parallel axes theorem. This results in the following alternative condition to Equation 16:

$$\frac{E_e h_e^3}{12} = \frac{E_1 h_1^3}{12} + E_1 h_1 \left(x - \frac{h_1}{2}\right)^2 + \frac{E_2 h_2}{12} + E_2 h_2 \left(h_1 - x + \frac{h_2}{2}\right)^2 \tag{39}$$

Equation 39 assumes that the neural axis of the composite system lies within layer 1 at a distance x from the top of layer 1, but the same expression is obtained if the neutral axis is assumed to lie within layer 2 (x is still measured from the top of layer 1). As done for the unbonded layers, it is assumed here that $E_e = E_1$ and that $\mu_e = \mu_1 = \mu_2$, which leads to the following expression for the thickness of the "effective" plate for the case of bonded layers:

$$h_e = \left\{ h_1^3 + \frac{E_2}{E_1} h_2^3 + 12 \left[\left(x - \frac{h_1}{2}\right)^2 h_1 + \frac{E_2}{E_1} \left(h_1 - x + \frac{h_2}{2}\right)^2 h_2 \right] \right\}^{1/3} \tag{40}$$

The depth to the neutral axis, x, is determined by considering the first moment of area of the original composite plate, as follows:

$$x = \frac{E_1 h_1 \frac{h_1}{2} + E_2 h_2 \left(h_1 + \frac{h_2}{2}\right)}{E_1 h_1 + E_2 h_2} \tag{41}$$

Noting that the derivation of Equations 39 through 41 follows the same reasoning as that used by Tabatabaie et al. (*7*), Equation 40 may be rewritten as

$$h_e = \left(h_{1F}^3 + \frac{E_2}{E_1} h_{2F}^3 \right)^{1/3} \tag{42}$$

where h_{1F} and h_{2F} are defined by

$$h_{1F} = \left(h_1^3 + 12\beta^2 h_1 \right)^{1/3} \tag{43}$$

$$h_{2F} = \left(h_2^3 + 12\alpha^2 h_2 \right)^{1/3} \tag{44}$$

with

$$\alpha = \left(h_1 + \frac{h_2}{2} - x \right) \tag{45}$$

and

$$\beta = \left(x - \frac{h_1}{2} \right) = \left(\frac{h_1 + h_2}{2} \right) - \alpha \tag{46}$$

It is observed that Equation 42 is identical to the corresponding Equation 21 for h_e for unbonded systems, the only substitution necessary being the introduction of the "fictitious" thicknesses, h_{1F} and h_{2F}, which are somewhat higher than the original thicknesses h_1 and h_2. It is also clear that the flexural stiffness of the original composite two-layer bonded plate is equal to the stiffness of an unbonded two-layer plate in which the plate layers retain the moduli E_1 and E_2 but are assigned "fictitious" thicknesses h_{1F} and h_{2F}. The fact that $h_{1F} > h_1$ and that $h_{2F} > h_2$ counterbalances the effect of "removing" the bond between the two plate layers.

A relationship between the bending stress at the bottom of the "effective" plate, σ_e, and that acting at the bottom of layer 1 of the original composite two-layer plate, σ_1, is then sought. This is obtained with reference to the geometry of the stress distribution diagrams pertaining to the two systems and recognition of their common slope above the neutral axis. As indicated in Figure 2,

$$\frac{\sigma_e}{\sigma_1} = \frac{h_e}{2y} \tag{47}$$

but

$$y = (h_1 - x) \tag{48}$$

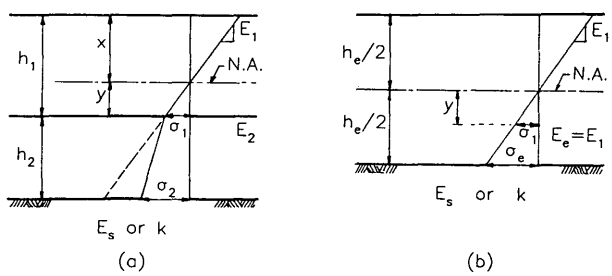

FIGURE 2 Stress distribution in bonded plate on elastic foundation system: (a) original composite two-layer plate; (b) "effective" homogeneous plate.

where

$$\sigma_1 = \sigma_e \frac{2(h_1 - x)}{h_e} \tag{49}$$

This formula is similar in form to the corresponding Equation 22 valid for unbonded systems, with the term $2(h_1 - x)/h_e$ replacing (h_1/h_e). The stress σ_e may be evaluated using the available plate theory solutions pertaining to the loading condition and foundation type of interest. Since plate theory ignores the compression in each of the two layers, σ_1 should be corrected as indicated in Equation 24. For the interior loading-elastic solid case, the necessary corrections are given by Equations 29 and 30. Note that the substitution of (h_1/h_e) by $2(h_1 - x)/h_e$ is also performed in Equation 29. Thus, the following expression is obtained for σ_{1L}, corresponding to Equation 31:

$$\sigma_{1L} = \frac{2(h_1 - x)}{h_e}\sigma(h_e, E_1, E_s) + \vartheta\left[\sigma(h_1, E_1, E_2) - \frac{2(h_1 - x)}{h_e}\sigma(h_e, E_1, E_2)\right] \tag{50}$$

with h_e as defined by Equation 42.

Graphical Solution

An alternative graphical solution is also possible. Using h_{1F} and h_{2F} instead of h_1 and h_2, the ratio $[\eta_{eF}^2/h_{1F}^2]$ may be calculated from Equation 35. Thus, Figure 1 may be used to calculate σ_{1L} in terms of $\sigma(h_{1F}, E_1, E_s)$.

VERIFICATION AND IMPLICATIONS OF PROPOSED APPROACH

The applicability of the proposed closed-form and graphical solutions for the maximum bending stress, σ_{1L}, occurring at the bottom of the top layer in a three-layer system was verified by comparing predicted values with the corresponding bending stresses from numerous analyses using computer program BISAR. It is noted that these verification runs were different from those included in the derivation of Equation 30 and of Figure 1. The predictions of the proposed procedures were also compared with the results of Odemark's method of equivalent thicknesses. These comparisons are shown in Figures 3 and 4 for the unbonded and bonded cases, respectively. It is observed that predictions are generally more reliable for the unbonded rather than the bonded cases. Furthermore, the proposed closed-form approach exhibits somewhat less scatter than the graphical approach, especially for the bonded cases. Both proposed procedures lead to improved estimates of σ_{1L} compared with Odemark's approach, verifying the wisdom of treating the base as primarily reinforcing the PCC slab rather than the subgrade. Odemark's solution leads to stresses that generally compare more favorably with BISAR stresses assuming unbonded layers.

It is noted that in writing Equation 31, no assumptions were made that would restrict it to the interior loading condition

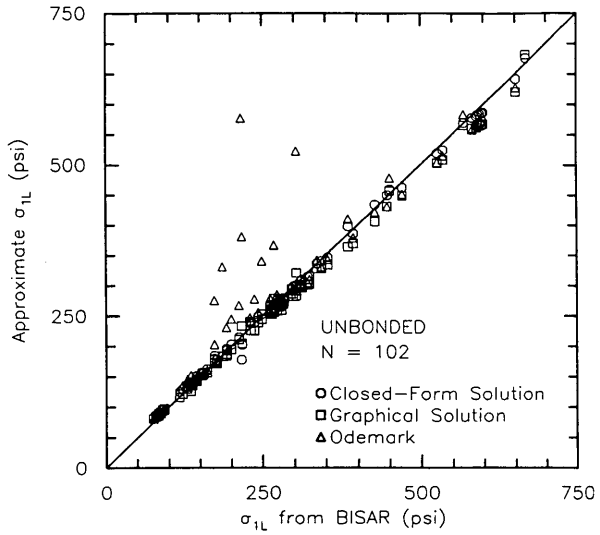

FIGURE 3 Validation of proposed procedures for σ_{1L} under interior loading (elastic solid foundation: unbonded layers).

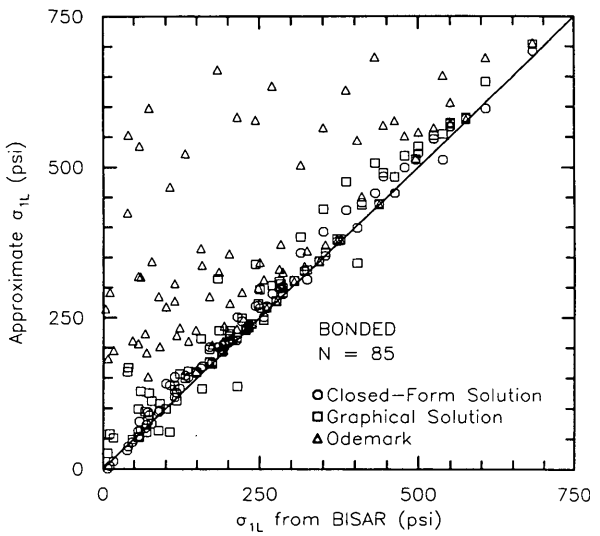

FIGURE 4 Validation of proposed procedures for σ_{1L} under interior loading (elastic solid foundation: bonded layers).

alone, with the exception of the fact that the axisymmetric program BISAR was used in the development of Equation 30 for the factor ϑ. Since, however, Equation 30 is valid for both unbonded and bonded layers, it is reasonable to assume that it is also applicable to edge and corner loading. Thus, it is suggested that Equation 31 may be used in the analysis of three-layer concrete pavement systems under these loading conditions as well. For this purpose, the plate theory expressions given by Ioannides (*3*) may be employed. Verification of this proposal would require the execution of a three-dimensional finite-element code (*16*).

Furthermore, it may be argued that it is possible to interpret the assumption of Equation 25 as also implying that the cor-

rection increment is independent of the *nature* of the foundation as well. Thus, Equation 31 may be applied to the case of a dense liquid foundation, the only necessary change being in the calculation of the plate theory stress using $\sigma(h_e, E_1, k)$ instead of $\sigma(h_e, E_1, E_s)$, where k is the modulus of subgrade reaction. The correction increment, $\Delta\sigma$, is calculated using Losberg's equation as before. This proposal dispenses with the need to define a "top-of-the-base" k-value, a procedure that often leads to erroneous conclusions (*17*). It is possible to examine the accuracy of the proposed procedure for the dense liquid-interior loading case using a general purpose two-dimensional finite-element code such as FINITE (*18*). That effort is continuing at this time. Verification of this proposal for the edge and loading conditions would require three-dimensional finite-element analysis.

Some evidence for the validity of the proposals pertaining to unbonded layers is provided by a comparison of plate theory maximum responses to finite-element results from the WINKLER option in ILLI-SLAB. For this purpose, a data base of 41 "typical" three-layer interior loading runs was assembled. It was found that Equation 22 yields the same stress as that calculated using ILLI-SLAB if $\mu_1 = \mu_2$; if $\mu_1 = \mu_2$, the predicted stress is about 5 percent lower. Furthermore, it was verified that these plate theory results can be predicted with sufficient accuracy by Equation 36, which was developed by Salsilli (*14*) for edge loading. This supports the assertion that the proposals above are applicable to all three fundamental loading conditions for both elastic solid and dense liquid foundations. Verification of the plate theory proposals for the elastic solid foundation is possible using the BOUSSINESQ option in ILLI-SLAB (*15*).

The maximum deflection calculated using ILLI-SLAB was found to be the same as that predicted by plate theory considering the "effective" plate (thickness, h_e; modulus, E_1). It is therefore suggested that the maximum deflection be taken as equal to the value computed using plate theory for any of the three fundamental loading conditions and for both elastic solid and dense liquid foundations. These plate theory predictions should be corrected for the compression of the two placed layers. An effort in this direction is also under way.

CONCLUSION

Analysis and design of concrete pavement systems have long been hampered by the restrictive assumption of available analytical solutions that the PCC slab rests directly on an elastic foundation. In reality—more often than not—concrete pavement slabs are placed on prepared bases, which are sometimes granular and sometimes bound. A number of approaches have been used in the last 40 years to overcome the "one placed layer" limitation. Most notable among these have been

1. Analyzing multilayered concrete pavement systems using Burmister's layered elastic analysis for axisymmetric conditions; such applications include Odemark's method of equivalent thicknesses and, more recently, computerized techniques as implemented, for example, in the program BISAR;
2. Analyzing three-layer concrete pavement systems using a finite-element program based exclusively on plate theory, for example, ILLI-SLAB;
3. Assigning an increased top-of-the-base subgrade modulus purporting to reflect the structural contribution of the base layer and analyzing three-layer concrete pavement systems using the available analytical or numerical procedures.

Such methodologies invariably suffer from considerable shortcomings and may in several cases lead to wrong conclusions. To remedy this situation, practical solutions to the problem posed by a three-layer concrete pavement system are presented in this paper based on sound theoretical precepts and interpretation of numerical results using dimensional analysis. The main difference of the proposed procedure from the popular "bump-the-k-value" approach is that the base layer is treated as a placed layer whose major structural contribution is to reinforce the upper placed layer—the PCC slab—rather than the natural supporting subgrade. The proposed closed-form and graphical solutions allow the calculation of maximum responses in concrete pavement systems—namely, deflection, bending stress, and subgrade stress—for all three fundamental loading conditions and for both dense liquid and elastic solid foundations. It is shown that responses obtained on the basis of plate theory alone must be corrected for the compression experienced by the two placed layers. The implications of the proposed approach with respect to current analysis and design methodologies are far reaching. Research activities for its full verification and refinement are continuing at this time. Most noteworthy among these efforts are those focusing on the development of a computerized model for a mutlilayered system supported by a dense liquid foundation (*19*).

ACKNOWLEDGMENTS

This material is based on work supported by the National Science Foundation. The government has certain rights to this material. Additional funding was provided by the University of Illinois Research Board thorugh an Arnold O. Beckman Research Award. The authors wish to acknowledge the contributions of Michael Duval and Bassam E. Touma, formerly graduate research assistants at the University of Illinois, in assembling the data base and other materials used as background to this study.

REFERENCES

1. H. M. Westergaard. New Formulas for Stresses in Concrete Pavements of Airfields. *Transactions*, ASCE, Vol. 113, 1948, pp. 425–439.
2. A. Losberg. *Structurally Reinforced Concrete Pavements*. Doktorsavhandlingar Vid Chalmers Tekniska Högskola, Göteborg, Sweden, 1960.
3. A. M. Ioannides. The Problem of a Slab on an Elastic Solid Foundation in the Light of the Finite Element Method. *Proceedings, 6th International Conference on Numerical Methods in Geomechanics*, Paper No. 408, April 11–15, 1988, Innsbruck, Austria, pp. 1059–1064.
4. W. R. Barker and C. R. Gonzalez. Pavement Design by Elastic Layer Theory. *Proceedings, Specialty Conference Aircraft/Pavement Interaction—An Integrated System*, (P. T. Foxworthy, ed.), ASCE/ATD/APC, Kansas City, Mo., Sept. 4–6, 1991, pp. 21–43.
5. D. M. Burmister. The Theory of Stresses and Displacements in Layered Systems and Application to the Design of Airport Run-

ways. *Proc.* HRB, Vol. 23, 1943, pp. 126–144; Discussion, pp. 144–148.
6. N. Odemark. *Investigations as to the Elastic Properties of Soils and Design of Pavements According to the Theory of Elasticity* (in Swedish). Meddelande 77, Statens Väginstitut, Stockholm, Sweden, 1949. [English translation, M. A. Hibbs and J. Silfwerbrand (A. M. Ioannides, ed.), 1990.]
7. A. M. Tabatabaie, E. J. Barenberg, and R. E. Smith. *Longitudinal Joint Systems in Slip-Formed Rigid Pavements, Vol. II: Analysis of Load Transfer Systems for Concrete Pavements*. Report DOT/FAA/RD-79/4, II. FAA, U.S. Department of Transportation, Nov. 1979.
8. J. Uzan and M. W. Witczak. Composite Subgrade Modulus for Airfield Pavement Design Based Upon Multilayer Theory. *Proceedings, Third International Conference on Concrete Pavement Design and Rehabilitation*, Purdue University, April 23–25, 1985, pp. 157–166.
9. E. J. Yoder. *Principles of Pavement Design*. John Wiley & Sons, Inc., New York, 1959, 569 pp.
10. L. W. Teller and E. C. Sutherland. The Structural Design of Concrete Pavements: Part 5. *Public Roads*, Vol. 23, No. 8, April, May, June, 1943, pp. 167–212.
11. A. J. Weissmann, B. F. McCullough, and W. R. Hudson. Back-Calculated Material Properties of Continuously Reinforced Concrete Pavements: A Comparison Between Two Approaches. Presented at the 69th Annual Meeting of the Transportation Research Board, Washington, D.C., 1990.
12. M. G. F. Peutz, H. P. M. Van Kempen, and A. Jones. Layered Systems Under Normal Surface Loads. In *Highway Research Record 228*, HRB, National Research Council, Washington, D.C., 1968, pp. 34–45.
13. S. P. Timoshenko and S. Woinowsky-Krieger. *Theory of Plates and Shells* 2nd ed. McGraw-Hill, New York, 1973, 580 pp.
14. R. A. Salsilli. *Development of Mechanistic Based Design Procedure for Concrete Pavements*. Ph.D. thesis. University of Illinois, Urbana, 1991.
15. A. M. Ioannides, M. R. Thompson, and E. J. Barenberg. Finite Element Analysis of Slabs-On-Grade Using a Variety of Support Models. *Proceedings, Third International Conference on Concrete Pavement Design and Rehabilitation*, Purdue University, April 23–25, 1985, pp. 309–324.
16. A. M. Ioannides and J. P. Donnelly. Three-Dimensional Analysis of Slab on Stress-Dependent Foundation. In *Transportation Research Record 1196*, TRB, National Research Council, Washington, D.C., 1988, pp. 72–84.
17. A. Ioannides. Subgrade Characterization for Portland Cement Concrete Pavement Systems. *Proceedings, International Conference on Geotechnical Engineering for Coastal Development Theory and Practice*, Port and Harbour Institute, Japan Ministry of Transport, Yokohama, Sept. 3–6, 1991.
18. L. A. Lopez. FINITE: An Approach to Structural Mechanics Systems. *International Journal for Numerical Methods in Engineering*, Vol. 11, 1977, pp. 851–866.
19. F. Van Cauwelaert. "Westergaard's Equations" for Thick Elastic Plates. *Proceedings, 2nd International Symposium on the Theoretical Design of Concrete Pavements*, Sigüenza, Spain, Oct. 4–5, 1990, pp. 165–175.

Expedient Stress Analysis of Jointed Concrete Pavement Loaded by Aircraft with Multiwheel Gear

WAYNE J. SEILER

The load-carrying capacity of an airport pavement is limited by the flexural stresses that aircraft induce in a jointed plain concrete pavement (JPCP). Aircraft gear characteristics have a significant effect on the magnitude of the slab edge stress. For those aircraft that have multiwheel gear, a pavement engineer cannot directly use Westergaard's analysis for loads placed at the interior, edge, or corner of a slab. In addition, Westergaard's analysis does not account for load transfer across a joint in a JPCP. Regression models were developed during research at the University of Illinois that allow the engineer to use an equivalent single-wheel radius to determine the free edge stress in a JPCP. These models have been developed for several gear configurations so that a free edge stress equation based on Westergaard's analysis and joint load transfer efficiency models can be used to quickly determine the stress in a JPCP. Thus, instead of a computer program such as the H51 or a finite-element program such as ILLI-SLAB, regression models may be used to more efficiently and expediently determine edge stresses with no sacrifice in accuracy of the results. The expediency of the stress analysis procedure presented in this paper makes it an appropriate tool for use in the field or for inclusion in knowledge-based expert systems (KBES). In lieu of a fielded KBES, a simple electronic spreadsheet has been developed as an interim approach for this stress analysis procedure.

In the past, agencies have made approximate assumptions in the calculation of flexural stresses in a jointed plain concrete pavement (JPCP) that result from aircraft loads (*1–3*). Agencies often assume that load transfer across a joint reduces slab edge stress by 25 percent regardless of the joint type. This assumption should no longer be used, since it does not describe a very important performance measure of a JPCP, namely, joint behavior. Foxworthy, Ioannides, and Korovesis have developed models that describe the load transfer behavior of concrete joints (*4–6*). Their work shows that temperature, joint type, and load radius significantly affect the deflection and stress load transfer efficiencies. This in turn affects the magnitude of the stress in a JPCP and the allowable aircraft loads that should be permitted on a pavement.

The variability of aircraft characteristics such as gross weight, gear configuration, tire pressure, and tire contact area makes it necessary for engineers to evaluate each aircraft in the design or evaluation of an airfield pavement. Many aircraft have multiwheel gear, so a stress analysis of a JPCP cannot directly use Westergaard's analysis (*7*) for any of the three load locations. This limitation can be overcome by using the equivalent single-wheel radius (ESWR) concept (*8–11*) to determine the free edge stress and the stress load transfer efficiency. Once the ESWR is known, the actual edge stress at the transverse joint of a JPCP can be computed for any type of aircraft. Next, the ratio of the edge stress to the portland cement concrete (PCC) modulus of rupture can be used to predict the allowable number of aircraft passes on a JPCP (*4*).

ERES Consultants, Inc., 8 Dunlap Court, Savoy, Ill. 61874-9501.

CURRENT METHODS OF ANALYSIS

At present, most design agencies use one of three methods to analyze the stress in a JPCP (*11*): Westergaard's analysis, an elastic layer analysis, or a finite-element program. In the past, most organizations have used the method that is most appropriate for the user's needs. Since the first two methods are generally more expedient, they are frequently used in the field. Finite-element programs are more powerful research tools, but the level of understanding and computer hardware required to use these programs restricts their use primarily to the research field.

Those agencies that use Westergaard's analysis normally use a computerized version of the Pickett and Ray influence charts (*12*). One program in widespread use today is H51 (*13*), which is used to determine the free edge stress of a JPCP. This program is widely used since it allows the user to enter more than one load for those aircraft that have main gear with multiple wheels. Its use is restricted to those situations that adhere to the semiinfinite plane assumptions in Westergaard's analysis (*14*). The free edge stress must be reduced to account for load transfer if the edge or corner loading location is considered in the design analysis. For this situation, most agencies assume that the average stress reduction is 25 percent, regardless of temperature, joint type, or aircraft gear configuration.

In order to simplify the analysis of a JPCP, the U.S. Army Corps of Engineers Waterways Experiment Station developed regression equations for common aircraft in the U.S. inventory. They used H51 to obtain regression constants for Equation 1 (*15*). Equation 1 is included in airfield design and analysis programs:

$$\sigma_e = \frac{P}{h^2}[a_0 + a_1 (\ln l) + a_2 (\ln l)^2] \quad (1)$$

where

σ_e = free edge stress (psi),
P = actual gear load (lb),
h = slab thickness (in.), and

a_i = regression constant calculated for a specific gear to match the computerized solutions of Pickett and Ray influence chart solutions.

$$l = \left[\frac{Eh^3}{12(1 - \mu^2)k}\right]^{1/4} \quad (2)$$

where

l = radius of relative stiffness (in.),
E = modulus of elasticity of the concrete (psi),
h = thickness of the concrete (in.),
μ = Poisson's ratio of the PCC slab, and
k = modulus of subgrade reaction (psi/in.).

Equations 1 and 2 are used by the U.S. Army Corps of Engineers and the U.S. Air Force because they are fast and efficient methods of determining free edge stresses.

The regression constants that were developed for each aircraft using Equation 1 are based on aircraft main gear that were positioned at either the transverse or longitudinal joint of a JPCP. Foxworthy found that the transverse joint is normally the critical location in the design of a PCC pavement (*4*) because of the magnitude of the stress in the concrete slab and the pass-to-coverage ratio of each aircraft's gear with respect to the transverse and longitudinal joints of the pavement.

Another method of analyzing the stress in a JPCP is to use an elastic layer analysis. The U.S. Army Corps of Engineers is developing computer programs for elastic layer analysis of airfield pavements. Elastic layer analysis is more representative of the layer material properties than is Westergaard's analysis (*15*). An elastic layer program also has the advantage of allowing the engineer to consider several layers in a pavement structure. However, a major disadvantage of an elastic layer analysis is that it cannot model joint behavior in concrete pavements. Therefore, this method must also use an assumed joint load transfer efficiency to attempt to model tensile stresses that occur in the JPCP slab. This is important since JPC pavements in the field do not have 100 percent load transfer efficiencies.

The last method of analysis uses a finite-element program such as ILLI-SLAB to consider specific JPCP issues like slab curing and nonuniform subgrade support conditions. Unlike the previous two methods, this program considers joint load transfer and computes the stress at any point in the JPCP slab with a high degree of accuracy (*16*). However, use of a finite-element program requires a good theoretical understanding of JPCP performance, and it generally is not an appropriate tool for use in the field. In addition, a program such as ILLI-SLAB requires several inputs and more powerful computer hardware than is typically available in the field.

PROPOSED METHOD OF ANALYSIS

The work that was conducted by the Waterways Experiment Station using H51 provided a fast and efficient method for determining the free edge stress in a JPCP, but a prototype expert system developed at the University of Illinois needed a tool that could also be used to determine joint load transfer efficiencies (*10*). This objective was met by using the equivalent single-axle radius (ESAR) concept (*8–10*) to develop ESWR regression models for several aircraft (*11*). It appears that the equivalent radius concept was first introduced for dual truck tires by Bradbury in 1934, but no further research was conducted in this area until Ioannides began his studies in 1989 (*8–10*).

The definition of ESWR is identical to the definition of an equivalent single-wheel load (ESWL) given by Yoder and Witczak (*18*), except that the words "load on" replace "radius of." The corresponding modification of Yoder and Witczak's ESWL definition for ESWR reads as follows:

> An equivalent single-wheel radius (ESWR) is defined as the radius of a single tire that will cause an equal magnitude of a preselected parameter (stress, strain, deflection, or distress) at a given location within a specific pavement system to that resulting from a multiple-wheel load at the same location within the pavement structure. (*18*)

Once the ESWR regression models had been developed, a pavement engineer could easily compute the ESWR for an aircraft's main gear for each JPCP trial section. After the ESWR is computed for a trial section, the engineer can compute the free edge stress at the transverse joint and the stress load transfer efficiency. Finally, the designer can use these values to compute the edge stress at the transverse joint of the pavement.

Aircraft ESWR Model Development

Ioannides et al. used the finite-element program ILLI-SLAB to review and identify the correct form of Westergaard's free edge stress equation (*7,19*), which is shown as Equation 3. Like all the original Westergaard equations, Equation 3 is limited in applicability to a single load with a radius a (i.e., it is not applicable for larger aircraft with multiwheel gear). However, Equation 3 can be used for an aircraft with multiwheel gear if the ESWR is substituted for a and the entire gear load is used to compute the free edge stress.

The procedure used to develop an ESWR model for an aircraft is shown in Figure 1 (*11*). Equation 4 shows the general form of this regression model. For very large aircraft, as many as six tires on a gear had to be converted to an ESWR before the engineer could use Equation 3 to calculate the free edge stress in a JPCP slab.

$$\sigma = \frac{3(1 + \mu)P}{\pi(3 + \mu)h^2}\left[\ln\frac{Eh^3}{100ka^4} + 1.84 - \frac{4\mu}{3} + \frac{1 - \mu}{2} + 1.18\,(1 + 2\mu)\,(a/l)\right] \quad (3)$$

where

σ = free edge stress (psi),
E = modulus of elasticity of the concrete (psi),
h = thickness of the concrete (in.),
μ = Poisson's ratio of the pavement,
k = modulus of subgrade reaction (psi/in.),
a = actual load radius for single-wheel gear or ESWR for multiwheel gear (in.),
l = radius of relative stiffness (in.), and

STEP 1:	Use the H51 computer program to determine the flexural stress for the transverse edge loading condition. Determine edge stresses for pavement structures with ℓ (EQN 2) values ranging from 12 to 130.
STEP 2:	Solve for "a" in EQN 3 using the total gear load and the H51-determined edge stress. This results in a unique ESWR for each trial JPCP section, or ℓ value, which can then be used to compute the free edge stress.
STEP 3:	Use multiple regression to determine equation models for ESWR as a function of ℓ.
STEP 4:	Validate the regression equations using an independent set of ℓ values. Compare stresses using the H51 program and Equations 1 through 4.

FIGURE 1 Procedure used to develop aircraft ESWR models.

P = tire load (lb) for single-wheel gear or gear load (lb) if the gear ESWR is used for multiwheel gear.

The procedure shown in Figure 1 was used to obtain Equation 4 coefficients presented in Table 1 for common military and commercial aircraft in the U.S. inventory. Figure 2 compares the ESWR of those aircraft with twin (two wheels) main gear.

$$\text{ESWR} = c_1 + c_2 l + c_3 l^2 + c_4 l^3 + c_5 l^4 \quad (4)$$

where l is the radius of relative stiffness (in.) and c_i are constants developed for a specific aircraft.

If all aircraft in Figure 2 had equal main gear weights and it was assumed that aircraft tire contact areas remained constant, these figures would show which aircraft gear configurations cause the most damage to a JPCP. In other words, Figure 2 shows which aircraft gear configurations cause the highest flexural stresses, thereby causing the most PCC fatigue damage for each gear coverage of the JPCP. As the ESWR for a given l-value decreases, the JPCP fatigue damage caused by that gear configuration increases.

Free Edge Stress Determination Using ESWR

Once the aircraft ESWR models had been developed for their respective multiwheel gear, determining the free edge stress for any aircraft at the transverse joint became a simple two step process. After the ESWR for an aircraft is computed using Equation 4, Equation 3 can be used to determine the free edge stress. Since the ESWR is used in this procedure, the total gear load is used in Equation 3. Because the ESWR indicates how well aircraft manufacturers have designed main gear to minimize pavement fatigue damage, it is advantageous to compare the free edge stress of a JPCP when all gear have the same load.

Figure 3 shows what the free edge stress in a 12-in. JPCP would be if each aircraft had a 100-kip load placed on the main gear. Figure 3 shows which aircraft gear configurations would

TABLE 1 ESWR Regression Model Coefficients

	EQUATION 4 COEFFICIENTS						
AIRCRAFT	c_1	c_2	c_3	c_4	c_5	R^2	**STD ERR**
A-300 ::	8.1753E+00	1.2817E+00	-2.4122E-02	2.0038E-04	-5.9445E-07	0.9985	0.1976
B-52 ..	7.2390E+00	8.3507E-01	-1.7009E-02	1.4602E-04	-4.3636E-07	0.9927	0.2924
B-707 ::	5.9076E+00	1.4834E+00	-2.8093E-02	2.3290E-04	-6.8985E-07	0.9967	0.3199
B-727 ..	9.4562E+00	7.2066E-01	-1.4560E-02	1.2220E-04	-3.5460E-07	0.9891	0.2957
B-737 ..	9.2827E+00	6.1666E-01	-1.3310E-02	1.2028E-04	-3.7428E-07	0.9934	0.2011
B-747 ::	2.0012E+00	1.8159E+00	-3.3448E-02	2.7245E-04	-7.9985E-07	0.9983	0.2998
C-9 ..	11.0601E+00	3.8631E-01	-8.6895E-03	8.1913E-05	-2.6306E-07	0.9858	0.2050
C-135 ::	5.1489E+00	1.5557E+00	-2.8865E-02	2.3541E-04	-6.8847E-07	0.9974	0.3089
C-141 ::	7.5708E+00	1.3139E+00	-2.5723E-02	2.1923E-04	-6.6525E-07	0.9937	0.3682
DC-10 ::	-0.8767E+00	2.0834E+00	-3.5900E-02	2.7808E-04	-7.8675E-07	0.9994	0.2277

NOTES: 1. :: - Twin-tandem main gear.
2. .. - Twin main gear.

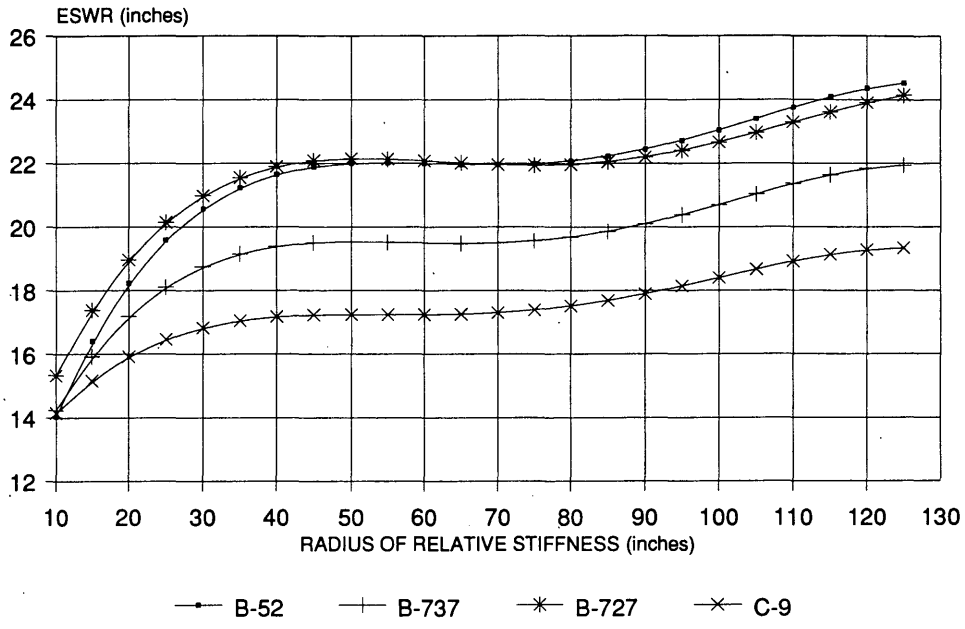

FIGURE 2 ESWR of several twin gear configurations.

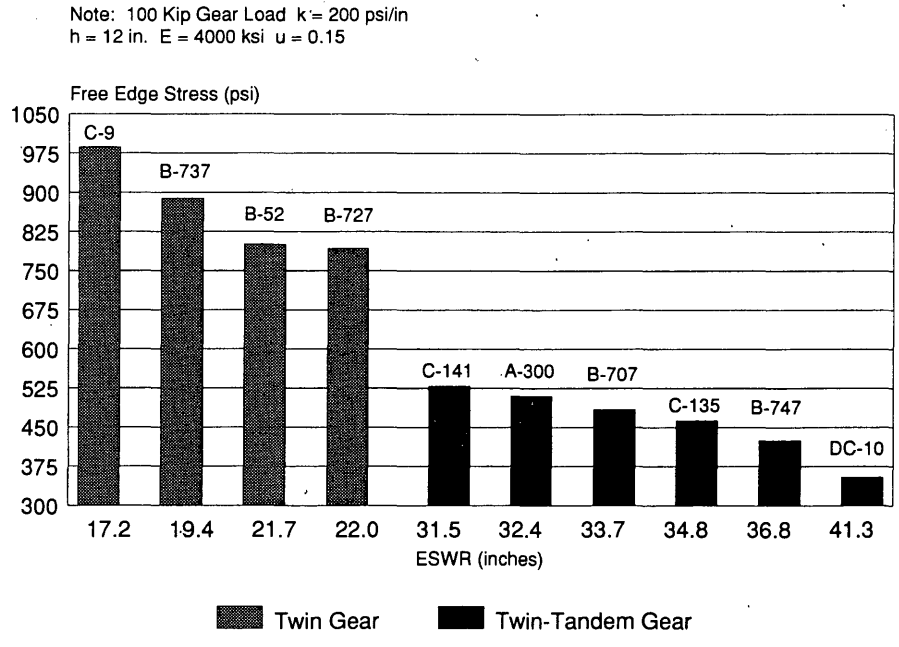

FIGURE 3 Relationship between gear configuration and JPCP edge stress.

cause the most fatigue damage in the JPCP if tire contact areas remained the same. Aircraft with the smallest ESWR induce the highest free edge stress for a 100-kip gear load.

The statistical analysis of Figure 3 shown in Table 2 emphasizes how the free edge stress in a JPCP can be reduced by increasing the number of wheels on the main gear to distribute the gear load over a larger area, but it also shows that other gear characteristics affect the magnitude of the free edge stress and the ESWR. The characteristics that contribute to the ESWR and edge stress variation within the twin and twin-tandem gear groups include the tire contact area and tire spacing. Although additional wheels, larger tire contact areas, and increased tire spacings may increase the production cost of an aircraft, airline companies may recoup this cost since future landing fees may be based on the JPCP damage caused by each aircraft (*20*).

TABLE 2 Edge Stress Variance due to Gear Configuration

	TWIN GEAR			TWIN TANDEM GEAR		
	Mean	S.D.	C.V. (%)	Mean	S.D.	C.V. (%)
ESWR (in)	20.09	2.24	11.1	35.07	3.57	10.2
Free Edge Stress (psi)	867	91	10.5	461	64	13.9
Tire Contact Area (in^2)	212.3	37.4	17.6	237.2	39.7	16.7
Transverse Tire Spacing (in)	29.4	5.7	19.4	37.9	9.6	25.3
Longitudinal Tire Spacing (in)	NA	NA	NA	58.5	6.2	10.6

NOTES:
1. Analysis is for only those aircraft shown in Figure 3.
2. Main gear load is 100 kips for all aircraft.
3. h = 12 in, E = 4000 ksi, u = 0.15, k = 200 psi/in.

As Step 4 in Figure 1 indicates, H51 computer runs were used to validate the aircraft ESWR equation coefficients shown in Table 1. Since the free edge stresses obtained from H51 are usually within 3 percent of the free edge stresses obtained from using a finite-element program, the H51 results were the basis for comparison. Figure 4 shows that the use of the ESWR concept as originally proposed by Bradbury (*8*) leads to accurate determination of free edge stresses. The results shown in Figure 4 are typical for other aircraft models developed during this research and demonstrate that use of an ESWR usually produces better results than those obtained using Equation 1.

Load Transfer Efficiency

Now that the ESWR for several aircraft can be used to accurately determine the free edge stress at the transverse joint of a JPCP, the aircraft gear ESWR can next be used to determine stress load transfer efficiency. This allows field engineers to accurately estimate JPCP flexural stresses for "semiinfinite" slab conditions without the use of a finite-element program.

Figure 5 shows models that have been developed by Ioannides and Korovesis to express the relationship between deflection load transfer efficiency (DLTE) and stress load transfer efficiency (SLTE). DLTE and SLTE are defined in Equations 5 and 6, respectively. Equation 7 coefficients for each of the curves shown in Figure 5 are presented in Table 3. The coefficient of determination (r^2) for each curve is 1.0 and the standard error of SLTE estimation in Figure 5 ranges from 0.0064 to 0.062.

$$\text{DLTE} = \frac{\delta_u}{\delta_l} * 100\% \tag{5}$$

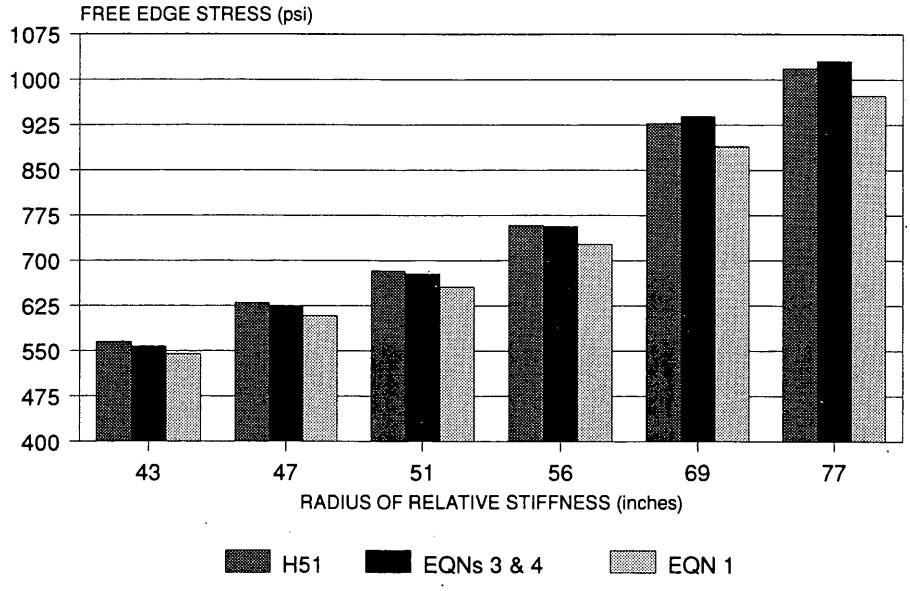

FIGURE 4 B-747 induced free edge stress in a 15-in. JPCP.

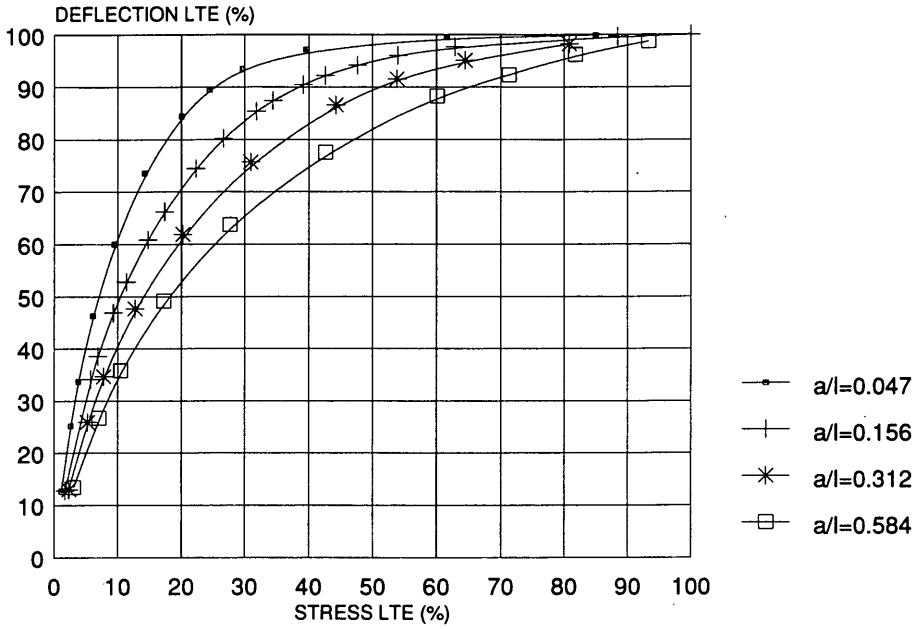

FIGURE 5 SLTE versus DLTE for a symmetric edge load (*9*).

TABLE 3 SLTE Regression Model Coefficients

a/ℓ	c_1	c_2	c_3	c_4	c_5
0.047	-0.12231E-00	0.63129E-02	0.93482E-03	-0.18447E-04	0.10421E-06
0.156	0.64787E-01	0.47221E-02	0.89586E-03	-0.16478E-04	0.89222E-07
0.312	-0.74232E-01	0.37497E-01	-0.28618E-03	-0.15080E-06	0.12778E-07
0.584	-0.20500E-03	0.42797E-01	-0.51432E-03	0.35116E-05	-0.6599E-08

where δ_u is the deflection of the adjacent unloaded slab and δ_l is the deflection of the loaded slab.

$$\text{SLTE} = \frac{\sigma_u}{\sigma_l} * 100\% \quad (6)$$

where σ_u is the edge stress of the adjacent unloaded slab and σ_l is the edge stress of the loaded slab.

$$\text{LOG}_{10}(\text{SLTE}) = c_1 + c_2(\text{DLTE}) + c_3(\text{DLTE})^2 + c_4(\text{DLTE})^3 + c_5(\text{DLTE})^4 \quad (7)$$

where c_i are the constants developed for one *a/l* curve in Figure 5.

Figure 5 also shows that the DLTE versus SLTE relationship depends on the load size ratio, *a/l* (*10*). Since the slab length over *l*(*L/l*) and slab width over *l*(*W/l*) ratio assumptions (i.e., semiinfinite slab response) of Figure 5 represent typical ratios in the field, the curves in this figure can be used to estimate SLTE. DLTE values in the field are usually determined using a falling weight deflectometer (FWD) during a nondestructive pavement evaluation, but if no evaluation results are available, a mean DLTE must be estimated for the pavement design life. Darter et al. reported the range of typical DLTE values shown below for the various types of joints in JPCP (*1*). These DLTE values can be used for design of a new or reconstructed JPCP, or local FWD data can be used to estimate the LTE behavior of each joint type.

Joint Type	*Base Type*	*DLTE (%)*
Weakened plane	Granular	40 to 60
Weakened plane	Stabilized	50 to 70
Keyway	Granular	50 to 70
Keyway	Stabilized	60 to 70
Doweled	Any type	70 to 90

An objective of the airfield pavement research conducted at the University of Illinois was to acquire as much existing pavement technology as possible for rehabilitation designs of a JPCP. The *a/l* ratios shown in Figure 5 were developed for single loads, but not for multiple wheel loads. In addition, single-load radii ranged from 1.70 to 21.03 in. (*6*), but the ESWRs for aircraft with twin-tandem gear are greater than 30 for typical field *l*-values (i.e., typical pavement cross sections). Therefore, if Figure 5 were to be used in this prototype expert system, it would be important to validate the use of these *a/l* curves for multiwheel gear. The finite-element program ILLI-SLAB was used to validate the curves using the parameters and values shown in Table 4. Ideally, the ILLI-

TABLE 4 Aircraft SLTEs

	DLTE	40%		70%		90%	
	ℓ (in)	69.7	53.8	69.7	53.8	69.7	53.8
F-15 (1 Wheel)	$SLTE_{ioan}$	6	7	16	19	31	38
	$SLTE_{whls}$	7	7	16	18	32	35
	$SLTE_{eswr}$	NA	NA	NA	NA	NA	NA
B-727 (2 Wheels)	$SLTE_{ioan}$	10	11	27	29	51	57
	$SLTE_{whls}$	13	14	30	32	55	59
	$SLTE_{eswr}$	12	13	28	32	56	61
B-1 (4 Wheels)	$SLTE_{ioan}$	11	13	30	37	59	69
	$SLTE_{whls}$	14	15	33	35	60	62
	$SLTE_{eswr}$	14	16	34	37	64	69

NOTES:

1. $SLTE_{ioan}$ is the stress load transfer efficiency interpolated from Figure 5 by using ESWR/ℓ.

2. $SLTE_{whls}$ is the stress load transfer efficiency obtained from using the finite element program ILLI-SLAB with actual wheel locations. For the B-727 the two wheels were placed at the transverse joint while the two front wheels of the B-1 main gear were placed at the transverse joint.

3. $SLTE_{eswr}$ is the stress load transfer efficiency obtained from using the finite element program ILLI-SLAB and the ESWR of the B-727 and B-1 main gears.

4. "ℓ" values are based on thicknesses of 24 and 17 inches, Poisson's ratio of 0.15, PCC modulus of elasticity of 4 million psi, and a modulus of subgrade reaction of 200 psi/in.

SLAB runs would show that the *a/l* curves in Figure 5 could be used for multiwheel gear by converting the exact configuration to an ESWR and then using the ESWR/*l* ratios shown in Figure 5.

This hypothesis was validated by performing two ILLI-SLAB runs for each combination of *l* and DLTE values for an aircraft. The objective of the first run was to determine the SLTE by using a mesh that included the exact tire location and contact area for all wheels of a main gear. Next, Equation 4 was used to compute the ESWR for a main gear and then use that radius in the finite-element mesh to determine the SLTE. Finally, the ESWR/*l* ratio could be used in Figure 5 to interpolate between the curves as necessary to arrive at a third SLTE.

The results of these finite-element runs are shown in Table 4 and support the hypothesis that the *a/l* curves in Figure 5 apply for multiwheel gear. Figure 6 shows that if the DLTE is plotted against the SLTE for an ESWR/*l* ratio, there is good agreement between both finite-element runs. In addition, the results of the finite-element runs correlate well with the original curves developed by Ioannides and shown in Figure 5.

ESWR Stress Analysis Example

The stress analysis procedure presented in this paper is summarized through an example problem. The example presented in Figure 7 assumes that a pavement engineer is designing a new JPCP pavement and that the critical aircraft is B-727. The current trial PCC thickness is 17 in. and includes the same thickness design inputs shown in Table 4. Figure 7 gives the steps required to use the ESWR concept to determine the edge stress at the transverse joint of the JPCP. For this example, the assumed DLTE is 70 percent.

The ESWR method of determining the actual edge stress in the JPCP is based on the assumption that the sum of the stresses of the loaded and unloaded slabs is approximately equal to the free edge stress of a loaded slab. This is a reasonable assumption regardless of the type of load transfer (aggregate interlock or dowels) because Ioannides and Korovesis have shown that the primary mechanism of load transfer is through shear forces (*21*). If dowels are used for load transfer, a small percentage of the load is transferred through the moment at the joint. If it is assumed that the load transferred through the moment at a doweled joint is negligible and a SLTE of 28 percent is used, this example shows that the edge stresses of 313 and 88 psi in the loaded and unloaded slabs equal the total free edge stress of 401 psi.

Figure 8 shows that the stress analysis procedure presented in this paper compares very well with the results that were obtained using the finite-element program ILLI-SLAB. Figure 8 also shows that the edge stresses in the loaded and unloaded slabs approach 50 percent of the free edge stress as the DLTE approaches 100 percent. Finally, the vertical line

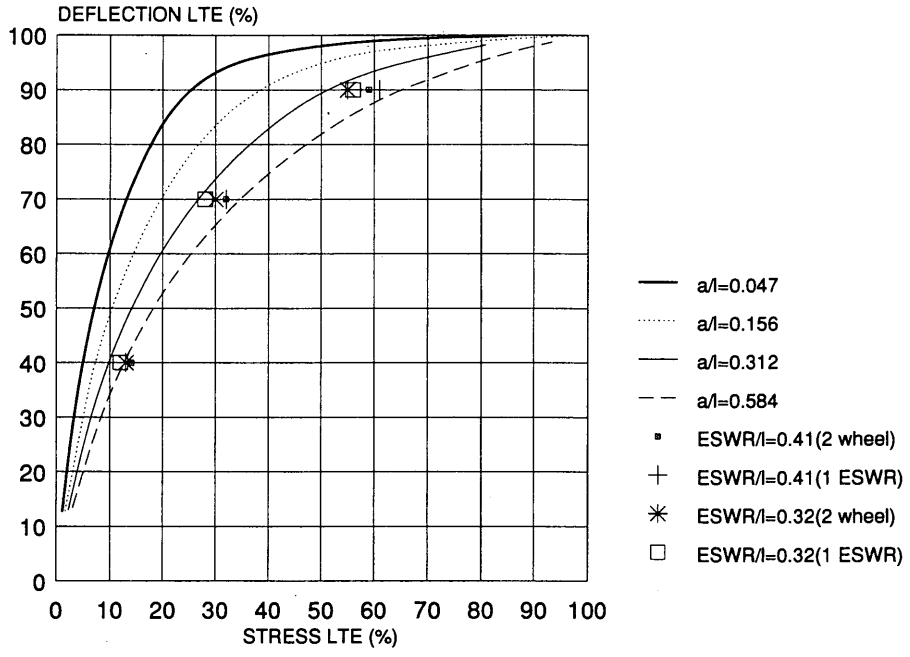

FIGURE 6 B-727 load transfer efficiencies.

STEP	INPUT	OUTPUT	REFERENCE
1. Calculate ℓ	h = 17 in E_{PCC} = 4,000,000 psi u = 0.15 k = 200 psi/in	ℓ = 53.7 in	EQN 2
2. Calculate ESWR	ℓ = 53.7 in	ESWR = 22.1 in	EQN 4 TABLE 1 FIGURE 2
3. Calculate Free Edge Stress	h = 17 in E_{PCC} = 4,000,000 psi u = 0.15 k = 200 psi/in ESWR = 22.1 in ℓ = 53.7 in P = 81 kips	σ_{free} = 401.2 psi	EQN 3
4. Calculate ESWR/ℓ	ESWR = 22.1 in ℓ = 53.7 in	ESWR/ℓ = 0.412	
5. Determine SLTE	DLTE = 70% ESWR/ℓ = 0.412	SLTE = 28%	FIGURE 5 EQN 7 TABLE 4 FIGURE 6
6. Calculate Actual Edge Stress	σ_{free} = 401.2 psi SLTE = 28%	σ_l = 313.1 psi σ_u = 88.0 psi	EQN 6

FIGURE 7 Example problem using a B-727 ESWR to compute an edge stress.

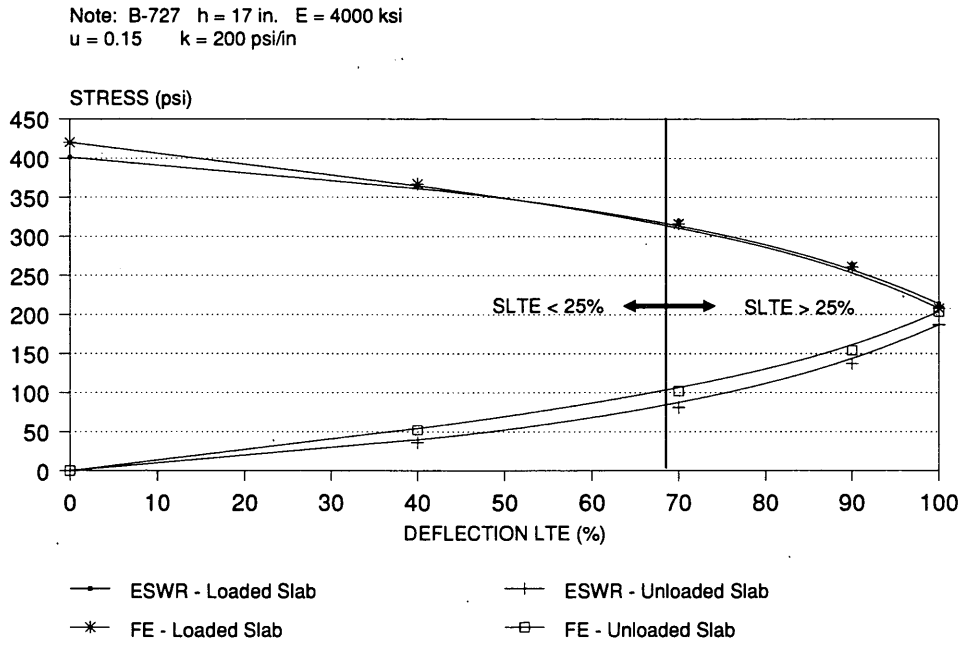

FIGURE 8 Edge stresses obtained using an ESWR and a finite-element program.

in Figure 8 represents an SLTE of 25 percent. If all joints in the JPCP are not doweled, the expected DLTEs will lead to edge stresses that are higher than those obtained using current FAA and U.S. Air Force design procedures, since each agency assumes a constant SLTE of 25 percent. As one moves to the left of the 25 percent SLTE line in Figure 8, the increase in edge stress in the loaded slab will decrease the fatigue life of the PCC and lead to early failure of the JPCP.

CONCLUSIONS

This paper presents a method for determining the flexural stress in a new or existing JPCP for aircraft with multiwheel main gear. ESWR regression models were developed for loading at the transverse joint of a JPCP for several aircraft. Once the ESWR is known for a trial JPCP section, Westergaard's analysis is used to determine the free edge stress. This research demonstrated that the ESWR can also be used to determine the SLTE, given the DLTE. Finally, the actual edge stress in a JPCP at the transverse joint can be determined using the free edge stress and the SLTE.

This analysis procedure is a fast and efficient means of accurately modeling JPCP behavior. Stress analysis results obtained from this procedure are almost as accurate as the results that would be obtained from a finite-element analysis and do not require the more powerful hardware that is used to run finite-element computer programs. Since this procedure also considers joint behavior, which is crucial to JPCP performance, it is a good tool for use in the field or for research checks of finite-element analyses.

This procedure has been incorporated into a prototype expert system that was developed at the University of Illinois. Future work on the edge stress analysis procedure presented in this paper should include ESWR regression models developed for main gear placed at the longitudinal joint of a JPCP. The results of this work could be added to the prototype expert system, which could then be programmed to evaluate both the transverse and longitudinal loading conditions and identify situations in which the longitudinal joint may be the critical location in a design analysis.

ACKNOWLEDGMENT

The author wishes to express his appreciation to Kathleen Hall for her editorial support. Her reviews and suggestions helped to improve the presentation of the research results obtained at the University of Illinois. Her efforts and those of the author should help agencies understand the benefit of using the ESWR concept to quickly compute free edge stresses and joint load transfer efficiencies in an airport JPCP.

REFERENCES

1. *Rigid Pavement Design for Airfields*, NAVFAC DM-21.04. U.S. Navy, May 1986.
2. *Airport Pavement Design and Evaluation.* FAA Advisory Circular AC 150/5320-6C. FAA, U.S. Department of Transportation, Dec. 1978.
3. *Rigid Pavements for Airfields.* AFM 88-6. Chapter 3. U.S. Air Force, Aug. 1988.
4. P. T. Foxworthy. *Concepts for the Development of a Destructive Testing and Evaluation System for Rigid Airfield Pavements.* Ph.D. thesis. University of Illinois, Urbana-Champaign, 1985.
5. A. M. Ioannides. *Analysis of Slabs-on-Grade for a Variety of Loading and Support Conditions.* AFOSR-83-0143. U.S. Air Force, Dec. 1984.
6. G. T. Korovesis. *Analysis of Slab-on-Grade Pavement Systems Subjected to Wheel and Temperature Loadings.* Ph.D. thesis. University of Illinois, Urbana-Champaign, 1990.
7. A. M. Ioannides, E. J. Barenberg, and M. R. Thompson. The Westergaard Solutions Reconsidered. Presented at 64th Annual

Meeting of the Transportation Research Board, Washington, D.C., 1985.
8. R. D. Bradbury. Evaluation of Wheel-Load Distribution for the Purpose of Computing Stresses in Concrete Pavements. *HRB Proc.*, Vol. 14, 1934, pp. 225–254.
9. A. M. Ioannides and R. A. Salsilli. Temperature Curling in Rigid Pavements: An Application of Dimensional Analysis. In *Transportation Research Record 1227*, TRB, National Research Council, Washington, D.C., 1989, pp. 1–11.
10. A. M. Ioannides and G. T. Korovesis. Aggregate Interlock: A Pure-Shear Load Transfer Mechanism. In *Transportation Research Record 1286*, TRB, National Research Council, Washington, D.C., 1990.
11. W. J. Seiler. *A Knowledge-Base for Rehabilitation of Airfield Concrete Pavements*. Ph.D. thesis. University of Illinois, Urbana-Champaign, 1991.
12. R. P. Rawe, T. A. Ruhl, and R. J. Sunta. Results of the 1989 ASCE Airfield Pavement Survey. Presented at ASCE Specialty Conference on Aircraft/Pavement Interaction, Kansas City, Mo., September 1991.
13. W. C. Kreger. *Computerized Aircraft Ground Flotation Analysis—Edge Loaded Rigid Pavement*. Research Report ERR-FW-572. General Dynamics Corporation, Fort Worth, Tex., Jan. 1967.
14. G. Pickett, and S. Badaruddin. Influence Chart for Bending of a Semi-Infinite Pavement Slab. *Proceedings, 9th International Congress on Applied Mechanics*, Vol. 6, Université de Bruxelles, 1957.
15. H. M. Westergaard. Stresses in Concrete Pavements Computed by Theoretical Analysis. *Public Roads*, Vol. 7, No. 2, April 1926, pp. 25–35.
16. A. M. Tabatabaie, E. J. Barenberg, and R. E. Smith. *Longitudinal Joint Systems in Slip-Formed Rigid Pavements*, Vol. II: *Analysis of Load Transfer Systems for Concrete Pavements*. Report FAA-RD-79-4. II. U.S. Department of Transportation, Nov. 1979.
17. R. S. Rollings. Developments in the Corps of Engineers Rigid Airfield Design Procedures. *Proceedings of the 4th International Conference on Concrete Pavement Design and Rehabilitation*, Purdue University, West Lafayette, Ind., April 1989.
18. E. J. Yoder and M. W. Witczak. *Principles of Pavement Design*, 2nd ed. John Wiley & Sons, Inc., 1975.
19. A. M. Ioannides. Analytical Procedures for Concrete Pavements. In *Concrete Rafts* (John W. Bull, ed.), Blackie and Son, Ltd., Bishopbriggs, Glasgow, Scotland, 1990.
20. D. R. Alexander and J. W. Hall. ACN-PCN Concepts for Airport Pavement Management. Presented at ASCE Specialty Conference on Aircraft/Pavement Interaction, Kansas City, Mo., September 1991.
21. A. M. Ioannides and G. T. Korovesis. Analysis and Design of Doweled Slab-on-Grade Pavement Systems. *Journal of Transportation Engineering*, ASCE, March 1990.

Abridgment

Concrete Pavement Performance: A 23-Year Report

SHIE-SHIN WU

In 1966 an experimental concrete pavement road was constructed in the eastern part of North Carolina. This test road included a control section and eight test sections with different design features. The purpose was to evaluate the relative merits of several types of surface and base course treatments. Pavement performance information was collected periodically. It is concluded that base type affects the performance of the concrete surface, and the current design equation underestimates the performance of the concrete pavement.

A test road of concrete pavement in eastern North Carolina was opened to traffic on December 1, 1967. Pavement condition was surveyed periodically. The results and findings of this study are summarized in this paper.

TEST SECTIONS

The experimental road is a 15.758-mi portion of I-95 from Mile Post 144.45 to 159.87.

The southbound lane, which serves as the control section, is 9-in. jointed plain concrete pavement (JPCP) with 30-ft joint spacing on a 4-in. coarse aggregate base course (ABC). The northbound lane was divided into eight sections designated as Sections A through H. Different features in each section are as follows:

Section A: 9-in. JPCP on 4-in. ABC, 30-ft skew joints (4 ft at 24 ft), 7,035 ft long;

Section B: 9-in. JPCP on 6-in. soil-cement base (SCB), 30-ft joints with dowels, 10,200 ft long;

Section C: 9-in. JPCP on 6-in. SCB, 30-ft joints, 10,200 ft long;

Section D: 9-in. JPCP on 4-in. ABC, 30-ft joints with dowels, 9,495.94 ft long;

Section E: 9-in. JPCP on 4-in. cement-treated base course (CTBC), 30-ft joints, 10,200 ft long;

Section F: 9-in. JPCP on 4-in. bituminous concrete base course (BCBC), 30-ft joints, 11,450.06 ft long;

Section G: 8-in. continuously reinforced concrete (CRC) with 0.6 percent steel and transverse No. 4 bar at 30-in. center to center on 4-in. ABC, 11,825.44 ft long; and

Section H: 8-in. jointed reinforced concrete (JRCP) with 8-in. mesh reinforcement on 4-in. ABC, 60-ft joints with dowels, 12,000 ft long.

State of North Carolina Department of Transportation, P.O. Box 25201, Raleigh, N.C. 27611-5201.

For all these sections, a 4-in. sand blanket was constructed under the shoulder. The sand layer, which extended from the base course to the ditch slope, is designed for subsurface drainage.

CONSTRUCTION NOTES

A few notes on construction:

1. The concrete was mixed in a central plant and placed in one layer using forms.
2. The longitudinal and transverse bars on the CRC section were assembled and tied on site.
3. Core samples revealed that pavement depth varied from 8.90 to 9.95 in. for the 9-in. pavement and 7.97 to 9.13 in. for the 8-in. pavement. Compression strength varied from 4,280 to 7,460 psi.

DATA COLLECTION

Data pertaining to performance were collected and recorded. Information collected was as follows.

Road Roughness

A Bureau of Public Roads (BPR) type roughometer was used to collect roughness data. Since 1988, a South Dakota Road Profilor (SDRP) has been used to acquire pavement roughness information. Results of roughness surveys are summarized in Tables 1 and 2.

Joint Faulting

Faulting development in all sections was measured in 1974, 1980, and 1988. The results are summarized in Table 3.

Skid Resistance

Locked-wheel skid resistance tests have been conducted along the outside travel lane since early 1970. Test results are inconsistent (see Table 4).

TABLE 1 Road Roughness Index in Inches per Mile

SECTION	FEB. 68	OCT. 68	FEB. 70	APR. 71	APR. 72	JAN. 74
			OUTSIDE LANE			
A	82	*	*	79	78	*
B	76	79	78	77	77	79
C	78	83	88	79	74	84
D	70	76	79	78	76	77
E	78	80	87	80	78	87
F	79	80	82	77	74	84
G	70	69	76	71	68	73
H	68	69	74	71	69	72
CONTROL	77	79	86	87	83	90
			MEDIAN LANE			
A	78	*	*	79	79	*
B	76	79	78	75	77	75
C	74	76	79	76	75	80
D	69	76	73	73	75	71
E	75	77	79	74	76	77
F	79	78	77	77	75	78
G	73	72	77	73	73	74
H	70	72	72	72	72	70
CONTROL	76	79	79	76	77	78

* NO READINGS TAKEN SINCE ONLY VERY SHORT PORTION OF SECTION IS OPEN TO TRAFFIC.

TABLE 2 Roughness Summary: IRI in Meters per Kilometer

SECTION	1988	1990	1991
A	1.86	1.91	2.04
B	2.03	2.06	2.18
C	1.83	1.86	1.97
D	1.90	1.92	2.11
E	2.03	2.07	2.12
F	1.89	1.85	1.99
G	1.54	1.45	1.59
H	1.70	1.69	1.79
CONTROL	1.94	1.98	2.61

TABLE 3 Average Joint Faulting in Inches

SECTIONS	MEDIAN LANE 1974	MEDIAN LANE 1980	OUTSIDE LANE 1974	OUTSIDE LANE 1980	OUTSIDE LANE 1988(3)
A(1)	0.0	0.0	0.0	0.025	0.10
B	0.050	0.038	0.125	0.113	0.15
C	0.088	0.113	0.125	0.125	0.20
D	0.0	0.063	0.125	0.138	0.10
E	0.113	0.10	0.138	0.138	0.15
F	0.038	0.088	0.075	0.088	0.10
G(2)	-	-	-	-	-
H	0.038	0.075	0.125	0.150	0.15
CONTROL	0.039	0.094	0.141	0.189	0.194

NOTES: Ten joints were randomly selected from each section for measurements.
(1) Not open to traffic until late 1970's
(2) Continuously reinforced concrete pavement.
(3) Average of the first 18 joints from the Milepost.

TABLE 4 Average Skid Number

Section	1985	1986	1987
A	*	34	44
B	45	46	43
C	41	47	44
D	47	42	47
E	43	49	45
F	50	51	52
G	41	48	44
H	42	49	50
Control	44	45	45

* no data

Traffic Loading

Annual average daily traffic (AADT) data were used to estimate the truck traffic. The 18-kip equivalent single-axle load (ESAL) factors were applied to the estimated truck traffic to calculate the estimated loading.

On the basis of the given pavement structure, the design loading was backcalculated by using the 1972 AASHTO *Interim Guide for Design of Pavement Structures*.

TABLE 5 Surface Condition Summary

Sec	A	B	C	D	E	F	G	H	CONT.
1969	*	exc	F(m)	exc	F(l) S(l)	exc	exc	exc	exc
1970	*	exc	F(m)	exc	F(l) S(l)	exc	exc	exc	F(l)
1972	*	exc	F(m)	exc	F(l) S(l)	exc	exc	exc	F(l)
1973	*	exc	F(m)	exc	F(l) S(l)	exc	vg	exc	F(l)
1974	*	F(l)	F(m)	F(l)	F(m+)	F(l-)	vg	F(l)	F(m+)
1977	F(l)	F(l) C(l)	F(m)	F(l)	F(m+) S(l)	F(l)	vg	F(l)	F(m+)
1982	F(l)	F(l) C(l)	F(m) P(l)	F(l)	F(m+)	F(l)	vg	F(l) C(l-)	F(m+)
1983	F(l)	F(l)	F(m) C(l)		F(m+)	F(l)	vg	F(l) C(l-)	F(m+)
1984	F(l)	F(l) C(l)	F(m) C(m)	F(l)	F(m+)	F(l)	vg	F(l) C(l-)	F(m+) C(l)
1990	F(l) C(l-)	F(l) C(m) S(l)	F(m+) C(m+) P(l)	F(l) C(l-)	F(s) C(m)	F(l)	vg	F(l) C(l-)	F(s) C(m)

F : faulting
S : spalling
C : cracking
P : pumping
exc: excellent
vg : very good
* : section not open to traffic
l : low
m : medium
s : severe

Surface Condition

During every field investigation, subjective surveys of pavement surface condition were made. Only relational surface conditions were recorded. Results are summarized in Table 5.

FINAL SURVEY

The final survey was performed in November 1991. A 300-ft segment within each test section was randomly selected, and the number of cracks was counted. The sample was compared with the whole section visually to ensure that it was representative.

RESULTS AND FINDINGS

The results indicated that some test sections are showing signs of minor deficiency. However, all sections are structurally sound.

The actual loading of 12.3 million ESALs on the design lane is more than twice the design loading of 5.5 million ESALs for the unstabilized base and 1.5 times the design loading of 8 million ESALs for the stabilized base. Although some sections are in better condition than others, none of the test sections is in bad condition. This indicates that the pavement outperformed the prediction model.

Soil samples indicate that subgrade soils are predominantly A-6 soils. Traffic loading for all sections except Section A, which was opened to traffic 7 years later than the other sections, is essentially the same. There is no evidence to suggest that the northbound and southbound lanes carried different traffic loadings. Under these conditions, it is reasonable to assume that the difference in performance of the various sections is due to different treatments.

Pavement Surface Condition

In summary, the pavement in all sections outperformed the performance model. CRC pavement outperformed all other designs. As a matter of fact, this section of CRC outperformed any other CRC projects in North Carolina. The BCBC section (F) also performed well. Both Sections D and H are still in good condition. These two doweled sections, which have the same type of base as the control section, performed better than the control section.

Performance of the control and Section E is at the same level. Sections B and C (soil-cement base) are the worst-performing designs. Section B, which was constructed with dowels, is somewhat better than Section C (without dowels).

Section A was opened to traffic 7 years later than all other sections. Therefore no direct comparison can be carried out. On the basis of data collected, this section's performance is similar to that of the control section.

Roughness

From the latest International Roughness Index (IRI) data, Section G has the best ride quality. Sections H, C, and F

follow. Sections D and E are on the next level, and Section B is the worst.

Load Transfer

Regardless of the base material, sections with dowels outperform the same base without dowels. Providing load transfer devices reduces joint faulting, hence improves ride quality.

Base Material

Concrete pavement with an asphalt base outperforms that with any other type of base. Aggregate bases are next in performance, and cement-treated aggregate bases are next to the last. Soil-cement bases are the worst.

CONCLUSIONS AND RECOMMENDATIONS

On the basis of this project, it is concluded that

1. Having transverse tie bars on the CRC provides reinforcement in the transverse direction and hence eliminates the punch-out problem.
2. JPCP on SCB performs poorly.
3. CTBC may provide a strong, nonerodible base that fulfills the functions of a base as defined by Yoder and Witczak (*1*). Wu and Hearne (*2*) found that concrete slabs actually lift up and separate from an econocrete base as the surface temperature changes. Curling of concrete slabs on stiff CTBC results in loss of uniform support and shortened fatigue life. Therefore, relative stiffness should be considered in the selection of base material for a concrete pavement.
4. BCBC is the best of all base materials tested in this project. Nonerodibility and flexibility contribute to the good performance.
5. A sand blanket provides an outlet for trapped water and hence eliminates this destructive factor. Pavement drainage design should be an integral part of the pavement structural design procedure.
6. Providing load transfer at joints reduces faulting and vertical movement at the joint. It therefore decreases pumping problems and improves ride quality.
7. Long joint spacing provides a better ride quality.
8. The current pavement performance model underestimates concrete pavement performance. Development of a model that is calibrated with North Carolina data is essential.
9. Over the years, IRI values show deterioration of the pavement surface condition. Considering its low cost of operation and its safety, the SDRP could be the primary source of objective pavement condition information to support the Pavement Management System.

ACKNOWLEDGMENTS

The author is indebted to Frank Pace, Tom Hearne, and many other North Carolina Department of Transportation employees for their valuable work in collecting the data.

REFERENCES

1. E. J. Yoder and M. W. Witczak. *Principles of Pavement Design*, 2nd ed. John Wiley & Son, Inc., New York, 1975.
2. S. Wu and T. Hearne. Performance of Concrete Pavement with Econocrete Base. *Proceedings, 4th International Conference on Concrete Pavement Design and Rehabilitation*, Purdue University, April 1989.

Dynamic Response of Rigid Pavement Joints

THEODOR KRAUTHAMMER AND LUCIO PALMIERI

A recent experimental study on the relationship between aggregate interlock shear transfer across a concrete interface and its dynamic response frequency is described. The analysis of the data recorded during the tests was performed in both the time and the frequency domains. The results demonstrate a clear relationship between the internal aggregate interlock conditions of the concrete interface and its response frequency, and the study may serve as a basis for an innovative testing approach for joints in rigid pavements.

Pavement maintenance for ensuring acceptable serviceability conditions requires the assessment of a pavement's internal conditions. However, the determination of such conditions in extensively damaged pavement can be difficult. In rigid pavements, one of the most critical areas is the joint where spalling of concrete and cracking and pumping of the base may occur. These phenomena can adversely affect the load transfer across pavement joints and the pavement's behavior. In the last decades, significant efforts have been undertaken to develop nondestructive testing techniques for pavement evaluation. Most of these techniques, however, provide information on pavement deflection, an indirect parameter largely used for pavement structural evaluation. Furthermore, deflections depend on the modality of loading and on its magnitude, and one of the major problems is to identify an experimental loading mode representative of traffic loads.

The objective of this paper is to describe a recent experimental study on the assessment of shear transfer conditions by aggregate interlock in a rigid pavement joint on the basis of the frequency analysis of its dynamic response (*1,2*). The analysis of the data recorded during the tests was performed in both the time and the frequency domains. The correlation between the results obtained in these two domains highlighted a unique relationship between the shear transfer ability and the dynamic response frequency.

BACKGROUND

Joints are locations where geometric discontinuities are introduced into the pavement slab, and the provision of load transfer across a joint is one of the main concerns in concrete pavement design. In undowelled joints, load transfer is provided by shear forces across an undowelled discontinuity between adjacent edges in the form of aggregate interlock. In reinforced concrete pavements the reinforcing steel is expected to resist the opening of undesired cracks to ensure adequate aggregate interlock and to provide dowel action across discontinuities in the pavement. These mechanisms have been described in a report by American Concrete Institute–American Society of Civil Engineers Committee 426 (*3*) and in well-known books on reinforced concrete (*4,5*). Furthermore, it is known that the development of good aggregate interlock can greatly prevent the development of critical edge stresses (*6,7*).

Application of shear to planes of discontinuity (cracks, interfaces between different materials, interfaces between concretes cast at different times) causes relative slip between the two sides of the discontinuity. As reported by Park and Paulay and by MacGregor (*4,5*), if reinforcement is present, the shear is transferred across the interface mainly by the following two mechanisms:

1. Under the shear action the surfaces tend to separate or to slip, or both; in both cases the reinforcement is subjected to tension, and for equilibrium the concrete is subjected to compression. Consequent to these compressive stresses, friction develops in the interface.
2. Shear is also transferred by aggregate interlock between the particles of concrete and by dowel action of the reinforcement crossing the surface.

According to Mattock and Hawkins (*8*), the shear strength V_n when shear friction reinforcement is perpendicular to the shear plane can be evaluated from

$$V_n = 0.8A_{vf}f_y + A_cK_1 \quad (1)$$

where

A_{vf} = area of reinforcement crossing the surface,
A_c = area of concrete surface resisting the friction,
K_1 = constant equal to 400 for normal-weight concrete, and
f_y = reinforcement's yield strength.

The first term in Equation 1 represents mechanism 1 (friction) with a coefficient of friction for concrete sliding on concrete of 0.8, and the second term represents mechanism 2. Furthermore, the first term in Equation 1 should be notified if the two concrete surfaces are pressed against each other by an externally applied in-plane force, and such a modification could be based on the Coulomb friction theory. This shear force is expected to control the load transfer across joints in rigid pavements.

T. Krauthammer, Department of Civil Engineering, 212 Sackett Building, Penn State University, University Park, Pa. 16802. L. Palmieri, Department of Civil and Mineral Engineering, University of Minnesota, 500 Pillsbury Drive S.E., Minneapolis, Minn. 55455.

Current joint assessment approaches employ the concept of joint efficiency for classification of its internal condition. Load transfer efficiency (or joint efficiency) is defined as the ratio of the deflection of the unloaded side of the joint divided by the deflection of the loaded side of the joint (for convenience this ratio is usually expressed as a percentage), and it is related to the joint shear transfer capacity. From the study by Foxworthy (*9*) it has been shown that the load transfer efficiency of a joint is closely related to the stresses that are developed on the bottom of the slab and therefore to the slab's performance under loading. Tabataie and Barenberg (*10*) showed that the load transfer efficiency across a joint affects the maximum stresses in the slab, especially under edge and corner loading conditions.

Since the stress transmitted to the subgrade, assuming linear behavior, is the slab deflection times a base stiffness K, the subgrade stress will be affected in proportion to the deflection. The critical point to note is that just a small reduction from a full joint efficiency may result in a large change in the stress ratio, and therefore significant benefits correspond to designing joints with high load transfer efficiencies. The joint efficiency depends on several factors, such as temperature, moisture, and frost, but, according to Foxworthy (*9*), not on the load magnitude.

Nondestructive Evaluation Techniques for Pavements

Nondestructive techniques are methods for evaluating the characteristics of a system without harming it. In this case, the goal is to determine the strength and integrity of the pavement, usually by employing deflection measurements. The deflection of a rigid pavement under loading is generally due to comparison of the base rather then to compression of the pavement layers (*6,7*). Pavement deflections depend on pavement properties and on the loading type (e.g., static, dynamic) and magnitude. The ideal testing procedure should closely represent a design moving load. According to a classification by Moore et al. (*11*), the four major categories of nondestructive structural evaluation of pavements are static deflection, steady-state deflection, impact load response, and wave propagation techniques. The impact load response techniques have several advantages over the others (*6,7*), and this approach was employed for the present study.

In impact load response techniques, a transient load is applied to the pavement, and the response, usually in terms of displacement, is measured. The short-duration loading is generated by a weight dropped on a plate that is placed on the pavement surface, but according to Moore et al. (*11*), the duration of the pulse should not exceed 1 msec for the loading to be considered transient. This is because the rise time, defined as the time the pavement needs to deflect from 10 to 90 percent of its maximum deflection, can vary between 3 to 6 msec. Furthermore, the response to longer loadings will contain not only information on short-duration pavement response, but also information on the longer-frequency characteristics of the system and disturbances from wave reflections. It is difficult to obtain such short pulses in the field, and the devices used for impact load tests usually have pulses that last 20 msec or longer.

One such testing device is the falling weight deflectometer (FWD), which consists of a large mass that is dropped vertically on a plate resting on the pavement surface while a spring-damping system is interposed between the mass and the plate. The mass, dimensions of the plate, and drop height vary, depending on different versions of the device. For example, the Phoenix FWD has a 330-lb weight, it is dropped from a height of 15.7 in. on an 11.8-in.-diameter circular plate, and the pavement's deflection is measured with a linear variable differential transformer (LVDT). The corresponding pulse has a duration of about 26 msec, and the magnitude of the peak load is about 5.5 tons.

Different types of FWD devices generate pulses with different durations, but always in the interval from 20 to 40 msec. The theoretical accelerations transmitted to the pavement by these devices are of the order of 10 to 30 g (where g is the acceleration of gravity). For example, the accelerations measured in the field by Hoffman and Thompson (*12*) were about 4 g, and this difference was probably due to the FWD-pavement interaction and to the rubber mat interposed between the loading plate and pavement surface. However, even a 4 g peak acceleration is about 10 times higher than those due to traffic, as pointed out by Sebaaly et al. (*13*), who also noted that the duration of typical pulses from traffic loading is of the order of several hundred milliseconds. Despite these discrepancies, the deflections measured by Hoffman and Thompson (*12*) were consistent with the ones due to traffic; however, better results are obtained by using velocity transducers (geophones) instead of LVDTs. This is because geophones, like accelerometers, do not need an immovable reference system as required by an LVDT.

It is clear that all impact load response techniques are based on measuring the dynamic response of a pavement under a short-duration load pulse. Furthermore, dynamic analyses can be performed both in the time and the frequency domains, and the information obtained by one approach supplements the other. The traditional dynamic analysis has been based on time domain methods (*14*); however, much can be learned from frequency domain analysis. Data acquired during tests represent the time history of a certain variable. The Fourier transform is one of the tools used to study a function's characteristics in the frequency domain, and the analysis in the frequency domain was done using the fast Fourier transform (FFT) techniques, as discussed by Oppenheim and Schafer (*15*). The FFT operation was applied through the scientific software Asystant+ (*16*). In fact, what was actually done in this study was the power spectrum operation, defined as the square magnitude of the FFT.

Structural Response Under Impulsive Loads

Structures behave differently under dynamic loads than when subjected to static forces. However, not all types of dynamic loads produce the same modes of behavior, as discussed by Clough and Penzien (*14*) and Biggs (*17*), who showed that impulsive loads can excite specific behavioral modes that do not exist under slower loading conditions. Krauthammer et al. (*18,19*) showed that under very short impulsive loads there is a complete separation between flexural and shear responses. These findings were confirmed and carefully examined also by Assadi-Lamouki and Krauthammer (*20*), who found that the interaction between structural response mechanisms depends on their corresponding natural frequencies.

Furthermore, it has been found by Krauthammer and others (*18–20*) that such time separation between flexural and shear response modes indicates hardly any influence of flexural behavior on shear behavior.

For example, a reinforced concrete slab with the dimensions 60 × 30 × 6 in. has a fundamental (flexural) frequency of about 0.0737 Hz, and a 30 × 30 × 6 in. slab has a fundamental frequency of about 0.1178 Hz (these frequencies correspond to periods of about 13.5 and 8.5 sec, respectively). Impulsive loads, however, can excite shear response modes in the frequency range of several hundred, or even thousands, of hertz (i.e., corresponding to periods that could be less than 1 msec). Under such conditions, the structure will exhibit its thickness shear responses first, and the flexural response modes may appear much later. Obviously, one can perform experiments in which the early shear response is captured by high-speed data acquisition systems, and any possible flexural response would not affect that behavior since it only appears much later. It was shown earlier that typical FWD devices use relatively heavy weights dropped from a low height onto an elastic layer that is placed over the pavement surface. Increasing the drop height and reducing the flexibility of the elastic layer and the weight enable one to obtain shorter load pulses with comparable magnitudes. The experimental approach adopted for this study is based on the early time shear response of concrete slabs.

APPROACH OF THE STUDY

The present study (*1*) was aimed at developing an experimental procedure for evaluating aggregate interlock shear transfer capabilities across portland cement concrete (PCC) pavement joints. Furthermore, on the basis of the separation between flexure and shear response modes, as discussed above, only the early time (i.e., shear) behavior would be of interest for this method, and there is no need to study the flexural behavior (i.e., the moment transfer) also, which has no effect on the early response. Krauthammer and Western (*21*) showed that the shear transfer across a joint in rigid pavements can be described accurately by the relationship between shear stress and shear slip. A deterioration in the joint shear transfer capability was correlated to a reduction in the joint shear stiffness. Such a reduction in the joint's stiffness should cause a decrease in the shear response frequency, as discussed by Clough and Penzien and Biggs (*14,17*).

This study was based on the anticipated finding of a relationship between the frequency response of a joint to dynamic loading and the joint shear transfer capability. If a relationship between the internal aggregate interlock shear transfer conditions of the joint and its response frequencies exists, it would be possible, by measuring a corresponding frequency shift in situ, to determine the joint's internal condition in a unique manner. Such information would then be used to decide on the required corrective measures, which would enhance roadway management procedures. The experimental approach has been described elsewhere (*2*), and a brief summary is presented here.

The following two reinforced concrete slab systems were employed in modeling the pavement-joint configuration in this study, as shown in Figure 1:

1. System 1: One concrete slab 60 in. long, 30 in. wide, and 6 in. deep.
2. System 2: Two concrete slabs each 30 in. long, 30 in. wide, and 6 in. deep.

Although these systems were not intended to model a full-scale pavement joint, they contain all material and geometric features to provide meaningful information on aggregate interlock across a concrete interface. System 1 represents the ideal case of full shear transfer across an imaginary joint, and the two slabs of System 2 represent a realistic concrete-to-concrete interface in a pavement. The two systems were placed

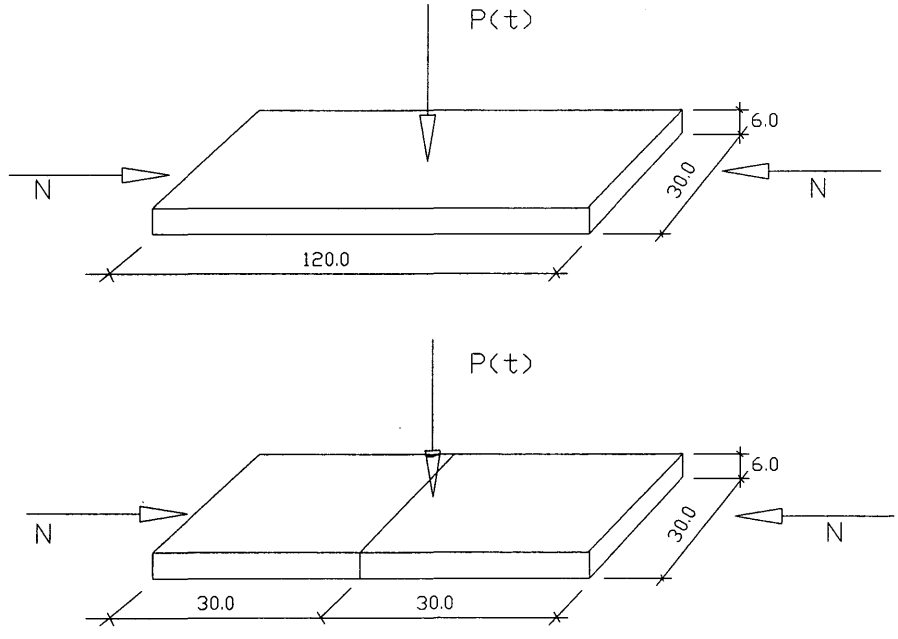

FIGURE 1 Slabs and force systems.

on a sand bed 1 ft deep to simulate an underlying base material.

The simulation of different conditions of joint shear transfer in System 2 was done by applying to the system an in-plane compressive force N, as shown in Figure 1. The application of this force was realized by means of two 1-in.-diameter steel rods connected to steel angles placed at the ends of the slabs. When the nuts at the end of the rods were torqued, tensile forces were induced in the rods and a corresponding compressive force was induced in the plane of the slabs. The axial forces in the rods were calculated from the measured strains obtained from two strain gages that were mounted diametrically opposite, and their readings were averaged to remove possible bending effects. The average strain in each rod was multiplied by the steel modulus of elasticity and by the cross-sectional area to compute the axial force.

Under loading, when the vertical force $F(t)$ is applied, the two slabs are forced to move relative to each other, and a frictional force T, as defined in Equation 1, develops at the interface opposing this relative movement. Varying the values of the force N, the values of T change accordingly, as will the total resistant forces acting on the two sides of the interface. Neglecting the friction between the slabs and the sand, this force will be close to $F(t) - T$ on the loaded side of the joint, whereas on the unloaded side it will be T. Changing the magnitude of these resultant forces causes a difference in the corresponding displacements of the two sides of the joint; hence, the value of joint efficiency can be computed. This approach permits one to vary the value of N for simulating different shear transfer conditions and corresponding joint efficiencies.

The dynamic load was generated by a 30-lb weight dropped from a height of 3 ft. The impulsive force obtained in this manner had a recorded maximum amplitude of 22,500 lb and a duration of about 1.6 msec. These pulse characteristics are close to the limit of 1 msec, as recommended by Moore et al. (*11*), and they have peak force values comparable with in-service loads or FWD tests. The impact load was uniformly distributed over a steel plate with an area of 144 in.^{2} to prevent cracking and breaking of the concrete. The plate was positioned along the major axis of symmetry of the slab 3 in. from the joint and firmly attached to the slab by four steel bolts to prevent rebound. Two rubber pads were interposed between the plate and the concrete slab and between the plate and the weight to prevent steel-to-steel high-acceleration impact, to keep the accelerations under the maximum value of 500 g, and to obtain a more even distribution of the load from the steel plate onto the concrete slab. This approach ensured that the same impact conditions would exist for all tests.

Experimental data consisted of acceleration-time histories obtained from accelerometers glued to the reinforced concrete slabs. Two accelerometers were positioned 2.5 in. from the joint along the major axis of symmetry of the slab on both sides of the joint, and they were connected to the data acquisition system through a channel coupler. Data acquisition was performed at an effective sampling rate of 500 kHz per channel. Data were acquired for 10 msec, and the number of samples acquired from each channel was 5,000. This duration was sufficient to capture the vibrations of the systems under the main impact. As noted earlier, the flexural response of the slabs could appear between about 8.5 to 13.5 sec later, well after the data had been acquired. The experimental data were then transferred for analysis in both the time and frequency domains by the scientific software Asystant+ (*16*).

Tests on System 1

A set of eight tests, marked B1 through B8, was conducted without applying in-plane compression to the slab through the rods, and they represented an ideal condition of full shear transfer. The data were acceleration-time histories on both sides of the joint in the positions previously described. However, any comparison between the results from System 1 and the results from System 2 must be made only at parity of conditions. Therefore, it was necessary to eliminate all influences on the results by any test parameter except the joint shear transfer. Preliminary experiments were conducted and it was determined that neither large in-plane forces nor possible background noise had an effect on this experiment.

Tests on System 2

System 2 represented variable shear transfer conditions across a joint induced by externally applied in-plane forces to the pavement slabs, as described above. Different values of in-plane compression were applied to the slabs, tests were conducted, and the corresponding values of joint efficiency were calculated. On the basis of the data obtained, and according to the classification by Krauthammer and Western (*21*), values of axial force were selected to represent the following three joint conditions: a new joint, a deteriorated joint, and a dead joint, as shown below:

	Joint Efficiency
New joint	≥0.9
Deteriorated joint	≈0.6
Dead joint	<0.4

Six values of the force N were selected to be applied in each rod to represent the different joint conditions and, correspondingly, six sets of three tests each were conducted on System 2. Every test was marked by two letters followed by a number from 1 to 3, and their corresponding in-plane forces are as follows:

Test Set	*In-Plane Force, Each Rod (lb)*
ST	2,000
SU	4,000
SV	5,000
SP	6,000
SQ	8,800
SR	9,500

RESULTS AND DISCUSSION

Experimental data consisted of acceleration-time histories obtained from the accelerometers attached to the reinforced concrete slabs in the positions previously described. The displacement-time histories at those points were obtained by integrating twice the acceleration records. On the basis of the frequency analysis of the acceleration data, it was decided to

concentrate on the frequency range between 0 and 5,000 Hz. The results obtained for the two systems under consideration are discussed next.

Results for System 1

As described previously, a set of preliminary tests was conducted on System 1 to evaluate the effort of in-plane forces on the system's response frequency, and it was noted that the frequencies were the same as those obtained without the application of in-plane forces. From this observation it was decided to consider the results for the case without in-plane forces as the main set of tests, and the corresponding data would be compared with that from the tests on System 2.

The assumption that System 1 represents an ideal condition of full shear transfer capability is confirmed by the test results, and the initial assumption of a joint efficiency value was 0.9, as shown earlier. The experimental values obtained for the maximum displacements, the time at which they occur, and the corresponding joint efficiency are given in Table 1.

It is noted that for six of the eight cases these values are very close to 0.9. However, a value of 0.628 was obtained for case B3 and a value of 1.132 for case B6, most probably because of poor adherence between accelerometers and the slab. It was noted earlier that the joint efficiency ratio is obtained when the peak deflection of the unloaded side of the joint is divided by the peak deflection of the loaded side. Ratios considerably lower or higher than unity are possible since either one of the accelerometers may not have been adequately bonded to the surface. From Table 1 it is noted that the maximum displacements for System 1 occur at the same time on both sides of the joint. In general for every test, all time histories of these displacements almost overlap: the two sides of the imaginary joint move at the same time and with displacements of the same amplitude. This indicates that the load is properly transferred from one side of the ideal joint to the other, as expected. The data were used to obtain a description of the response in the frequency domain for all cases. It should be noted again that the flexural (i.e., bending) response would appear much later, well after the test is over.

Results for System 2

System 2 represents the variable joint conditions through the applications of different values of in-plane force N. Table 2 contains the average values of maximum displacements, the time at which they occur, and the corresponding joint efficiency values (i.e., the ratio of the peak displacement of the unloaded side to the peak displacement of the loaded side). The selection of in-plane compression, reported in the previous section, as representative of variable shear transfer conditions seems to be confirmed by these results. Comparing the selected joint efficiencies tabulated in the previous section with the corresponding test values of Table 2 demonstrates that the pairs of sets ST-SU, SV-SP, and SQ-SR represent the cases of dead, deteriorated, and new joints, respectively. From the data in Table 2 it is noted that the interval of time between the peaks in the displacement plots decreases as the value of in-plane compression increases.

TABLE 1 Maximum Displacements and Joint Efficiency for System 1

	Loaded Node		Unloaded Node		
Test No.	Max. Displ. in./g[a]	Time (msec)	Max. Displ. in./g	Time (msec)	JE[b]
B 1	-5.200 E-5	7.76	-4.680 E-5	7.77	0.900
B 2	-5.000 E-5	6.30	-4.200 E-5	6.38	0.840
B 3	-5.240 E-5	6.99	-3.288 E-5	6.55	0.628
B 4	-4.720 E-5	6.74	-4.040 E-5	6.61	0.856
B 5	-3.864 E-5	6.49	-3.440 E-5	6.51	0.890
B 6	-3.780 E-5	6.63	-4.280 E-5	6.77	1.132
B 7	-3.528 E-5	8.25	-2.924 E-5	8.19	0.829
B 8	-3.024 E-5	7.16	-2.872 E-5	7.05	0.950

[a] g = Acceleration of Gravity
[b] JE = Joint Efficiency

TABLE 2 Maximum Displacements, Time, and Joint Efficiencies for System 2

TEST	LOAD PER ROD (lbs)	LOADED SIDE		UNLOADED SIDE	
		Max. Disp. (in.*10^{-6})	Time (msec)	Max. Disp. (in.*10^{-6})	Time (msec)
ST	2,000	-7.22	6.11	-1.5	7.1
SU	4,000	-6.35	5.4	-2.31	6.16
SV	5,000	-5.99	5.65	-3.17	6.72
SP	6,000	-5.13	5.35	-3.75	5.82
SQ	8,800	-4.02	5.82	-3.78	5.78
SR	9,500	-3.91	5.47	-3.81	5.52

TABLE 3 Frequency Variations on Unloaded Side of Joint

Test	Power Spectrum Peaks' Frequencies, Hz					
ST	244	488	976	1586	/	2562
SU	244	610	976	1586	2440	2562
SV	244	732	1098	1586	2440	2562
SP	244	1098	/	1586	/	2684
SQ	244	1098	/	1708	2440	2684
SR	244	1098	/	1708	2440	/

/ = Peak too small to be significant, or no response.

Also it is noted that the amplitude of the displacements decreases, as does the difference between the values of the displacements on the two sides of the joint at any time, when the in-plane compression forces increase. These behavioral aspects demonstrate that the application of variable in-plane compressive forces to the slabs simulates effectively different aggregate interlock shear transfer conditions across a pavement joint. As the value of this force increases, the two slabs tend to behave more as one. For high values of applied force (for example, sets SQ and SR), the two sides of the interface move almost simultaneously and with displacements of almost the same amplitude.

The information in Table 2 is used to provide further insight into impact load response approaches. It is noted that for joints with good load transfer the peak displacements on both sides of the joint occur at almost the same time (the largest time difference was measured for case SQ 2 at 0.64 msec). However, that time difference increases as the load transfer deteriorates. This indicates that there could be a problem if traditional FWD data are used for the assessment of PCC pavements with poor joints. If one employs the peak displacements from the two sides of the joint, the corresponding joint efficiency ratio is based on events that do not occur at the same time. If, however, the joint efficiency ratio is derived on the basis of readings for the same time, they may not represent the peak displacements on both sides of the joint. This problem does not exist with the present approach, because the entire time history is used to obtain the corresponding power spectra.

The data for all cases were transformed into the frequency domain, and representative results were tabulated for each in-plane force set. Frequency data for each in-plane force set for the unloaded side of the joint are presented in Table 3.

Comparison of Results

The following observations are made on the basis of the results presented in Table 3:

1. The data indicate that the second response frequency is affected by the shear transfer capability of the joint. An increase in the quality of the contact across the joint (i.e., better aggregate interlock) increases the second response frequency, as shown in Figure 2. A further increase in the in-plane force caused the second frequency to reach and remain at 1,098 Hz on the unloaded side. A similar trend was observed from readings on the loaded side.
2. The response of the larger slab (System 1) is very close to the response of the two slabs (System 2) subjected to a large in-plane force. The main difference is in the first frequency, which is a function of the slab's dimensions and dynamic characteristics. This difference, observable for both sides of the joint, indicates that the large slab has a rigid body motion that is different from that of the two smaller slabs.
3. For higher frequencies, no appreciable differences can be related to changes in the quality of the contact between the sides of the joint, and the frequency values on both sides remain almost constant for all the tests.

CONCLUSIONS

An exploratory experimental approach has been presented for nondestructive testing of pavement joints with aggregate interlock load transfer capabilities. The approach is based on the shear vibration response of structural systems under impulsive loads, and on the considerable time separation between shear and flexural behavior modes. Experimental data were acquired on models representing different aggregate interlock shear transfer capabilities across concrete interfaces. Those data were analyzed both in the time domain and in the frequency domain utilizing the Fourier analysis technique.

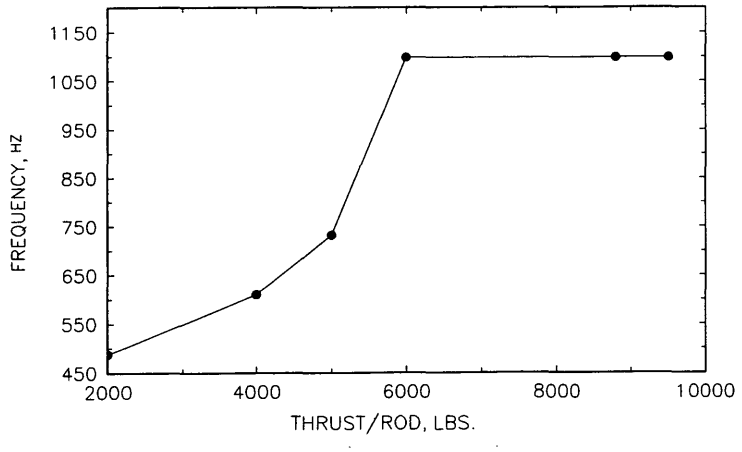

FIGURE 2 Frequency shift and interface contact conditions.

The results obtained confirm the initial expectation that response frequencies in the dynamically loaded structure are closely related to the shear transfer capacity of the interface. The following conclusions are drawn from this study:

1. The model that has been adopted to simulate different aggregate interlock shear transfer conditions is reliable, and it has been confirmed by experimental data.
2. On the basis of the obtained results, frequency variation of modal response is an excellent tool for deciphering the internal aggregate interlock conditions of concrete interfaces. Different vibration frequencies are representative of different values of corresponding joint shear transfer.
3. It is concluded from these results that this approach, after further development, could be employed for the determination of the internal shear transfer capabilities of interfaces in rigid pavement joints.

ACKNOWLEDGMENT

The study reported herein was performed by the University of Minnesota under contract with the Minnesota Department of Transportation. The authors wish to express their deep appreciation to George Cochran and his staff for their cooperation and support.

REFERENCES

1. L. Palmieri and T. Krauthammer. *Vibration Spectroscopy for Rigid Pavement Joint Assessment.* Report MN/RD-91/04. Minnesota Department of Transportation, St. Paul, Aug. 1990.
2. T. Krauthammer and L. Palmieri. Concrete Interface Shear Vibration Spectroscopy. *Journal of Engineering Mechanics*, ASCE, Vol. 117, No. 10, Oct. 1991, pp. 2251–2264.
3. ACI-ASCE Committee 426. The Shear Strength of Reinforced Concrete Members. *ASCE Journal of Structural Division*, Vol. 99, June 1973, pp. 1091–1187.
4. R. Park and T. Paulay. *Reinforced Concrete Structures*. Wiley-Interscience, New York, 1975.
5. G. J. MacGregor. *Reinforced Concrete, Mechanics and Design*, 2nd ed. Prentice Hall, Englewood Cliffs, N.J., 1991.
6. R. I. T. Williams. *Cement-Treated Pavements*. Elsevier Applied Science Publishers, New York, 1986.
7. E. J. Yoder and M. W. Witczak. *Principles of Pavement Design*. Wiley, New York, 1975.
8. H. A. Mattock and N. M. Hawkins. Shear Transfer in Reinforced Concrete—Recent Research. *Journal of Prestressed Concrete Institute*, Vol. 17, No. 2, March–April 1972.
9. P. T. Foxworthy. *Concepts for the Development of a Nondestructive Testing Evaluation System for Rigid Airfield Pavements*. Ph.D. thesis. Department of Civil Engineering, University of Illinois at Urbana-Champaign, June 1985.
10. A. M. Tabataie and E. J. Barenberg. Structural Analysis of Concrete Pavement Systems. *Journal of Transportation Engineering*, ASCE, Vol. 106, No. TE5, Sep. 1980.
11. W. M. Moore, D. I. Hanson, and J. W. Hall. *Transportation Research Circular 189: An Introduction to Nondestructive Structural Evaluation of Pavements*. TRB, National Research Council, Washington, D.C., Jan. 1978.
12. M. S. Hoffman and M. R. Thompson. Comparative Study of Selected Nondestructive Testing Devices. In *Transportation Research Record 852*, TRB, National Research Council, Washington, D.C., 1982.
13. B. Sebaaly, T. G. Davis, and M. S. Mamlouk. Dynamics of Falling Weight Deflectometer. *Journal of Transportation Engineering*, ASCE, Vol. 111, No. 6, Nov. 1985.
14. R. W. Clough and J. Penzien. *Dynamics of Structures*. McGraw-Hill, New York, 1975.
15. A. V. Oppenheim and R. W. Schafer. *Digital Signal Processing*. Prentice-Hall, Englewood Cliffs, N.J., 1975.
16. *Asystant+, Scientific Software for Data Acquisition and Analysis*. Asyst Software Technologies, Inc., Rochester, N.Y., 1987.
17. J. M. Biggs, *Introduction to Structural Dynamics*. McGraw-Hill, New York, 1964.
18. T. Krauthammer, N. Bazeos, and T. J. Holmquist. Modified SDOF Analysis of RC Box-type Structures. *Journal of Structural Engineering*, ASCE, Vol. 112, No. 4, April 1986, pp. 726–744.
19. T. Krauthammer, S. Shahriar, and H. M. Shanaa. Response of RC Elements to Severe Impulsive Loads. *Journal of Structural Engineering*, ASCE, Vol. 116, No. 4, April 1990, pp. 1061–1079.
20. A. Assadi-Lamouki and T. Krauthammer. *Development of Improved Timoshenko Beam and Mindlin Plate Theories for the Analysis of Reinforced Concrete Structures Subjected to Impulsive Loads*. Structural Engineering Report ST-88-02. Department of Civil and Mineral Engineering, University of Minnesota, May 1988.
21. T. Krauthammer and K. L. Western. Joint Shear Transfer Effects on Pavement Behavior. *Journal of Transportation Engineering*, ASCE, Vol. 114, No. 5, Sept. 1988, pp. 505–529.